UNIVERSITY OF SOUTHAMPTON

LATTICE CALCULATIONS IN THE B AND K SYSTEMS

by

Alistair Kyles Ewing

A thesis submitted for the degree of

Doctor of Philosophy

Department of Physics

October 1994

To my family

UNIVERSITY OF SOUTHAMPTON

ABSTRACT

FACULTY OF SCIENCE

PHYSICS

Doctor of Philosophy

LATTICE CALCULATIONS IN THE B AND K SYSTEMS

Alistair Kyles Ewing

Accurate measurements of the CKM matrix elements can be used to probe the consistency of the Standard Model. The main uncertainties in these measurements are involved in the theoretical calculation of the strong interaction effects on weak decays. Lattice QCD offers the only non–perturbative method to calculate these effects in a model independent way.

Neutral kaon mixing is driven in the low energy effective theory by the $\Delta S = 2$ four fermion operator. We study the weak matrix element of this operator in terms of the kaon B-parameter using Lattice QCD with an improved fermion action. The chiral behaviour of the matrix elements compared with the Wilson results show no significant improvement.

Extraction of CKM matrix elements from B-meson mixing is restricted by the uncertainty in the B-meson decay constant. We calculate this matrix element using b quarks simulated in the static limit of the Heavy Quark Effective Theory (HQET). Smeared interpolating operators are used to extract the ground state and the effectiveness of several smearing functions is studied.

We calculate the $B_s - B_d$ and $\Lambda_b - B$ mass differences from the lowest order contribution to the static theory. The spin dependent first order corrections are studied in a calculation of the vector–pseudoscalar mass splitting, $B^* - B$. Comparison is made to calculations with Wilson fermions and experimentally measured values.

Contents

List of Figures

List of Tables

Preface

The work described in this thesis was carried out within the UKQCD Collaboration. The contents of Chapters 1 and 2 are standard. The work described in Chapters 3, 4 and 5 were carried out in collaboration with J. Mehegan, University of Edinburgh , and C.T. Sachrajda, University of Southampton. The results contained in Chapters 4 and 5 were presented at 'Lattice 94' conference held in Bielefeld, Germany and will appear in the conference proceedings.

Acknowledgements

First and foremost, I would like to thank my family–Douglas, Catherine and Catriona Ewing–and Fiona Dow without whose love and support this PhD would have been a much longer and lonelier experience. I think this thesis has caused them more pain than it did me.

None of this would have been possible without the guidance of my supervisor, Professor C.T. Sachrajda, *el señor que tiene los ojos azules*, and I thank him for his time and patience. Equally invaluable were the many contributions from John Mehegan, my collaborator and friend in Edinburgh. We learned to *lettura delle configurazioni di gauge* and enjoyed a good few pints of *heavy* into the bargain.

Southampton is a long way from home, but the warmth and friendship of all the staff, postdocs and students of the Southampton High Energy Physics group has made my time here very pleasant. In particular I would like to thank Professor K.J. Barnes, for giving me the opportunity to work in his group, and `bjg` and `te` for their guidance on all things computational and horticultural, respectively.

Thanks also to EPSRC for funding this work.

Finally I would like to thank Nancy Hey for getting an A in her GCSE Maths, so making this whole PhD worthwhile.

Chapter 1

Introduction

Nineteen eighty–three was a good year for particle physics. The detection of the W and Z bosons at CERN's UA1 detector were in spectacular agreement with the predictions of the electroweak theory of Glashow, Salam and Weinberg. Arguably, this was one of the great successes of the Standard Model of Particle Physics and was celebrated by Nobel Prizes for the experimentalists Rubbia and Van der Meer in 1983. Since then it could be said that most of particle physics, both experimentally and theoretically, has been involved in testing this Standard Model and as yet it has survived remarkably well.

In this chapter we include a brief sketch of the Standard Model and outline in more detail one aspect of the theory of particular interest to this thesis, CP violation in the Standard Model. A detailed account of the Standard Model can be found in a multitude of text books on the subject, [7, 8, 9]. This chapter is ended with some motivations for the calculations attempted in this work.

1.1 The Standard Model

The Standard Model of Particle Physics describes the interactions of elementary particles (*quarks* and *leptons*) in terms of three forces (*strong*, *weak* and *electro-magnetic.*) though as yet fails to provide a quantum theory of gravity. All three theories fall into the class of Quantum Field Theories (QFT), with particles represented by fields over all space–time. Interactions can be introduced in a very natural way by the requirement of gauge invariance. This involves constructing a theory which is invariant under local, *gauge*, transformations. In this way, *gauge bosons* are introduced into the theory. These are massless spin 1 particles, which mediate the interactions, acting as force carriers. A further requirement placed on the Standard Model is that of renormalisability, which allows the extraction of finite physical predictions from the theory.

The 'blue–print' QFT is QuantumElectroDynamics (QED). This describes the interactions of electrons and photons in a gauge covariant formalism as a theory of electromagnetism. Historically, this arose from Dirac's work on spin–$\frac{1}{2}$ particles, but can be constructed from invariance under the U(1) gauge group, forming an abelian gauge theory. With the technical problems involved in the renormalisation of this theory solved by Feynman, QED offers the most accurate theory known to science.

The ideas of gauge invariance introduced in QED were generalised to non-abelian gauge groups by Yang and Mills (1954). A theory of the strong interaction was formulated from the work of Gell–Mann and Zweig (1964). This involved interpreting hadrons as bound states of elementary particles, quarks, carrying a new quantum number, colour. A gauge theory describing the interactions of quarks was constructed in analogy to QED; invariance under the $SU(3)_{colour}$ gauge group with force carriers called gluons. This theory is known as QuantumChromoDynamics (QCD). The final piece, came in terms of a theory of the weak interaction. Originating from the Fermi theory of β decay, the ideas of gauge theories and intermediate vector bosons, culminated in the unified electroweak theory of Glashow(1961), Salam(1967) and Weinberg (1968), in terms of the $SU(2)_L \otimes U(1)_Y$ gauge group. However, it was only with the the proof of renormalisation of the electroweak theory by 't Hooft (1971), that gauge theories were adopted as the Standard Model of Particle Physics.

With hindsight, the Standard Model can be completely determined from three requirements,

- specification of the gauge group,

  $$SU(3) \otimes (SU(2)_L \otimes U(1)_Y)\,.$$

  This is the combined gauge group of the strong, weak and electromagnetic interactions. Each force is mediated by a gauge boson; gluons, W and Z bosons and the photon, respectively.

- choice of matter fields in the theory and how they transform under the above gauge group. A minimal choice in the fermion content of the theory consists of three generations of quarks and leptons. These are usually arranged as left–handed doublets and right–handed singlets for the electroweak theory.

$$\begin{pmatrix} u \\ d \end{pmatrix}_L \quad \begin{pmatrix} c \\ s \end{pmatrix}_L \quad \begin{pmatrix} t \\ b \end{pmatrix}_L \quad ; \quad \begin{pmatrix} \nu_e \\ e \end{pmatrix}_L \quad \begin{pmatrix} \nu_\mu \\ \mu \end{pmatrix}_L \quad \begin{pmatrix} \nu_\tau \\ \tau \end{pmatrix}_L$$

$$u_R, d_R \qquad c_R, s_R \qquad t_R, b_R \quad ; \qquad e_R \qquad\quad \mu_R \qquad\quad \tau_R$$

- and the final requirement that all possible renormalisable couplings are included.

With these requirements satisfied, all the information concerning the dynamics of the Standard Model can be contained in a Lagrangian,

$$\mathcal{L}_{SM} = \mathcal{L}_{Gauge} + \mathcal{L}_{Fermion} + \mathcal{L}^{\theta}. \tag{1.1}$$

All the pure gauge dynamics are contained in $\mathcal{L}_{Gauge}$, $\mathcal{L}_{Fermion}$ describes the interactions between the fermion content of the theory and the gauge bosons and $\mathcal{L}^{\theta}$ is a topological term. The full Standard Model Lagrangian is given in Appendix A.

The requirement of renormalisability forbids the inclusion of mass terms, for either the fermions or gauge bosons. This is a major problem, as fermion masses are experimentally observed and it is known that the weak interaction is short ranged, mediated with very heavy gauge bosons. One way of introducing mass terms in a renormalisable way, was introduced by Higgs, [10]. In the simplest case this involves the introduction of a charged scalar (Higgs) doublet, into the particle count,

$$\Phi = \begin{pmatrix} \phi^+ \\ \phi^0 \end{pmatrix}. \tag{1.2}$$

This gives rise to another two terms in the Standard Model Lagrangian, $\mathcal{L}_{Higgs}$ dealing with the dynamics of the scalar fields, including gauge couplings, and $\mathcal{L}_{Yukawa}$ containing all interactions between the scalar Higgs and the fermions in the theory.

Masses are introduced by means of spontaneous symmetry breaking (SSB). The choice of one particular physical vacuum from all possible degenerate ground states breaks the symmetry. This vacuum keeps only a subgroup of the full symmetry, while the Lagrangian itself is still fully invariant under the symmetry transformations. The Higgs mechanism involves the SSB of the electroweak symmetry to the electromagnetic symmetry,

$$SU(2)_L \otimes U(1)_Y \stackrel{\langle\Phi\rangle_0}{\rightarrow} U(1)_{EM}. \tag{1.3}$$

In terms of Standard Model fields, one component of the Higgs obtains a non–zero vacuum expectation value (v.e.v.),

$$\langle\Phi\rangle_0 \equiv \langle 0|\Phi|0\rangle_0 = \begin{pmatrix} 0 \\ \frac{v}{\sqrt{2}} \end{pmatrix}. \tag{1.4}$$

As a result, this component of the Higgs obtains a large mass. In turn, these degrees of freedom are 'eaten' by the electroweak gauge bosons resulting in very massive W and Z bosons and the massless photon. The effect of this symmetry breaking on the Yukawa sector of the Standard Model is to give rise to fermion mass terms.

This concludes the barest outline of the Standard Model. Although there have been many successes, the story is far from complete. There are still many problems with the current theory; 19 free parameters still have to be put in 'by hand', the arbitrary nature of the Higgs sector to introduce fermion masses, no explanation of the mass hierarchy (why the top mass is so much greater than the other quark masses), why there should be just three generations and whether there is some underlying structure to the whole scheme. Further to this is the fundamental question of baryon number violation, leading to a matter/anti-matter asymmetry in the universe, which is related to the phenomenon of CP violation.

It is hoped that study of CP violation can probe the rare parts of the Standard Model, really testing the details and searching for inconsistencies which could perhaps indicate a path beyond the Standard Model. With this as motivation, we give a brief outline of how CP violation enters the Standard Model, then describe a method for studying it.

1.2 CKM Matrix and CP Violation

The arbitrary nature of the fermion masses in the Standard Model is closely tied to the phenomena of CP violation, in that they both arise from the Yukawa term in the Lagrangian.

The most general Yukawa coupling of quarks and leptons with the scalar fields is,

$$\mathcal{L}_{Yukawa} = \lambda^l_{ij}\bar{l}^i_L \Phi e^j_R + \lambda^u_{ij}\bar{Q}^i_L \tilde{\Phi} u^j_R + \lambda^d_{ij}\bar{Q}^i_L \Phi d^j_R + h.c.. \tag{1.5}$$

For all three generations $i, j = 1, 2, 3$, λ_{ij} are the Yukawa couplings, l_L are the left–handed lepton doublets, e_R the right–handed leptons, Q_L the left–handed quark doublets and q_R the right–handed quark singlets. The dual Higgs field is defined as $\tilde{\Phi} = i\tau_2\Phi^*$.

After SSB the Yukawa terms obtain a form reminiscent of a mass term, though at this point the mass matrix is cross-generational (i.e. not diagonal in flavour),

$$\mathcal{L}_{Yukawa} = \bar{e}^i_L m^e_{ij} e^j_R + \bar{u}^i_L m^u_{ij} u^j_R + \bar{d}^i_L m^d_{ij} d^j_R + h.c., \tag{1.6}$$

with $m_{ij} = \lambda_{ij}\frac{v}{\sqrt{2}}$.

However, it is known that any matrix can be diagonalised by two unitary transformations, $M_{diag} = U^\dagger M V$. By rotating the quark fields in the Yukawa terms,

$$u^i_{(L,R)} = U^{(u)ij}_{(L,R)} u'^j_{(L,R)} \ \ ; \ \ d^i_{(L,R)} = U^{(d)ij}_{(L,R)} d'^j_{(L,R)}, \tag{1.7}$$

the quark mass matrices can be diagonalised,

$$U^{(u)\dagger i}_L m^u_{ij} U^{(u)j}_R = \begin{pmatrix} m_u & 0 & 0 \\ 0 & m_c & 0 \\ 0 & 0 & m_t \end{pmatrix} \ ; \ U^{(d)\dagger i}_L m^d_{ij} U^{(d)j}_R = \begin{pmatrix} m_d & 0 & 0 \\ 0 & m_s & 0 \\ 0 & 0 & m_b \end{pmatrix}. \tag{1.8}$$

In this way the Standard Model obtains quark mass terms, $m_i \bar{f}'_i f'_i$, for all quarks, f'_i. These new fields are known as the mass eigenstates of the theory, compared with the weak eigenstates which were the original quark fields.

These rotations of the fields to the mass eigenstates can be carried out in the other sectors of the Standard Model. Of particular interest is the effect on the electroweak sector, governing the weak decays of quarks. Consider, for example a neutral current,

$$J^0_\mu = \bar{u}_i\gamma_\mu(\alpha^u + \beta^u\gamma_5)u_i + \bar{d}_i\gamma_\mu(\alpha^d + \beta^d\gamma_5)d_i + h.c., \tag{1.9}$$

involved in the decays of quarks u_i and d_i of all chiralities. Being diagonal in flavour the neutral currents are clearly unaffected by the rotation to the mass eigenbasis, as the rotation matrices are unitary. This means there are no flavour changing neutral currents at tree level.

Quarks also decay weakly through the emission of charged W bosons. The dynamics of these decays are contained in the charged currents, $J_\mu^{+/-}$. The effect of the transformation of the quark fields on these currents is as follows,

$$J_\mu^+ = \frac{g}{\sqrt{2}} \sum_i \bar{u}_L^i \gamma_\mu d_L^i + h.c. = \frac{g}{\sqrt{2}} \sum_i \bar{u}_L'^i \gamma_\mu V d_L'^i + h.c.. \tag{1.10}$$

The unitary matrix $V = U_L^{(u)\dagger} U_L^{(d)}$ arises from the combination of the rotations on the upper and lower components of the quark doublets. This is known as the Cabibbo-Kobayshi-Maskawa (CKM) quark mixing matrix, [11, 12]. Its matrix elements tell us of the coupling strength of weak quark decays,

$$V = \begin{pmatrix} V_{ud} & V_{us} & V_{ub} \\ V_{cd} & V_{cs} & V_{cb} \\ V_{td} & V_{ts} & V_{tb} \end{pmatrix}. \tag{1.11}$$

This CKM mixing matrix is a unitary 3×3 complex matrix. Generalising for a complex $n \times n$ unitary matrix, there are $2n^2$ free parameters, which the unitarity condition reduces to n^2. This can be reduced further, by $2n - 1$, by exploiting the freedoms to redefine the phase on the $2n$ quark fields, though the matrix is invariant when all quarks are rotated by the same phase. Comparison with an $n \times n$ orthogonal matrix with $n(n-1)/2$ real angles, indicates that a complex unitary matrix can be parameterised in terms of $n(n-1)/2$ real angles and $(n-1)(n-2)/2$ complex phases[1]. For the CKM matrix of a three generation Standard Model, this means a parameterisation in terms of three real angles and one complex phase. It is this complex phase which is the origin of CP violation in the Standard Model.

So why can't the CKM matrix elements be better defined by experiment? One reason is the uncertainty in the mass of the top quark. This plays a crucial role in extracting the CKM matrix elements from experimental measurements. Despite great excitement earlier this year with the publication of ref. [13], quoting

$$m_t = 174 \pm 10 \ {}^{+13}_{-12}\mathrm{GeV}, \tag{1.12}$$

the experimentalists at the CDF detector at Fermilab were very careful to point out this was evidence *for*, not discovery *of* the top quark. Clearly time will ascertain the validity of this result.

[1] $n \geq 3$ for a complex phase

However, the main problem involves theoretical uncertainties in calculating the strong interaction effects on weak matrix elements. These are vital if we are to exploit the full predictive power of the CKM matrix as a probe of the Standard Model. To see this further, the next section offers a parameterisation of the CKM matrix, and outlines a set of steps, including both experimental and theoretical input, which can be used to determine the CKM matrix elements.

1.3 The CKM Matrix and the Wolfenstein Parameterisation

The last section ended with the introduction of the CKM matrix as a means of introducing CP violation in the Standard Model. This, however, goes only a small way into describing the full utility of the CKM matrix. In terms of the Standard Model itself, the CKM matrix contains many of the free parameters, including the poorly known top couplings[2]. It also probes both strong and weak sectors of the theory, covering much of the dynamics of the Standard Model. Further to this, given that many of the processes involving the CKM matrix occur only above tree level, it tests the very quantum nature of the theory and could also give the clues to the existence of new physics.

In attempting to determine the couplings within the CKM matrix, it is possible to parameterise this matrix with three real angles and one complex phase. Many such parameterisations exist. The Particle Data Group, [14], recommend a 'standard' form, because of the simple relations between the parameters and the experimental measurements. Instead, the Wolfenstein parameterisation, [15], only will be given here, because of its useful geometrical representation.

The Wolfenstein parameterisation is based on an expansion in $\lambda = |V_{us}|$, originally founded from empirical observation, and displaying the relative sizes of the couplings,

$$V = \begin{pmatrix} 1-\frac{\lambda^2}{2} & \lambda & A\lambda^3(\rho - i\eta) \\ -\lambda & 1-\frac{\lambda^2}{2} & A\lambda^2 \\ A\lambda^3(1-\rho-i\eta) & -A\lambda^2 & 1 \end{pmatrix} + \mathcal{O}(\lambda^4), \tag{1.13}$$

for real angles λ, A and ρ and phase η representing CP violation contributions. This parameterisation clearly shows the hierarchy of couplings between genera-

[2]accurate determination of CKM matrix elements could also constrain the top mass

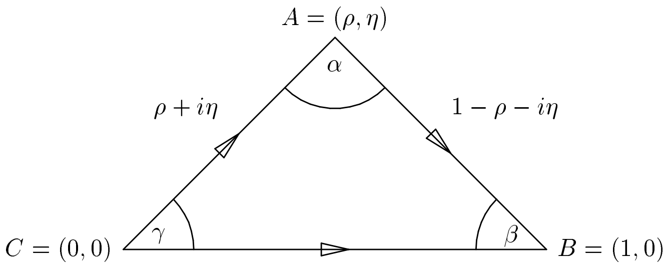

Figure 1.1: The unitarity triangle in the (ρ, η) plane.

tions, largest within one generation and smallest between first and third. Also, all CP violating phases only occur in the couplings of heavy quarks. The utility of this parameterisation becomes clear in the next section, where a simple geometric representation of the contents of the CKM matrix is given in terms of the unitarity triangle.

1.4 The Unitarity Triangle

Unitarity of the CKM matrix offers nine relations between the rows and columns of the matrix. By considering the CKM matrix elements as vectors in the complex plane, these unitarity relations can be described in terms of 'unitarity triangles', the area of which give a measure of CP violation. These triangles offer means to represent the structure of the CKM matrix in a simple geometrical form. This is particularly useful for studying CP violation with the inclusion of much experimental data and theoretical predictions from B and K decays.

The most interesting of these triangles, from a phenomenological point of view, is,

$$V_{ud}V_{ub}^* + V_{cd}V_{cb}^* + V_{td}V_{tb}^* = 0, \tag{1.14}$$

which contains the poorly known V_{ub} and V_{td}. Rescaling each side of this triangle by $|V_{cb}V_{cd}^*| = A\lambda^3$, transforms the unitarity triangle into the (ρ, η) plane, shown in Figure 1.1. Unitarity of this triangle is simply given by the condition,

$$\alpha + \beta + \gamma = 180^o. \tag{1.15}$$

Using this triangle, with the Wolfenstein parameterisation, it is possible to combine experimental and theoretical results to determine values for λ, A, ρ and

η, or at least offer constraints to the values. A typical strategy, [16, 17], for this involves, at least, a five step process,

- parameter λ:
  measured to a good accuracy from K and hyperon decays,

$$\lambda = |V_{us}| = 0.2205 \pm 0.0018. \tag{1.16}$$

- parameter A:
  related to V_{cb}, this can be extracted from the semi–leptonic B decays. Originally measured from inclusive decay processes, an alternative more theoretical approach is to use the formalism of Heavy Quark Effective Theory (HQET) and the non–perturbative calculation of the Isgur–Wise function. Using $|V_{cb}| = 0.044 \pm 0.006$ gives,

$$A = \frac{1}{\lambda^2}|V_{cb}| = 0.90 \pm 0.12. \tag{1.17}$$

In order to determine point $A = (\rho, \eta)$ for a given value of m_t, it is usual to consider at least three experimental measurements, from which it is possible to determine unambiguous solutions for (ρ, η).

- Experimental measurement of $|V_{ub}/V_{cb}|$:
  Measured at ARGUS/CLEO from inclusive semi–leptonic B decays, we take $|V_{ub}/V_{cb}| = 0.085 \pm 0.015$. This defines a circle, centre (0,0),

$$\sqrt{\rho^2 + \eta^2} = \frac{1}{\lambda}\frac{|V_{ub}|}{|V_{cb}|} = 0.39 \pm 0.07. \tag{1.18}$$

- Mixing in neutral kaon system : ϵ:
  CP violation has only been seen in neutral kaon mixing and a measure of this CP violation is given by the parameter ϵ, discussed in more detail in Chapter 3. Experimental measurements from kaon mixing give $|\epsilon| = (2.26 \pm 0.02) \times 10^{-3}$. The theoretical input to this process comes from evaluation of the box diagram, described in Section 3.1. The non–perturbative strong interaction effects of the weak decay are contained in the kaon B-parameter, $B_K = 0.66 \pm 0.08$, calculated in Chapter 3. The result of Equation (3.7), relating the experimentally measured ϵ to terms involving CKM matrix

elements, known factors and the weak matrix elements, defines a hyperbola in (ρ, η) space,

$$|\epsilon| = \frac{G_F^2 M_W^2 f_K^2 m_K}{6\sqrt{2}\pi^2 \Delta m_K} B_K A^2 \lambda^6 \eta \left[x_c\left(\eta_{ct} f_3(x_c, x_t) - \eta_{cc}\right) + \eta_{tt} x_t f_2(x_t) A^2 \lambda^4 (1-\rho)\right]. \quad (1.19)$$

We have used the notation of ref. [18], defining the CP violating parameter in terms of the Wolfenstein parameters, QCD corrections $\eta_{ct}, \eta_{tt}, \eta_{cc}$ and known functions f_2 and f_3.

- Mixing in the B-system : x_d:
  Neutral meson mixing is also observed in the B-system, discussed in Chapter 4, with many similarities to kaon mixing. Experimental input comes from the mixing parameter, $x_d = 0.67 \pm 0.10$. Theoretical input can be obtained from the associated box diagram, Section 4.1, where now the main uncertainty is in the determination of the decay constant, $f_B = 200 \pm 30$ MeV. Expressing the CKM matrix dependence to the mixing parameter in Equation (4.1) in terms of the Wolfenstein parameterisation, defines a circle, centre (1,0),

$$x_d = \tau_B \frac{G_F^2 M_W^2}{6\pi^2} \eta_{QCD} m_B f_B^2 B_B x_t f_2(x_t) A^2 \lambda^6 \left[(1-\rho)^2 + \eta^2\right]. \quad (1.20)$$

These experimental measurements and theoretical predictions can be combined using the geometrical representation of these relations. In principle this could uniquely determine the unitarity triangle from point $A = (\rho, \eta)$ and hence all four parameters of the CKM matrix. Realistically, however, accurate measurements of all these quantities are not attainable. We attempt to show this by plotting the three curves outlined above, including the experimental errors, to show the constraints on the unitarity triangle. Figure 1.2(a) shows the (ρ, η) parameter space for the current experimental and theoretical estimates listed in Table 1.1.

Without further improvements in both theoretical and experimental calculations, only vague predictions can be made about the unitarity triangle. For example, if all the measurements required for the unitarity plot were obtained to an accuracy of 5%, Figure 1.2(b) would be obtained. To sharpen the predictive power of such an analysis several improvements would be welcome.

Experimental Measurements			
$\lvert V_{us}\rvert$	0.2205 ± 0.0018 [18]	$\lvert V_{cb}\rvert$	0.044 ± 0.005 [18]
$\lvert V_{ub}/V_{cb}\rvert$	$0.08 \ \pm 0.02$ [18]		
ϵ	$(2.26 \pm 0.02) \times 10^{-3}$ [53]	x_d	$0.67 \ \pm 0.10$ [67]
m_t	$175 \quad \pm 15$ GeV [13]	m_c	1.4 GeV [53]
M_W	80.2 GeV [53]	G_F	1.17×10^{-5} GeV^{-2} [53]
m_K	0.498 GeV [53]	Δm_K	$3.5 \ \times 10^{-15}$ GeV [53]
f_K	0.161 GeV [53]		
m_B	5.279 GeV [53]	$1/\tau_B$	4.388×10^{-13} GeV [53]
Theoretical Predictions			
B_K	0.66 ± 0.08 (this work)	$f_B\sqrt{B_B}$	0.2 ± 0.03 GeV [16]
η_{cc}	0.82[16]	η_{tt}	0.62 [16]
η_{ct}	0.35 [16]	η_{QCD}	0.55 [16]

Table 1.1: Input values for constraints on the unitarity triangle.

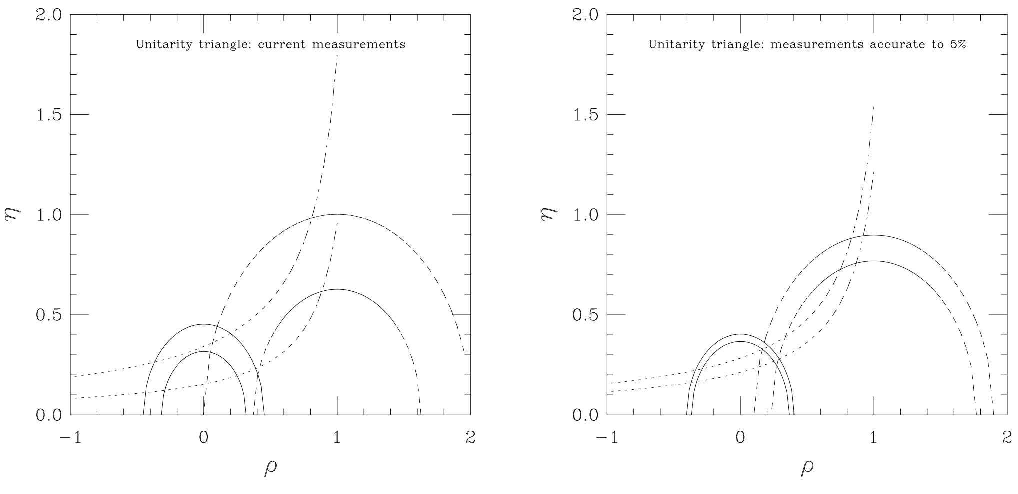

Figure 1.2: Constraints on the unitarity triangle, (a) for present experimental and theoretical measurements and (b) for all measurements accurate to 5%.

1. Experimentally:

    - accurate measurement of the top quark mass would remove a large uncertainty from all the m_t dependence,
    - measurement of mixing in $B_s^0\bar{B}_s^0$ to determine $|V_{td}|$ without precise knowledge of m_t,
    - further study of semi–leptonic B decays (and associated theory) to improve measurements of $|V_{ub}|$ and $|V_{cb}|$,
    - experimental determination of f_B from leptonic B decays,

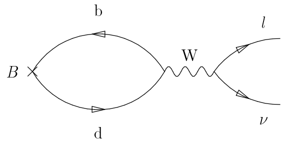

$$\Gamma\left[B \to l\nu\right] = \left[\frac{G_F^2 m_l^2 m_B}{8\pi}\eta_{em}\left(1-\frac{m_l^2}{m_B^2}\right)\right] f_B^2|V_{ub}|^2.$$

    - measurement of direct CP violation in various kaon decays,
    - study of CP asymmetries in B-decays, allowing for direct determination of angle of unitarity triangle, free from theoretical uncertainties.

The continued huge experimental effort focused on the above experimental improvements, will undoubtedly shed a good deal of light on the quark mixing matrix and CP violation in coming years. This will be further strengthened by the arrival of dedicated B-factories, producing the necessary luminosities required for study of some of the more elusive decay modes.

2. Theoretically:

    - improved calculations of B_K,
    - f_B and B_B.

In studying CP violation and the CKM matrix, we are probing the weak decays of quarks. However, quarks also interact strongly and what is needed is a better understanding of these strong interaction effects. The non–perturbative nature of these calculations is the main stumbling block to an accurate determination of these quantities. At present Lattice QCD, offers the best method by which to attack these calculations. Its utility

> and possibilities have been demonstrated by successes in realms of light quark spectroscopy and hadronic matrix elements with recent developments opening up new possibilities in heavy quark physics.

The Standard Model of Particle Physics has been very successful in describing a huge variety of experimental data. In this chapter we introduced this model in terms of gauge theories. We focus on the phenomenon of CP violation, introduced into the Standard Model primarily through the CKM quark mixing matrix. This was developed into a strategy for the determination of the CKM matrix elements, with the main uncertainties involved in the theoretical calculation of weak matrix elements. In Chapter 2 we outline a method to attempt these non–perturbative calculations, Lattice QCD, in Chapter 3 we continue with calculation of B_K, and in Chapter 4 f_B, Chapter 4 mentioned above. The last chapter, Chapter 5, involves the spectroscopy of systems containing one heavy quark.

Chapter 2

Lattice Field Theory

The Standard Model of Particle Physics has achieved great success in describing the interactions of elementary particles and classifying the 'zoo' of particles discovered from accelerator experiments. In terms of the strong force, the success in understanding the dynamics of this theory is only partial. The theory describes the interactions only of the constituent particles, quarks and gluons, but what is of primary interest is a description of the low energy behaviour of the particles, hadrons, existing in nature and studied by experiment. The standard field theoretic techniques of perturbation theory, relying on the asymptotic freedom of the strong interaction, can only accurately investigate the high energy, short distance physics. Clearly this is a problem, when many quantities of interest, such as hadronic masses and matrix elements, are inherently non–perturbative. It was Wilson, [19], who suggested a possible 'first principles solution' to the strong interaction problem.

His solution was a non–perturbative formulation of a field theory on a discrete space–time lattice. In formulating a field theory on a lattice, the finite lattice spacing serves as an ultraviolet regulator to cut–off the high energy behaviour, which then requires renormalisation group techniques to regain the continuum physics. Further to this, it was possible to take full advantage of the machinery of statistical mechanics which is well developed for study of systems with high numbers of micro–degrees of freedom to obtain macroscopic predictions. In tackling the strong interaction problem this way, the theory simulated is 'true' QCD containing all the physics of the continuum theory and not some model approximation.

As was mentioned, one of the main aims of Lattice QCD is the calculation of the strong interaction effects on hadronic matrix elements[1]. The standard way of calculating this is in the Path Integral formalism, [20], which in Minkowski space involves the following integral,

$$\langle \mathcal{O} \rangle_M = \frac{\int \mathcal{D}U\mathcal{D}\bar{\psi}\mathcal{D}\psi \, \mathcal{O} e^{iS_M[U,\bar{\psi},\psi]}}{\int \mathcal{D}U\mathcal{D}\bar{\psi}\mathcal{D}\psi \, e^{iS_M[U,\bar{\psi},\psi]}}. \tag{2.1}$$

Numerically this integral is not well defined, due to the complex exponent. However, Wick rotating to Euclidean space recovers a more useful form,

$$\langle \mathcal{O} \rangle_E = \frac{\int \mathcal{D}U\mathcal{D}\bar{\psi}\mathcal{D}\psi \, \mathcal{O} e^{-S_E[U,\bar{\psi},\psi]}}{\int \mathcal{D}U\mathcal{D}\bar{\psi}\mathcal{D}\psi \, e^{-S_E[U,\bar{\psi},\psi]}}, \tag{2.2}$$

and Dirac matrices with the following properties,

$$\{\gamma^E_\mu, \gamma^E_\nu\} = 2\delta_{\mu\nu} \qquad \text{and} \qquad \left(\gamma^E_\mu\right)^\dagger = \gamma^E_\mu. \tag{2.3}$$

In everything that follows, Euclidean space will be assumed, and 'E' labels dropped. In fact there will be no need to return to Minkowski space, as all quantities of interest can be extracted directly from Euclidean correlators.

In general, a Lattice Field Theory (LFT) is required to satisfy the same conditions of gauge invariance and renormalisability as a continuum field theory. Further to this, the LFT is required to recover the continuum form as the lattice spacing is removed. With this in mind this chapter outlines the discretisation of spacetime, the construction of a lattice version of the full QCD action and then some of the techniques needed for numerical simulation of a field theory. A simple example of the generic lattice calculation is given at the end.

2.1 Free Fermion Action

With the aim of introducing the basic ingredients to formulate a field theory on a discrete lattice, the free fermion action is considered. In Euclidean space, the Dirac action for a free fermion has the following form,

$$S = \int d^4x \, \bar{\psi}(x)(\gamma_\mu \partial^\mu + m)\psi(x), \tag{2.4}$$

where for simplicity and clarity all spin, α, colour, a and flavour, f, indices have been omitted, $\psi(x) = \psi^f(x)^a_\alpha$.

[1]in this thesis we focus on a lattice formulation of the strong force, described by QCD.

To obtain a lattice version of this action it is necessary to discretise spacetime. This involves replacing the continuous spacetime variables, x_μ, with the dimensionless, n_μ, where n_μ is an integer, and dimensionful parameter, a, the lattice spacing. Then the quantum field, $\psi(x)$, is replaced by $\psi(n)$ on a lattice site, representing the field over some small region of space. Often in numerical calculations it is useful to work with a dimensionless theory. This can be constructed by rescaling all quantities by powers[2] of the only dimensionful scale available to the theory; the lattice spacing.

$$x_\mu \to a n_\mu \tag{2.5}$$

$$\int d^4x \to a^4 \sum_n \tag{2.6}$$

$$\psi(x) \to a^{-\frac{3}{2}} \psi(n) \tag{2.7}$$

$$m \to a^{-1} m. \tag{2.8}$$

In constructing the discrete version of the derivative, many possible choices exist. The simplest case which obeys the requirement of anti-hermiticity is the symmetric difference,

$$\partial_\mu \psi(x) \to \frac{1}{2a} \left(\psi(n+\hat{\mu}) - \psi(n-\hat{\mu}) \right), \tag{2.9}$$

which ensure that quarks and anti-quarks propagate in the same manner. Here we use $\hat{\mu}$ as the unit vector in the μth direction, as opposed to μ the Lorentz index.

With such a definition, the following naive fermion action is obtained,

$$S_{NF} = \sum_n \left[\sum_\mu \Big(\bar{\psi}(n)\gamma_\mu(\psi(n+\hat{\mu}) - \psi(n-\hat{\mu})) \Big) + m\bar{\psi}(n)\psi(n) \right] \tag{2.10}$$

$$= \sum_{n,m} \bar{\psi}(n) M(n,m) \psi(m). \tag{2.11}$$

In writing the action as a term quadratic in quark fields, with some fermion matrix, $M(n,m)$, it is suggestive of the continuum formalism from which the free propagator can be obtained. Similarly, a free lattice propagator can be defined in terms of the two point correlation function,

$$\langle \psi(n)\bar{\psi}(m) \rangle = G(n,m) = M^{-1}(n,m). \tag{2.12}$$

[2]the power is given by the engineering dimensions of the quantity

A convenient way to determine this is in momentum space. With the field theory formulated on a discrete spacetime lattice, momentum space is continuous, periodic and restricted to the Brillouin Zone $\hat{k} \in [-\pi, \pi]$.[3] In this way it is clear that introducing a discrete lattice has regulated the field theory by a momentum cut–off. The momentum space representation of the quark fields, in terms of dimensionless momentum $\hat{k}$, are,

$$\psi(n) = \int_{-\pi}^{\pi} \frac{d^4\hat{k}}{(2\pi)^4}\, e^{-i\hat{k}\cdot n}\psi(\hat{k}) \quad ; \quad \bar{\psi}(n) = \int_{-\pi}^{\pi} \frac{d^4\hat{k}}{(2\pi)^4}\, e^{i\hat{k}\cdot n}\bar{\psi}(\hat{k}), \tag{2.13}$$

from which the free propagator in lattice units is,

$$G(n,m) = \int_{-\pi}^{\pi} \frac{d^4\hat{k}}{(2\pi)^4}\, e^{-i\hat{k}\cdot(n-m)} \frac{-i\sum_\mu \gamma_\mu \sin\hat{k} + m}{\sum_\mu \sin^2\hat{k} + m^2}. \tag{2.14}$$

The naive continuum limit of this is obtained by rescaling all quantities by appropriate factors of a and then taking the $a \to 0$ limit,

$$\langle\psi(x)\bar{\psi}(y)\rangle = \lim_{a\to 0}\frac{1}{a^3}G(\frac{x}{a},\frac{y}{a}) = \int_{-\pi/a}^{\pi/a} \frac{d^4k}{(2\pi)^4}\, e^{-ik\cdot(x-y)} \frac{-i\not{s} + m}{s^2 + m^2}, \tag{2.15}$$

where, $s = \frac{1}{a}\sin k_\mu a$.

For finite k, $s_\mu \to k_\mu$ in the $a \to 0$ limit, and the free lattice propagator regains the usual continuum formulation of the Dirac action,

$$G(k) \to \frac{-i\not{k} + m}{k^2 + m^2}, \tag{2.16}$$

corresponding to a physical particle with mass m. However, with this formulation of the free quark propagator, the naive continuum limit is also regained for momenta in the neighborhood of $k_\mu \approx \pm\pi/a$, at the edges of the Brillouin Zone.

These extra contributions correspond in physical terms to mass degenerate fermions, a 'doubler' in each dimension, i.e. 2^4 fermions in all. This is the infamous 'doubling problem' for naive fermions on the lattice. Clearly no such degenerate fermions are seen in nature. Fortunately, there are ways around this problem, but as always there must be some compromise. The two main ways used in practical Lattice QCD calculations are the Kogut-Susskind formulation, [21, 22], using 'staggered' fermions, or the one proposed by Wilson, [23]. It is this latter approach which is followed in all the work carried out in this thesis, with a review of staggered fermions given in ref. [24].

[3] this assumes translational invariance and infinite spatial volume.

With an outline of the procedure to discretise spacetime and construct a naive free fermion lattice action, the next section describes the Wilson formulation to overcome fermion doubling.

2.2 Wilson Fermions

The formulation of Lattice QCD used in this study is based on the Wilson action. The idea behind this lies in the fact that the lattice action is only required to regain the continuum in the limit $a \to 0$, leaving considerable choice in the definition of a lattice action. Wilson, [23], exploited this ambiguity by adding irrelevant operators, ones which vanish in the continuum limit, to reduce the fermion content of the lattice theory to one fermion.

Wilson's choice was to add a second derivative term to the naive action,

$$S_F = S_{NF} + S_W, \tag{2.17}$$

where the Wilson term is,

$$S_W = -\frac{ar}{2}\sum_n \bar{\psi}(n)\Delta\psi(n), \tag{2.18}$$

with Wilson coefficient, r, and Δ is the lattice discretisation of the second derivative,

$$\Delta\psi(n) = \sum_\mu \frac{1}{a^2}\left(\psi(n+\hat{\mu}) - 2\psi(n) + \psi(n-\hat{\mu})\right). \tag{2.19}$$

This gives for free fermions,

$$\begin{aligned} S_F = &\sum_n (m+4r)\,\bar{\psi}(n)\psi(n) \\ &-\sum_{n,\mu}\bar{\psi}(n)\{\left(\frac{r-\gamma_\mu}{2}\right)\psi(n+\hat{\mu}) + \left(\frac{r+\gamma_\mu}{2}\right)\psi(n-\hat{\mu})\} && (2.20) \\ = &\sum_n \bar{\psi}(n)\psi(n) \\ &-\sum_{n,\mu}\kappa\bar{\psi}(n)\{(r-\gamma_\mu)\psi(n+\hat{\mu}) + (r+\gamma_\mu)\psi(n-\hat{\mu})\}. && (2.21) \end{aligned}$$

In passing to Equation (2.21) we have redefined the quark fields,

$$\psi \to \frac{\psi}{\sqrt{m+4r}} = \psi\sqrt{2\kappa}, \tag{2.22}$$

in terms of the 'hopping parameter', κ, which measures the 'strength' of nearest neighbour interactions in the lattice theory. In practical lattice calculations this is the input parameter which controls the bare mass of the quarks used and will be referred to frequently in the following.

The effect of adding this irrelevant operator is to introduce an explicit mass term which breaks the degeneracy of the quark masses. In terms of the free quark propagator, the naive continuum limit is modified to,

$$\langle\psi(x)\bar{\psi}(y)\rangle = \lim_{a\to 0}\frac{1}{a^3}G(\frac{x}{a},\frac{y}{a}) = \int_{-\pi/a}^{\pi/a}\frac{d^4k}{(2\pi)^4}\,e^{-ik\cdot(x-y)}\frac{-i\not{s}+M(k)}{s^2+M(k)^2}, \qquad (2.23)$$

where $M(k) = m + 2r/a\sum_\mu \sin^2 k_\mu a/2$. In the $a \to 0$ limit one quark retains its continuum mass, $M(k) \to m$, while the others obtain an infinite mass, $\mathcal{O}(r/a)$, and decouple from the theory. However, this term also breaks chiral symmetry in the lattice theory even in the $m \to 0$ limit, thus leaving Wilson fermions less useful for calculations which test the chiral symmetry of QCD, compared with the staggered formulation. In the Wilson formulation this hard broken chiral symmetry is accepted in preference to a multi–fermion interpretation required with the staggered fermion approach. However, it will be seen later, (Section 2.8), that it is possible to regain this chiral limit. In fact, Neilson and Ninomiya showed in [25] that this is a fundamental problem with a lattice regularisation (the No Go theorem), in that it is impossible to have a local fermion action while retaining full chiral symmetry and avoiding the problem of fermion doublers.

The final part in discretising the fermionic part of the Path Integral is the definition of the fermionic measure. A formal definition is,

$$\mathcal{D}\bar{\psi}\,\mathcal{D}\psi = \prod_{n,a} d\bar{\psi}^a(n)\,\prod_{m,b} d\psi^b(m), \qquad (2.24)$$

where the sum is over all lattice sites and all quantum numbers, a, b (colour, spin, flavour). These integrals of fermionic fields are in terms of anti–commuting (Grassman) variables which obey the Grassman algebra and as such have special integration rules. Consider a set of Grassman fields, $\{\eta_i\}$, with $\{\eta_i, \eta_j\} = 0$. The integration rules for these are,

$$\int d\eta_i = 0 \quad ; \quad \int d\eta_i\eta_i = 1. \qquad (2.25)$$

With the properties of Grassman variables outlined, the following integrals of particular interest are included,

$$\int \mathcal{D}\bar{\psi}\mathcal{D}\psi \exp\left(-\sum_{k,l}\bar{\eta}_k A_{kl}\eta_l\right) = \det A \tag{2.26}$$

and

$$\int \mathcal{D}\bar{\psi}\mathcal{D}\psi \eta_i \bar{\eta}_j \exp\left(-\sum_{k,l}\bar{\eta}_k A_{kl}\eta_l\right) = (\det A)\, A^{-1}_{ij}. \tag{2.27}$$

The introduction of the Wilson term reduces the fermion content of the Lattice QCD to one, though at the expense of chiral symmetry. This, with the definition of the fermion measure, completes the construction of a free fermion action in Lattice QCD, with quark masses characterised by a free parameter, κ. However the real utility of Lattice QCD arises from calculations of an interacting field theory, with the inclusion of gauge fields.

2.3 Gauge Fields

The requirement of local gauge invariance in continuum field theories introduces the concept of gauge fields into the theory to correct the transformation properties of the action. This gauge symmetry manifests itself in the invariance of the action under the following local transformations of quark fields,

$$\psi(x) \to g(x)\psi(x) \quad ; \quad \bar{\psi}(x) \to \bar{\psi}(x)g^{-1}(x), \tag{2.28}$$

where $g(x)$ are local transformations belonging to some gauge group $\mathcal{G}$.

Exactly the same is required for a lattice gauge theory. However, the free fermion action defined earlier contains non–local quark bilinear terms which clearly are not invariant under such a gauge transformation.

In the continuum this problem was overcome by the introduction of gauge fields and construction of a covariant derivative from the simple derivative of the Dirac action. The continuum gauge fields transform as follows,

$$A_\mu(x) \to g(x)A_\mu(x)g^{-1}(x) - \frac{i}{g_0}g(x)\partial_\mu g^{-1}(x), \tag{2.29}$$

where g_0 is the bare gauge coupling parameter of the theory. With the success of this procedure in the continuum, it seems sensible to attempt the same for a lattice field theory. However, introducing gauge fields, $A_\mu(n)$ say, on the lattice sites does not remove the problem of gauge invariance. It took Wilson, [19], to formulate a covariant lattice gauge theory with the gauge fields represented on the links between sites. These links are members of a compact Lie Group compared with to elements of the Lie Algebra.

Again continuum field theory hints at what to use to correct the behaviour under gauge transformations. What is needed is a term, $U(x,y)$, such that,

$$\bar{\psi}(x)U(x,y)\psi(y) \rightarrow \bar{\psi}(x)U(x,y)\psi(y), \tag{2.30}$$

is gauge invariant. This term exists and is known as a Schwinger line integral,

$$U(x,y) = \mathcal{P}e^{ig_0 \int_y^x A_\mu(z)dz}, \tag{2.31}$$

which corresponds to the phase picked up by a fermion propagating in the presence of a gauge field.

In constructing a discrete version of Equation (2.31) for a lattice field theory, a natural definition is obtained in terms of the link variables,

$$U(n, n+\hat{\mu}) \equiv U_\mu(n) \simeq e^{ig_0 A_\mu(n+\frac{\hat{\mu}}{2})} \in SU(N), \tag{2.32}$$

corresponding to the 'hop' of a quark field from one lattice site to the next, along direction μ. The path ordering prescription in the continuum leads to the following identity,

$$U_{-\mu}(n+\hat{\mu}) = U_\mu(n)^\dagger, \tag{2.33}$$

for traversing a link in the opposite direction. The transformation properties of a link, following from the transformations of gauge field in Equation (2.29), are,

$$U_\mu(n) \rightarrow g(n)U_\mu(n)g^\dagger(n+\hat{\mu}). \tag{2.34}$$

With this in mind, it is now possible to construct a gauge invariant lattice action, by joining up the point–split quark bilinears, using the appropriate link variables. This gives the Wilson action,

$$\begin{aligned} S_W = \sum_n (m+4r)\,\bar{\psi}(n)\psi(n) - \sum_{n,\mu}\bar{\psi}(n)\Bigg[\left(\frac{r-\gamma_\mu}{2}\right)U_\mu(n)\psi(n+\hat{\mu})+ \\ \left(\frac{r+\gamma_\mu}{2}\right)U_\mu^\dagger(n-\hat{\mu})\psi(n-\hat{\mu})\Bigg]. \end{aligned} \tag{2.35}$$

In doing this, not only has the theory been made gauge invariant, but also interactions between quarks and gauge fields have been naturally included. In

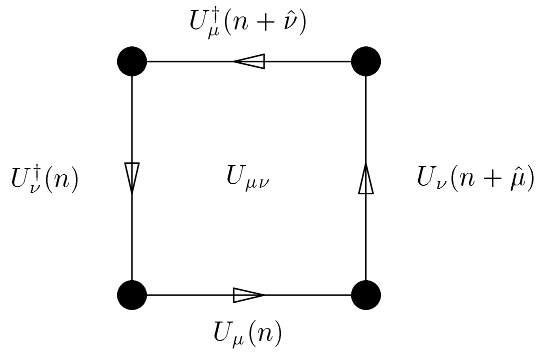

Figure 2.1: An elementary plaquette.

effect the combination of the links with the simple difference derivative has formed a lattice covariant derivative and the theory now resembles full interacting QCD.

To see this more clearly, the naive continuum limit can be taken as before. In the case of the link variables, this involves,

$$U_\mu(n) \equiv e^{iag_0 A_\mu(x)} \approx 1 + iag_0 A_\mu(x) + \mathcal{O}(a^2), \tag{2.36}$$

which, when included with the naive continuum limit of the Wilson action, results in,

$$S_W = \int d^4x\, \bar{\psi}(x) \left(\gamma_\mu \left(\partial_\mu + ig_0 A_\mu\right) + m\right) \psi(x) + \mathcal{O}(a) \tag{2.37}$$

Having now introduced gauge fields into the theory, the full QCD action requires a kinetic term for these gauge fields. The continuum definition of the pure gauge action is,

$$S_G^{cont} = \frac{1}{4} \int d^4x\, F^a_{\mu\nu} F^a_{\mu\nu}. \tag{2.38}$$

In looking for a lattice version of this, a gauge invariant quantity dependent only on link variables, $U_\mu(n)$, is sought. The simplest and most local gauge invariant object satisfying these criteria is known as a plaquette, the path ordered product of links shown in Figure 2.1,

$$U_{\mu\nu}(n) = U_\mu(n) U_\nu(n+\hat{\mu}) U_\mu^\dagger(n+\hat{\nu}) U_\nu^\dagger(n). \tag{2.39}$$

It is also useful to consider the naive continuum limit of a plaquette, using the definition (2.36) earlier and taking care to consider the non–Abelian nature of the gauge fields for QCD. This gives,

$$U_{\mu\nu} = 1 + ia^2 g_0 F_{\mu\nu} - \frac{g_0^2}{2} a^4 (F_{\mu\nu})^2 + \mathcal{O}(a^5). \tag{2.40}$$

Clearly the plaquette has a suitable continuum limit to be used for a lattice version of the gauge action. Gauge invariance is obtained in the continuum by taking the trace of the field tensor term. Taking the trace of the real part of a plaquette gives a definition of the pure gauge lattice action,

$$S_G^{latt} = -\beta \sum_{\mu\nu} \frac{Tr}{2N_c} \left(U_{\mu\nu} + U_{\mu\nu}^\dagger \right) \tag{2.41}$$

$$= \frac{1}{4} \int d^4x \, F_{\mu\nu}^a F_{\mu\nu}^a + \mathcal{O}(a^2), \tag{2.42}$$

where $\beta = 6/g_0^2$ for QCD, defines the parameter in lattice field theory for the bare coupling constant, g_0.

The final ingredient in this recipe for a lattice field theory, is a definition for a gauge invariant measure,

$$\mathcal{D}U = \prod_{n,\mu} dU_\mu(n), \tag{2.43}$$

where $dU_\mu(n)$ is the invariant Haar measure, with integration over all sites and directions, [26]. Again, the utility of defining the theory on the lattice in terms of members of the (compact) Lie group arises. For a lattice field theory there is no need to fix a gauge or introduce ghost fields, though these will be mentioned later with reference to other issues of lattice field theory.

In summary, the Wilson action for Lattice QCD is,

$$S_{QCD} = S_G[U] + S_W[U, \psi, \bar{\psi}] \tag{2.44}$$

$$S_G = -\frac{\beta}{6} \sum_{\mu\nu} Tr \left(U_{\mu\nu} + U_{\mu\nu}^\dagger \right) \tag{2.45}$$

$$S_W = \sum_n (m + 4r) \bar{\psi}(n)\psi(n) - \sum_{n,\mu} \bar{\psi}(n) \left[\left(\frac{r - \gamma_\mu}{2} \right) U_\mu(n)\psi(n + \hat{\mu}) + \left(\frac{r + \gamma_\mu}{2} \right) U_\mu^\dagger(n - \hat{\mu})\psi(n - \hat{\mu}) \right]. \tag{2.46}$$

Here, in principle at least, is the basis for a non–perturbative formulation of QCD, offering first principles calculation of the effects of the strong interaction. The practical application of this formulation is best dealt with by large numerical simulation, discussed in the following sections.

2.4 Improvement

In an attempt to reduce the $\mathcal{O}(a)$ systematic errors in lattice calculations without significant computational overhead, Symanzik, [27] and then Sheikholeslami and Wohlert, [28], outlined a programme of theoretical improvement to the lattice action. Looking at the naive continuum limit of the Wilson and gauge actions, as defined earlier in Sections 2.2 and 2.3,

$$S_G \to \frac{1}{4}\int d^4x\, F^a_{\mu\nu}F^a_{\mu\nu} + \mathcal{O}(a^2) \tag{2.47}$$

$$S_W \to \int d^4x\, \bar{\psi}\gamma_\mu\left(\partial_\mu + ig_0 A_\mu\right)\psi\, + \mathcal{O}(a). \tag{2.48}$$

The gauge action is automatically improved to $\mathcal{O}(a^2)$, with gauge symmetry protecting this improvement. However, the Wilson action has $\mathcal{O}(a)$ corrections to the continuum. For some matrix elements this is a significant effect, in particular when simulations with heavy quarks are performed.

Sheikholeslami and Wohlert proposed the exploitation of the flexibility in the choice of the discretisation of the fermion action and include extra irrelevant operators which exactly cancel the $\mathcal{O}(a)$ terms in the original Wilson action,

$$S^I_{QCD} = S_G + S_W + S_{IF}. \tag{2.49}$$

The fermion action improvement term, S_{IF}, in this study was of the form,

$$S_{IF} = \sum_n -\frac{ira}{4}\bar{\psi}(n)\sigma_{\mu\nu}F_{\mu\nu}\psi(n). \tag{2.50}$$

This improvement term, called SW or 'Clover' improvement, due to the shape of the lattice field tensor in terms of plaquettes, Figure 2.2, corrects the classical fermion action to $\mathcal{O}(a^2)$, but quantum corrections introduce terms of $\mathcal{O}(g_0^2 a)$, [29]. The added advantage of this choice of improvement term is that it only couples quarks locally. This offers improvement which can be easily incorporated in the numerical calculation of quark propagators, Section 2.5.2, without greatly increasing the computational effort.

It is also necessary to consider the effect of this improvement on the matrix elements of operators. Another way of introducing the improvement is as a transformation of quark fields, such as,

$$\psi \to \left(1 - \frac{ra}{2}\overrightarrow{\not{\Delta}}\right)\psi \tag{2.51}$$

$$\bar{\psi} \to \bar{\psi}\left(1 + \frac{ra}{2}\overleftarrow{\not{\Delta}}\right), \tag{2.52}$$

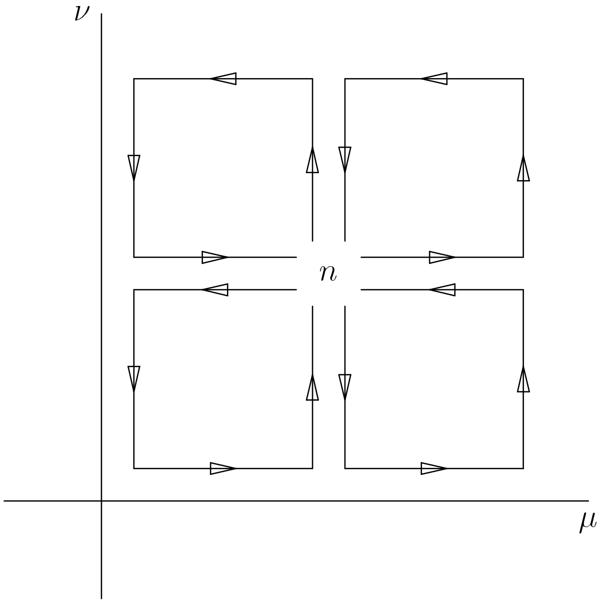

Figure 2.2: Contributions to field tensor for 'Clover' improvement.

with appropriate discretisation of lattice covariant derivative, Δ. It has been shown, [29], that the effect of these rotation of the quark fields is to improve the operator matrix elements to $\mathcal{O}(g_0^2 a)$. It should be noted that when matching to the continuum, the renormalisation constants for these improved operators are now different from those obtained from matching unimproved operators.

Throughout this study, the SW action is used. The effect of this improvement is one of the motivations in studying many of the quantities already calculated with Wilson fermions.

2.5 Numerical Techniques

Much time and effort in lattice field theory is spent in the numerical application of a field theory discretised on a finite lattice. In particular, the calculation of the expectation values of multi–local operators, $\mathcal{O}(x_1, x_2, \ldots)$, by means of a Euclidean Path Integral of the type,

$$\langle \mathcal{O} \rangle = \frac{1}{Z} \int \mathcal{D}U \mathcal{D}\bar{\psi} \mathcal{D}\psi \, \mathcal{O} e^{-S_G[U] - S_F[U,\bar{\psi},\psi]} \tag{2.53}$$

$$Z = \int \mathcal{D}U \mathcal{D}\bar{\psi} \mathcal{D}\psi \, e^{-S_G[U] - S_F[U,\bar{\psi},\psi]}. \tag{2.54}$$

This integral is complicated by the fact that fermion fields are anticommuting fields, which follow the rules for Grassman integration outlined in Section 2.2. To begin, the numerical calculation of a purely bosonic path integral is outlined,

$$\langle \mathcal{O} \rangle = \frac{1}{Z} \int \mathcal{D}U \, \mathcal{O} e^{-S_G[U]}, \tag{2.55}$$

and then a procedure for including fermions is mentioned.

Before attempting any sort of numerical integral, the dimension of the system must be made finite, which in the case of Lattice QCD involves simulating in a box of size $N_s^3 \times N_t$ lattice points[4]. Periodic boundary conditions are imposed on the lattice boundary, though, for technical reasons, anti–periodic boundary conditions are applied in the time direction. The physical effect of a spacetime lattice with finite extent is the introduction of an infrared red cutoff, in addition to the ultraviolet cutoff introduced at finite lattice spacing. For these reasons it is only possible to study phenomena with length scales large compared to the lattice spacing but short compared to the lattice size. Clearly, the lattice parameters must be chosen carefully, to minimise any systematic error from these compromises required in the light of finite computing resources.

2.5.1 Monte Carlo Methods

Clearly, it is impossible for an integral such as Equation (2.55) to be calculated numerically using the traditional techniques, due to the very large dimensionality of the integral[5]. Instead it is necessary to turn to statistical methods to calculate the expectation value as an ensemble average using some kind of Monte Carlo, (MC), integration method.

A straight forward MC application to the integral would be extremely inefficient because the action, $S[U]$, varies widely over the possible configurations[6]. However, the algorithm is made much more efficient if it can choose the configurations which contribute most, a procedure called 'importance sampling'. In particular if the configurations are chosen with probability,

$$P_{eq} \propto e^{-S_G[U]}, \tag{2.56}$$

[4]corresponding physical volume $V = (N_s a)^3 \times (N_t a)$.
[5]a numerical integration at every lattice site, for every direction and colour index.
[6]by configuration we mean the background fields, U, at all points on the lattice.

then the expectation value of the operator is estimated by an ensemble average,

$$\langle \mathcal{O} \rangle = \frac{1}{Z} \int \mathcal{D}U \, \mathcal{O} e^{-S_G[U]} \approx \frac{1}{N} \sum_{i=1}^{N} \mathcal{O} \left[\{U_i\} \right]. \tag{2.57}$$

This ensemble average is calculated over $\{U_i\}$, a set of N independent configurations chosen with the appropriate probability. The error of the ensemble average approximation is of the order $1/\sqrt{N}$. It is useful to think of these configurations as elements of some Markov process, which constructs a configuration from the previous, with the correct probability. Many such algorithms exist, though an efficient one would quickly sample the configuration space, thus generating independent configurations in the minimum of computer time, while limiting the amount of systematic error introduced in producing the next element. However, there is a constraint on the algorithm, in that it must satisfy a condition called detailed balance. This ensures the Markov process forces the configuration towards equilibrium with each step. Detailed balance requires the transition probability, P, from one configuration, C, to the next, C', to satisfy,

$$e^{-S[C]} P(C \to C') = e^{-S[C']} P(C' \to C). \tag{2.58}$$

The simplest algorithm satisfying detailed balance and selecting configurations with the appropriate probability was suggested by Metropolis, [30]. The idea behind it is as follows,

- suggest a change to a configuration, $C \to C'$,
- accept this change if,

  $$e^{-S[C']} > e^{-S[C]},$$

  change reduces the action,
- also accept this change if, for some random number, $r \in [0, 1]$,

  $$\frac{e^{-S(C')}}{e^{-S(C)}} \geq r,$$

  where this stage allows some deviation from the minimum action path, corresponding to quantum fluctuations,
- reject change otherwise.

A 'sweep' of the algorithm consists of the application of this update procedure at every lattice site. Sufficiently large numbers of sweeps are required to obtain a configuration in 'thermal' equilibrium on which the ensemble average can be based. This ensures that the system has no memory of its initial state and that a fully equilibrated configuration has the probability P_{eq}.

This algorithm, however, is not without its problems. Updating single variables at each step is very inefficient[7]. Similar inefficiencies exist for a single variable update of a widely non–local action[8]. In addition, the fact that we are treating the field theory as a statistical system results in the efficiency of the algorithm being effected by the choice of bare parameters. Near the continuum limit large fluctuations over all length scales result in critical slowing down and the algorithm has difficulty attaining an equilibrated configuration.

There is another class of algorithms, including the Langevin, Molecular Dynamic and Hybrid, which allow updates on all variables at one time and which are also efficient with non–local actions. These are based on considering the quantum field theory as a classical statistical mechanics system with four space dimensions. The dynamics of this system are governed by an associated Hamiltonian with the evolution of the system determined by numerically integrating out the equations of motion over some classical trajectory. Such algorithms progress very fast through configuration space, but suffer from a systematic error due to a finite step size required for numerical integration of the equations of motion.

In an attempt to overcome the problems associated with these two classes of algorithms, the Hybrid Monte Carlo algorithm was proposed by the authors of [31]. This algorithm contains all the advantages of the global update and non–local actions of Molecular Dynamics type, with the lack of systematic error of the Metropolis algorithm.

The above algorithms work well for MC integration over bosonic fields, however, integration over Grassman fields, as needed for the Path Integral with fermions, causes many problems. The standard approach to this problem is to use the properties of Grassman integration and analytically evaluate the fermionic

[7]cluster algorithms exist which update many sites, though these suffer from reduced acceptance rates, due to increased changes in the action.

[8]many lattice points must be considered for each update.

parts of the Path Integral,

$$\langle \mathcal{O} \rangle = \frac{1}{Z} \int \mathcal{D}U \mathcal{D}\bar{\psi} \mathcal{D}\psi \, \mathcal{O} e^{-S_G[U] - \bar{\psi} M[U] \psi} \tag{2.59}$$

$$= \frac{1}{Z} \int \mathcal{D}U \, \det\left(M[U]\right) \tilde{\mathcal{O}} \, e^{-S_G[U]}. \tag{2.60}$$

To obtain Equation (2.60) from integrating over fermion fields, Wick's Theorem has been used to contract pairs of quark fields to form propagators,

$$\psi(n)^\alpha_a \bar{\psi}(m)^\beta_b \equiv S(n,m)^{\alpha\beta}_{ab} = \left(M[U]^{-1}_{n,m} \right)^{\alpha\beta}_{ab}. \tag{2.61}$$

This results in a form of $\tilde{\mathcal{O}}$ which contains only traces over quark propagators and the relevant spin structure.

This analytic integration in principle leaves a form suitable for MC methods. The non–local determinant, $\det M[U]$, however, causes a huge problem numerically, perhaps the largest facing Lattice QCD at the present. Algorithms exist, such as pseudo-fermionic, which tackle this determinant directly as an integration over extra bosonic fields, though still the computational overhead is high. A more common approach, and the one followed in this work, is to simply set the determinant equal to a constant. This is the infamous 'quenched' or valence approximation of Lattice QCD which corresponds to generating gauge configurations without internal quark loops. Clearly this is a drastic approximation and cannot be fully understood until sufficient 'full' QCD calculations have been undertaken (this is discussed further in Section 2.10).

In principle, MC integration can be used to calculate the background gauge fields required for the first step in evaluating non–perturbative matrix elements in the Path Integral formalism. In an attempt to deal with fermionic fields, part of the Path Integral was calculated analytically, leaving an integral over functions of quark propagators and Dirac matrices only. The next section outlines how quark propagators are obtained from the background fields.

2.5.2 Quark Propagators

The basic building blocks for numerical simulation of Lattice QCD are quark propagators. In the continuum full quark propagators, $S(x,y)$, are calculated from inversion of the Euclidean Dirac operator,

$$(\not{D} + m) S(x,y) = \delta^{(4)}(x,y). \tag{2.62}$$

A similar procedure is followed numerically for lattice quark propagators. For a fermion action of the form (2.21), calculation of the quark propagators requires solution of the following system of equations,

$$(A-\kappa B)S(n,m)=\delta^{(4)}(n,m), \tag{2.63}$$

where the terms have spatial, colour and spin indices. For the Wilson action A is purely local and B connects only nearest neighbour terms. The bare quark masses of the simulation are effectively chosen by the κ, the hopping parameter.

Due to the actual forms of terms A and B, this is the inversion of a very large but sparse matrix which can efficiently be done numerically using conjugate gradient type algorithms. However, convergence of these algorithms is affected by choice of bare parameters. For this reason, simulations are restricted to unphysically high quark masses in order to avoid the problems of critical slowing down of the inversion algorithm. In practice, a vector equation is solved for each spin and colour component and at a single fixed point m. This point is called the origin and a set of propagators $S(x,0)$ are obtained.

A further complication in this study was due to the use of an improved fermion action. This improvement, covered in Section 2.4, was implemented by a rotation of quark fields (2.51). In terms of propagators this corresponds to the following rotation[9],

$$S^I(n,m)=\left(1-\frac{1}{2}\gamma\cdot\overrightarrow{\Delta}\right)S(n,m)\left(1+\frac{1}{2}\gamma\cdot\overleftarrow{\Delta}\right). \tag{2.64}$$

This is easily implemented numerically with no great increase in computational expense, by solving,

$$(A-\kappa B)S'(n,m)=\delta^{(4)}(n,m)+\frac{1}{2}\delta^{(4)}(n,m)\gamma\cdot\overleftarrow{\Delta} \tag{2.65}$$

$$\text{and}\quad S^I(n,m)=\left(1-\frac{1}{2}\gamma\cdot\overrightarrow{\Delta}\right)S'(n,m). \tag{2.66}$$

In this way, all the rotations of the quark fields have been included in the generation of the propagators so that all improved correlators can be calculated as with the unimproved action.

Thus, from the pure gauge configurations it is possible to construct the full quark propagators which include all gluonic interactions, for various quark masses. These form a basis for a non-perturbative calculation of the hadronic matrix elements of interest.

[9] here we have chosen the Wilson parameter, $r=1$.

2.5.3 Gauge Fixing

The final numerical component of a toolkit for Lattice QCD is that of numerical gauge fixing of the Monte Carlo produced gauge field configurations. As mentioned earlier, the compact nature of the group space over which gauge integrations are carried out removes the need to introduce a Fadeev–Popov type procedure. However, the study of gauge dependent objects such as gluonic or smeared hadron correlators[10] requires gauge fields fixed to a particular gauge. Indeed, the study of gauge fixing and the resulting Gribov copies on the lattice is a very interesting and involved subject in itself, [32, 33, 34].

In this work, gauge fixing to the Coulomb gauge was done numerically. Imposing the gauge condition was equivalent to minimising the function, $\mathcal{F}(U^g)$,

$$\mathcal{F}(U^g) = \frac{1}{N_t} \sum_{t=1}^{N_t} f[U^g](t), \tag{2.67}$$

where

$$f[U^g](t) = -\frac{1}{V_s} Tr \sum_{i=1}^{3} \sum_{\vec{n}} \left(U_i^g(\vec{n}, t) + U_i^{g\dagger}(\vec{n}, t) \right). \tag{2.68}$$

This is a function of the gauge transformed fields,

$$U_i^g(\vec{n}, t) = g(\vec{n}, t) U_i(\vec{n}, t) g^\dagger(\vec{n} + \hat{\imath}, t). \tag{2.69}$$

One of the advantages of using the Coulomb gauge is that it can be applied to each timeslice, as is explicitly shown in the above, which is useful numerically speaking, but also preserves the interpretation of the operators evolved by means of a transfer matrix formalism.

A measure of quality of the gauge fixing comes from a lattice version of the Coulomb gauge condition. In terms of $\Delta^g(n) = \sum_i \left[A_i^g(n) - A_i^g(n - \hat{\imath}) \right]$ the Coulomb gauge condition is expressed with the quantity, θ,

$$\theta = \frac{1}{V} \sum_n \theta(n) = \frac{1}{V} \sum_n Tr \left[\Delta^g(n) \Delta^{g\dagger}(n) \right] \tag{2.70}$$

$$\underset{a \to 0}{\rightarrow} Tr \int d^4x \, (\partial_k A_k^g)^2 , \tag{2.71}$$

which vanishes when the Coulomb gauge is obtained.

[10] Coulomb gauge smearing is of particular interest in this study, though gauge invariant smearing is also studied.

To numerically minimise the function, $\mathcal{F}$, an algorithm based on an over–relaxation technique of Mandula and Ogilvie, [35], was used. Small gauge transformations are applied on the gauge fields and used to force the function, $\mathcal{F}$, to a minimum, with the $SU(3)$ updates done by the $SU(2)$ subgroups. Over–relaxation is applied by introducing dependence of the gauge transformations, used to force $\mathcal{F}$ to a minimum, on parameter ω. This involves replacing transformations $g(n)$ by $g^\omega(n)$ which is expanded in a power series,

$$g^\omega = \sum_{n=0}^{N} \frac{\gamma_n}{n!}(g-I)^n, \quad \gamma_n = \frac{\Gamma(\omega+1)}{\Gamma(\omega+1-n)}. \tag{2.72}$$

In practise, the sum is truncated at $N = 2$ and matrices g^ω reunitarised before being used to transform the links. Tuning the over–relaxation parameter, ω, can increase the speed of convergence significantly. For this study, 600 iterations of the gauge fixing algorithm were applied, fixing the gauge to an accuracy of 10^{-4}, measured by quantity θ.

A detailed study, [34] of this gauge fixing has shown that there may be many local minima of $\mathcal{F}$. These correspond to Gribov copies of the background gauge field, which are related by some global gauge transformation. The number of such copies is difficult to quantify, though Coulomb gauge is seen to have larger numbers than, say, Landau gauge, because of the dependence of gauge fixing only on spatial extent, allowing gauge freedom between timeslices. Indeed the gauge fixing process can be thought of as some kind of non–linear system behaving chaotically. The evolution of the gauge fields through configuration space and the minimum the algorithm finds on the gauge plane is dependent on the initial conditions and the parameters on which the equations of evolution depend, such as the over–relaxation parameter, ω.

The existence of Gribov copies can affect the correlators generated from the gauge fixed links and propagators. The Coulomb gauge does not fix the gauge completely, some residual gauge freedom remaining. For example, smeared two point correlators can be used to extract smeared matrix elements, Z^S. These are some kind of average over all Gribov copies. With the Coulomb gauge, these smeared amplitudes are the same for all time, as the gauge is fixed independently at each timeslice. Further to this, for the quantities studied at the moment other statistical errors are such that this gauge uncertainty plays an insignificant role, though with increased lattice size and statistical samples these effects could become more important.

In summary, we quote the gauge transformations, in terms of Coulomb Gauge transformations, $g(n)$, of the elements Lattice QCD, which will be used later; the gauge fixing of background gauge fields and light quark propagators,

$$U_\mu^g(n) = g(n)U_\mu(n)g^\dagger(n+\mu) \tag{2.73}$$

$$S^g(n,0) = g(n)S(n,0)g^\dagger(0). \tag{2.74}$$

2.5.4 Summary

This concludes the outline of the three most computationally intensive parts of Lattice QCD; MC integration to produce the background fields, $\{U_\mu(\vec{n},t)\}$, inversion of the Dirac operator to obtain quark propagators, $\{S(n,0)\}$, and gauge fixing of the background fields to obtain an appropriate set of gauge transformations, $\{g(\vec{n},t)\}$. Although the emphasis in this thesis is not on the finer points of the algorithm industry spawned by Lattice QCD, any account of the lattice formalism would be incomplete without some mention of the technology involved. Indeed, the close relationship between technology and Lattice QCD has resulted in great improvement of results over the last few years and is one of the bright hopes for further progress.

2.6 Fixing the Input Parameters

Lattice QCD formulated in Sections 2.1 to 2.4 and implemented numerically, using the techniques outlined in Section 2.5 is a theory with n_f+1 free parameters; n_f quark flavours characterised by κ_f and bare gauge coupling constant $g_0 = 6/\beta$. Clearly with so few free parameters, the predictive power of such a theory has not been reduced, however an experimental measurement is needed to fix each free parameter.

2.6.1 Physical Scale

A finite lattice spacing was introduced in the formulation of a field theory on a discrete spacetime lattice. The size of this lattice spacing is not known from the outset of the numerical calculation. Instead, the coupling constant in terms of β is supplied as input and the lattice spacing is measured non–perturbatively from

physical quantity	a^{-1} (GeV)
$\sigma = \sqrt{K}$	2.73(5)
m_ρ	2.7(1)
f_π	3.4(2)

Table 2.1: Scale, a^{-1}, from different physical quantities, (taken from [6]).

the simulation. The scale of the lattice theory can be set by relating the lattice measurement of some dimensionful quantity to its physical value. Several such quantities are used,

- the string tension: the quark anti–quark potential is measured from various sized Wilson loops and fitted to a Coulomb plus linear potential of the following form,

$$V(R) = C - \frac{E}{R} + KR. \tag{2.75}$$

  The string tension is $\sigma^{latt} = \sqrt{K}$. The scale is set by comparing this lattice quantity to the experimental value measured from the charmonium spectrum, $(\sqrt{K})^{phys} = 0.44$ GeV.

- the rho mass,

$$m_\rho^{latt} = am_\rho^{phys}, \tag{2.76}$$

- the pion decay constant, f_π, and
- the $1P - 1S$ mass splitting in charmonium.

The values of a^{-1} were calculated in [6] and are listed in Table 2.1. Clearly there is a significant discrepancy in the values of lattice spacing obtained from different quantities. In this study we opt for a central value $a^{-1} = 2.7$. For the final dimensionful results we quote an additional error due to uncertainty in the lattice spacing $a^{-1} = 2.7\ ^{+0.7}_{-0.1}$, with the error on the lattice spacing encompassing the range of results measured for the scale, the upper value from the decay constant measurement and lower from the string tension. Error in the final results are quoted giving a range which include dimensions from the scale set by the different methods outlined above.

2.6.2 Quark Masses

The other free parameters of the theory enter in terms of quark masses, or in lattice terminology, kappa values, κ.

Light quarks, u and d, are assumed to be approximately massless. Numerically it is not possible to simulate light quarks at their physical values. Instead, simulations are performed at several light kappa values and the physical results are determined from an extrapolation in kappa to the chiral limit. The procedure for finding the critical kappa value for the chiral limit is outlined in Section 2.8. We use a critical kappa value, $\kappa_{crit} = 0.1431(2)$,[6].

Quantities containing strange quarks can be simulated directly. The corresponding kappa value, κ_s, is fixed by comparing the ratio of pseudoscalar to vector meson masses, m_P^2/m_V^2, from both lattice and experimental measurements, $(m_K^2/m_\rho^2)^{phys} = 0.413$. Following the results given in ref. [6] we use, $\kappa_s = 0.1419(1)$.

Similarly, it is possible to simulate directly quarks about the charm quark mass, though the heavy quark masses are now equivalent to about half a lattice spacing and there is the possibility of discretisation errors. In [36] they simulate with heavy kappa values around $\kappa_h = 0.129$, corresponding to approximately the mass of the charm quark. This was found from comparison with the experimental D-meson mass.

For hadrons containing beauty quarks, it is not possible to simulate directly at the quark mass. This topic is covered in detail in Section 4.2. One approach is to simulate heavy quarks at lower than physical masses around the charm quark mass. Results at the b quark mass are obtained from an extrapolation in the heavy–light pseudoscalar mass, M_P, to the physical B-meson mass. For light quark physics PCAC indicates a useful form for the extrapolation. However, no such simple form exists for systems of heavy quarks. For some quantities scaling relations from the Heavy Quark Effective Theory offer a guide to this extrapolation. The approach followed in this work takes the other extreme, attempting simulations with heavy quarks of infinite mass. In this limit the dynamics of the system simplify greatly and particularly simple forms for the heavy quark propagator are obtained. This is the so called static theory.

2.7 Continuum Limit

In constructing a gauge invariant lattice action the main constraint on the form of the action is that it must regain the correct form in the naive continuum limit, $a \to 0$. This offers much ambiguity in the definition of the action, exploited by the addition of the Wilson term and later with improvement, as outlined in Section 2.4. However, there is no reason why this continuum limit should be continuum QCD.

A lattice field theory has one dimensionful parameter, the lattice spacing a, and is dependent on several dimensionless parameters (β, $\kappa, \ldots$). To relate some dimensionless quantity, say a mass, m^{latt}, measured on the lattice to its physical value, m^{phys}, it is necessary to multiply by appropriate powers of lattice spacing,

$$m^{latt}(\beta, \kappa, \ldots) = a\, m^{phys}. \tag{2.77}$$

Indeed this is a way in which the lattice spacing can be determined (Section 2.6).

In taking the continuum limit, $a \to 0$, the physical mass must remain fixed, so for a consistent approach to the continuum limit the bare parameters must be tuned so that the lattice mass vanishes. This can be viewed in terms of a statistical mechanics system, defining a correlation length as,

$$\xi^{latt} = \frac{1}{m^{latt}}, \tag{2.78}$$

which diverges in the continuum limit. This suggests that continuum physics exists at the critical points of a lattice field theory, with bare parameters tuned to their critical values, $\beta \to \beta^{\star}$. Clearly this makes sense intuitively, the divergent correlation length corresponds to fluctuations over all length scales and the system 'forgets' it is on a discrete lattice, clearly a desirable aim.

However, the real utility to practical lattice simulations is a property of statistical systems know as scaling. This means for small enough lattice spacing, dimensionless ratios of quantities (both lattice and physical) are independent of a. If the bare coupling exists in a 'scaling window' then it is not necessary to simulate at $a = 0$, nor even extrapolate to the $a \to 0$ limit. Too small a lattice spacing introduces significant finite size effects. Too large a lattice spacing and the simulation can't account for fluctuations on small scales and the system moves away from the continuum limit. The simulations presented here are at $\beta = 6.2$, thought to be within the scaling window. However, even for this value of coupling constant there is the possibility for significant $\mathcal{O}(a)$ corrections, especially for quantities involving heavy quarks. An attempt to reduce these effects is made by the use of an improved action.

2.8 The Chiral Limit

The use of the Wilson formulation for lattice fermions breaks the chiral invariance of the field theory formulated on the lattice, even in the zero mass limit. In addition to this, light quarks, u and d, cannot be simulated at their physical masses. The former situation arises due to the need to overcome the fermion doubling problem, whereas the latter is required to avoid convergence problems in numerically inverting the Dirac operator.

The way to overcome both of these problems to some extent is to tune the bare parameters of the theory. This attempts to 'exactly' cancel the chiral symmetry breaking effects and obtain matrix elements containing light quarks at their physical masses. In a lattice simulation, the bare quark masses are controlled by the hopping parameter, κ, and this tuning procedure involves determining a critical kappa value, κ_{crit}. The criterion used for determining the chiral limit is the vanishing of the pion mass. The light pseudoscalar is thought to obey the PCAC relation, [37],

$$m_{PS}^2(\kappa) = a\left(\frac{1}{2\kappa_1} + \frac{1}{2\kappa_2} - \frac{1}{\kappa_{crit}}\right), \tag{2.79}$$

for light quarks of masses κ_1, κ_2. By plotting m_{PS}^2 against κ_1 and κ_2 the critical kappa value can be calculated non–perturbatively and indeed the PCAC relation is seen to be well satisfied (see Section 2.12).

For all lattice quantities containing light quarks it is necessary to extrapolate in terms of the light quark mass to the chiral limit at κ_{crit}. This extrapolation is assumed to be linear in inverse kappa value. For example, to extract some quantity at its physical value $Q(physical)$, say, from extrapolation of the lattice quantity $Q(\kappa_i)$ calculated at light kappa values κ_i, the extrapolation takes the form,

$$Q(\kappa_i) = Q(physical) + a_Q\left(\frac{1}{\kappa_i} - \frac{1}{\kappa_{crit}}\right), \tag{2.80}$$

with $Q(physical) = Q(\kappa_{crit})$.

The extrapolation to the chiral limit offers a means by which practical calculations of quantities involving light quarks can be obtained without simulating the light quarks at their physical masses. The final step to make contact with continuum physics is to reintroduce powers of the lattice spacing to obtain a dimensionful quantity and multiply by the relevant renormalisation constant. The need for this renormalisation constant and an outline of how they are determined are given in the following section.

2.9 Renormalisation and Operator Matching

Before matrix elements calculated by lattice methods can be incorporated into the study of continuum physics, it is necessary to first relate the operator defined on the lattice to that in the continuum, [38]. Calculation of renormalisation constants for this matching are the final input for obtaining physical results from Lattice QCD.

In essence, both continuum QCD and Lattice QCD are well defined field theories intended to describe the same continuum physics. The main differences arise when the quantum nature of the field theories is considered, i.e. on the inclusion of quantum loop corrections. The idea of renormalisation is to correct the bare theory, including the divergences introduced by loop effects, to give finite physical results.

In continuum field theory it is in principle possible to go beyond tree level and perturbatively calculate the loop corrections. However, the loop integrals involved in this process can diverge at high energies. In order to obtain finite results from these integrals it is necessary to regularise the theory. In the $\overline{\mathrm{MS}}$ regularisation scheme, for example, the dimension of the loop integrals is reduced to $d = 4 - \epsilon$. The divergent loop corrections are then parameterised in some systematic way, as poles in $1/\epsilon$, for example. These divergent terms are then subtracted from the bare theory and absorbed in a redefinition of the bare parameters. As a necessary consequence of this method to deal with these infinities a renormalisation scale, μ is introduced in the theory. This renormalisation procedure is intended to give finite physical predictions of the field theory.

In the same way, it is possible to consider the lattice as another perfectly good regularisation scheme. Expanding the lattice action in the weak coupling limit it is possible to produce a set of Feynman rules suitable for perturbative calculations. These perturbative calculations can in principle[11] determine the loop corrections to the lattice theory in exactly the same way as in the continuum. In this case the lattice spacing a is used as the UV cutoff to regularise the divergent loop integrals. In this case a also plays the role of the renormalisation scale.

As both lattice and continuum schemes aim to represent the same physics, renormalisation of operators in both schemes should match. In practise this matching procedure involves calculating the loop corrections to the operators using the continuum and lattice regularisation schemes. The aim of this is to obtain a relation of the type,

$$\mathcal{O}_i^{cont}(\mu) = Z_{ij}(\mu a, g_0(a))\mathcal{O}_j^{latt}(a), \tag{2.81}$$

for $Z_{ij}(\mu a, g_0)$, the renormalisation constants. The continuum operator should not depend on lattice cutoff, a, this dependence canceling exactly between the matching coefficients and operators $\mathcal{O}^{latt}$. This introduces the possibility of operator mixing under renormalisation, in that other operators must be considered in the lattice theory, for a complete matching. The main advantages of this type of matching are that only the high energy, short distance behaviour of the operators must be matched[12], which can be done perturbatively and also the renormalisation coefficients, Z_{ij}, depend only on the operators present and are independent of external states.

Perturbation theory is a widely used tool in continuum physics and involves an expansion in terms of $\alpha_{\overline{MS}}$, which is small at scales involved. A perturbation theory is also possible on the lattice in terms of the lattice coupling $\alpha_{latt} = g_0^2/4\pi$. However this involves the bare lattice coupling constant and recently, [39], it has been suggested that this is a poor expansion parameter. A better choice is to use some renormalised coupling, as was the case in continuum perturbation theory adopting $\alpha_{\overline{MS}}$. This leads to use of a 'boosted coupling' defined as $g^2 = 6/(\beta u_0^4)$, where u_0 is some measure of the average of a link variable. This is measured non–perturbatively from the expectation value of the plaquette or, as used in this work, defined by mean field arguments as $u_0 = (8\kappa_{crit})^{-1}$. In this way it is hoped to resum some of the tadpole graphs, which often appear in lattice perturbation theory and offer a more reliable perturbation theory. In this study

[11] in practise perturbative calculations are complicated significantly by the form of these Feynman rules.

[12] the low energy, infrared behaviour is the same for both regularisation schemes

Operator	Calculation	Renormalisation Constant			Reference
$\bar{q}\gamma_\mu\gamma_5 q$	f_π, f_K, B_K	Z_A	$\approx 1 - 0.0177g^2$	$= 0.97$	[40]
$(\bar{s}\gamma_\mu^L d)(\bar{s}\gamma_\mu^L d)$	B_K	Z_+	$\approx 1 - 0.069g^2$	$= 0.88$	[40]
$\bar{b}\gamma_\mu\gamma_5 q$	f_B^{static}, B_B^{static}	Z_A^{stat}	$\approx 1 - 0.127g^2$	$= 0.79$	[41, 42, 43]
$\bar{b}\sigma_i\epsilon_{ijk}F_{jk}^{latt}b$	$m_{B^*}^2 - m_B^2$	Z_σ	$\approx 1 + 0.245g^2$	$= 1.45$	[44]

Table 2.2: Renormalisation constants. Values for boosted coupling $g^2 = 1.63g_0^2$.

at $\beta = 6.2$, we use $g^2 = 1.63g_0^2$.

In summary, we list in Table 2.2, the renormalisation constants used in this work, with references to the original calculation.

2.10 Systematic Errors

In the search for a practical non–perturbative technique for the calculation of QCD matrix elements, Lattice QCD accepts various compromises required in light of limited resources. Indeed one of the main aims of current research in the field is to understand and attempt to quantify the systematic errors which unavoidably enter into any numerical simulation.

As outlined earlier, Section 2.5, the Path Integral expectation value for an operator is calculated by a Monte Carlo integration over a large but finite sample of configurations. Clearly this introduces some statistical error, the size of which can be estimated in the standard techniques, also outlined in Section 2.11. The present status of current simulations is such that these statistical errors seem for many, but not all quantities, to be under control with sample sizes of around 50-100 configurations.

The fact that these integrals are calculated on a discrete lattice of finite extent introduces 'finite size effects' with the quantities simulated 'feeling' the surrounding box. These effects can be quantified by varying the bare parameters (in terms of β and number of lattice points) of the theory to simulate over different volumes. Related to this is the need to simulate the quarks at much larger masses than is physical, which, as is mentioned elsewhere, requires an extrapolation in quark mass to the physical limit (Section 2.8).

Also arising from formulating the field theory on a discrete lattice are finite lattice spacing effects. These arise initially from terms in the action which agree with the continuum action only in the naive $a \to 0$ limit, but which introduce corrections to lattice quantities at finite a. Indeed these finite a corrections can sometimes greatly affect the properties of lattice matrix elements (of particular interest in this study is the chiral behaviour of the matrix element for the four fermion operator in neutral kaon mixing, Section 3.1). A 'brute force' way to attempt to quantify these lattice artefacts is to simulate at different lattice spacings and extrapolate to zero lattice spacing limit. However, in this work, a less computationally intensive approach was taken. By use of an improved action, Section 2.4, which formally removes the lowest order corrections to the matrix elements it is hoped that these lattice artifacts are reduced. Comparison of results with this action to unimproved operators is of continuing interest and will be one of the main themes of this study.

The other main systematic error arises from the wide use of the 'quenched approximation' (Section 2.5.1). The good agreement of quenched calculations with experiment for many quantities suggests quenching is a small effect, perhaps backed up by theoretical analysis of quenching using chiral perturbation theory. There are still, however, quantities such as the hyperfine splitting in quarkonia which suffer badly from quenching. In effect the full potential of lattice QCD as a truly 'first principles' solution to the effects of the strong interaction depends on the development of both theoretical and algorithmic methods to obtain 'full' unquenched QCD on a lattice.

Quantifying the systematic errors is a difficult subject and much work still needs to be done before many of the criticisms levelled at lattice QCD are silenced. But they are systematic and with experience and time there is hope that they can be understood and minimised.

2.11 Fitting and Error Analysis

The calculation of operator matrix elements in Lattice QCD usually involves the generation of sets of Euclidean correlators. The final step in the analysis of these correlators is the fit of the numerical data to some asymptotic form, f_i, as a function of time t_i.

$$C(t_i) = \langle \mathcal{O}(t_i)\mathcal{O}(0) \rangle = f_i(p), \tag{2.82}$$

The aim of this is to extract the parameters, $\{p\}$, which are related to the matrix elements and masses of the particles simulated. The χ^2 function offers a measure of how well the observed data compares with the theoretical prediction. A widely used way of determining the most probable set of parameters for a given set of data is by a maximum likelihood type fit achieved by minimising the χ^2 function. Further to this, error analysis of both the original data set and 'best fit' parameters is essential.

To estimate the errors, a set of averages are constructed from 'bootstrap' or 'jacknife' processes, [45, 46]. The spread of these averages offers a measure of the error. If the original data set contains N measurements at times t_i, $\{y_k(t_i)\}$, $k = 1, \ldots, N$. The central value for this data set is obtained from a simple mean,

$$\overline{Y}(t_i) = \sum_{k=1}^{N} y_k(t_i)/N. \tag{2.83}$$

The error on this value is calculated, not from the spread of the data, but from the spread of the biased averages. Bootstrap averages, $\{Y_k^B(t_i)\}$, $k = 1, \ldots, N_{boot}$, are constructed from N random samples from the original data set (including repeats). Similarly, jacknife clustering can be thought of as a systematic bootstrap, formed with one configuration dropped from the average in each sample, i.e. $Y_k^J(t_i) = (N\overline{Y}(t_i) - y_k(t_i))/(N-1)$. Errors for the jacknifed clusters can just be calculated in the usual way,

$$\sigma^2(t_i) = \sum_k (Y_k(t_i) - \overline{Y}(t_i))^2/(N-1), \tag{2.84}$$

whereas the errors on the bootstrapped clusters are fixed to contain the central 68% of the data. Everything is now expressed in terms of clustered averages (in this study we only use jacknife averages), $\{Y_k(t_i)\}$, with gaussian distribution, mean $\overline{Y}(t_i)$ and variance $\sigma(t_i)$.

A first estimate of the best fit parameters p of function f_i is gained from minimising an uncorrelated χ^2_{unc}, over some fit range $t_i \in \{t_{min}, t_{max}\}$, where the data is thought to fit the model,

$$\chi^2_{unc} = \sum_{t_i=t_{min}}^{t_{max}} \left(\frac{\overline{Y}(t_i) - f_i(p)}{\sigma(t_i)} \right)^2. \tag{2.85}$$

However, this takes no account of correlations which exist between data at different times. This is done by use of a correlated χ^2_{cor} function in terms of the covariance matrix, C_{ij}, [45, 47] (with prefactors changing dependent on whether bootstrap or jacknife error analysis was applied),

$$C_{ij} = \frac{1}{N-1}\left(\frac{1}{N}\sum_{k=1}^{N}\left(Y_k(t_i) - \overline{Y}(t_i)\right)\left(Y_k(t_j) - \overline{Y}(t_j)\right)\right) \tag{2.86}$$

$$\chi^2_{cor} = \sum_{i,j}\left(\overline{Y}(t_i) - f_i(p)\right) C^{-1}_{ij}\left(\overline{Y}(t_j) - f_j(p)\right). \tag{2.87}$$

In both cases the χ^2 functions are minimised numerically to determine the best fit parameters. This process is repeated for all biased clusters to obtain a distribution of the parameters, from which errors of the parameters can be obtained. The 'goodness of fit' for these correlated fits is indicated by χ^2 per degree of freedom, where the degree of freedom of a fit is the number of points fitted minus the number of free parameters in the fit. A $\chi^2/d.o.f. \sim 1$ suggests a good fit. A very small χ^2/dof could indicate an overestimate of errors. Alternatively, a large χ^2/dof indicates poor agreement between data and model.

Although not as computationally intensive as the other numerical parts of Lattice QCD, the analysis and fitting of correlators is without doubt the most labour intensive. Many strategies for obtaining the 'best fit' range exist. These can be based on comparison of uncorrelated and correlated fits and goodness of fit measures such as the χ^2 function. As such, choosing fit ranges is still as much an art as science.

At the end of this process a set of best fit parameters is obtained with a qualitative estimate of the statistical uncertainty of both the MC average and these fitted parameters.

2.12 An Example Lattice Calculation

To demonstrate the techniques outlined above, it may be useful to consider a simple example which uses the four main parts to any lattice calculation, that is,

- generation of the gauge configurations and quark propagators,
- construction of required correlation function from quark propagators,
- analysis of these by fitting to some model, to extract lattice quantities and,
- extrapolation of the results to the chiral limit, including factors of lattice spacing and renormalisation constants to obtain physical results.

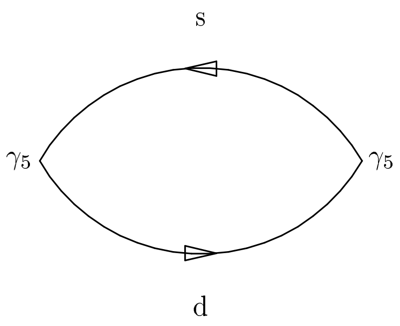

Figure 2.3: Two point pseudoscalar meson correlator

This example aims to calculate the critical kappa value required in extrapolation to the chiral limit, Section 2.8. This requires the measurement of the mass of the light pseudoscalar obtained from a simple two point function. This was chosen because it neatly and simply demonstrates the above steps, offers a good lattice example and is also a vital calculation for the rest of the work presented in this thesis.

Step 1. Generation of Propagators. It is assumed that a set of quark propagators exists, generated using the techniques outlined in in Section 2.5.

Step 2. From Propagators to Correlators.

As mentioned in Section 2.5 the expectation value of an operator is obtained with the Path Integral formalism and expressed in terms of an integral over configuration space. The further step of integrating over all fermion fields leaves an integral over gauge space, which in lattice field theory is done by Monte Carlo integration, of the trace of the Wick contracted operator.

In this example the correlator of interest is the product of operators which create/destroy a zero momentum pseudoscalar meson, $P_5 = (\bar{s}\gamma_5 d)$, which are Wick contracted to form propagators,

$$\begin{aligned} C(t) &= \sum_{\vec{x}} \left\langle P_5(x) P_5^\dagger(0) \right\rangle \\ &= \sum_{\vec{x}} \left\langle (\bar{s}(x)\gamma_5 d(x)) \left(\bar{d}(0)\gamma_5 s(0)\right) \right\rangle \\ &= -\sum_{\vec{x}} \left\langle Tr\left\{ S_d(x,0)\gamma_5 S_s(0,x)\gamma_5 \right\}\right\rangle \end{aligned} \tag{2.88}$$

$$= -\sum_{\vec{x}} \left\langle Tr\left\{ S_d(x,0) S_s(x,0)^\dagger \right\} \right\rangle. \tag{2.89}$$

This last step was possible by invoking a symmetry of lattice propagators, [48], namely,

$$S(x,0) = \gamma_5 S^\dagger(0,x)\gamma_5. \tag{2.90}$$

The function in Equation (2.89) is calculated for all configurations and for all combinations of quark masses.

Step 3. Analysing the Correlator.

Another route from the definition of the correlator, Equation (2.88), can be used to construct the asymptotic form to which the numerical results can be fitted. Inserting a complete set of states and allowing large Euclidean times to isolate the lowest state gives,

$$\begin{aligned}
C(t) &= \sum_{\vec{x}} \left\langle P_5(x) P_5^\dagger(0) \right\rangle \\
&= \sum_{\vec{x}} \int \frac{d^3p}{2E_p} \left\langle 0 | e^{p\cdot x} P_5(0) e^{-p\cdot x} P_5^\dagger(0) | 0 \right\rangle, \\
&= \sum_{n} \int \frac{d^3p}{2E_p} \delta^{(3)}(\vec{p}) \left\langle 0 | P_5(0) e^{-E_n|t|} | n \right\rangle \left\langle n | P_5^\dagger(0) | 0 \right\rangle, \\
&\underset{\text{large t}}{\rightarrow} \frac{|\left\langle 0 | P_5(0) | P \right\rangle|^2}{2m_P} \{\exp(-m_P t) + \exp(-m_P(N_t - t))\} \\
&= \frac{Z_5}{m_P} \exp(-m_P N_t/2) \cosh(m_P(N_t/2 - t)).
\end{aligned} \tag{2.91}$$

These last steps include the time reversed ordering of operators, with relative sign due to time reversal symmetry of propagators, [48]. The amplitude of the correlator is defined in terms of the matrix element, $Z_5 = |\langle 0|P_5(0)|P\rangle|^2$.

The expression in Equation (2.91) is the asymptotic form of the two point correlator to be used in extracting the amplitude, Z_5, and mass of the pseudoscalar, m_P, from the MC data by means discussed in Section 2.11.

Step 4. Chiral Extrapolation.

The final step in the process involves an extrapolation to the chiral limit, corresponding to physical light quark masses. This extrapolation depends on the particular physical quantity to be extracted, though it is assumed to

κ_1	κ_2	m_P
0.14144	0.14144	0.297 (2)
0.14144	0.14226	0.258 (2)
0.14144	0.14262	0.240 (2)
0.14226	0.14226	0.213 (2)
0.14226	0.14262	0.191 (3)
0.14262	0.14262	0.166 (3)
κ_{crit}	0.14313 (2)	-

Table 2.3: Pion mass composed of degenerate and non–degenerate quarks, measured in lattice units

be linear in inverse kappa, with the basic constituents the amplitudes and masses already fitted.

To actually calculate the value of the critical kappa, it is necessary to extrapolate the pseudoscalar mass to zero (corresponding to zero pion mass). The results of this are shown in Table 2.3 and Figure 2.4.

From this study, we find the critical kappa value,

$$\kappa_{crit} = 0.14313(2)$$

which agrees well with [6].

In other calculations it is at this point the factors of lattice spacing and the renormalisation constants are included to produce a result corresponding to the continuum value in physical units.

2.13 Numerical Details

All numerical results presented here are from the UKQCD Collaboration, with further details available elsewhere, [36, 2, 6, 46]. Simulations in the quenched approximation were performed on 60 gauge field configurations from a $24^3 \times 48$ lattice at $\beta = 6.2$, corresponding to lattice spacing, $a^{-1} = 2.7\ ^{+0.7}_{-0.1}$, [46], from the string tension and errors given from measurements of the scale from f_π and the rho mass.

Gauge configurations and quark propagators were calculated on a 64 i860–node Meiko computing Surface at Edinburgh. The gauge configurations were

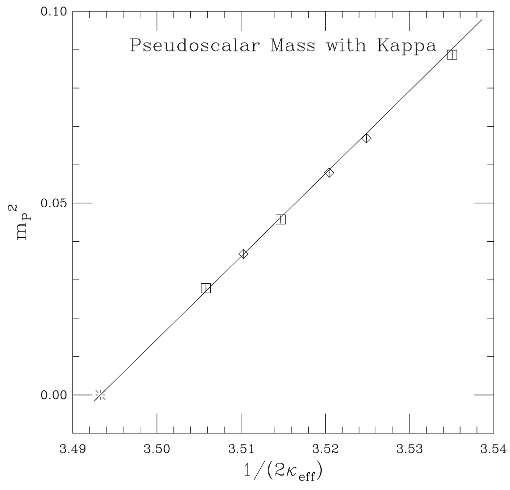

Figure 2.4: Chiral extrapolation of pion mass.

generated with a combination of over–relaxed and Cabibbo–Marinari subgroup updates, the so called Hybrid OverRelaxed algorithm, [46]. Propagators were generated with an $\mathcal{O}(a)$ improved, 'Clover', action, with $r = 1$ and coefficient of the clover term fixed to its tree–level value. These were calculated for light quark masses, $\kappa = 0.14144,\ 0.14226,\ 0.14262$, by means of an over–relaxed minimal residue algorithm with red–black preconditioning, [49].

Smeared propagators were generated by two methods, which will be discussed in more detail in Section 4.3. Coulomb gauge smearing techniques, Section 4.3.1, required the gauge fixing of the 60 gauge configurations to Coulomb gauge. An outline of this gauge fixing method was given in Section 2.5.3. This was done numerically, [34] on the CRAY YMP8 at the Rutherford Appleton Laboratory. For the gauge invariant smearing, [2], discussed in Section 4.3.2, smeared propagators were generated on a Thinking Machines CM–200 at The University of Edinburgh.

The analysis of the gauge configurations and propagators, to produce the hadronic correlators was carried out on a variety of DEC ALPHA machines at Edinburgh.

Chapter 3

Light Quark Phenomenology

Neutral kaon mixing is the perfect place to test the Standard Model. Not only was it the first phenomena to exhibit CP violation, [50], or offer the first prediction of the charm mass before its discovery, [51], but it is also an ideal example of the effects of the strong interaction in weak hadronic decays, at both long and short distances. Further, experimental measurement and theoretical prediction of the mixing are central to constraining some of the free parameters of the Standard Model; the CKM quark mixing angles, especially the top couplings, and also the top mass, to which kaon mixing is especially sensitive.

In terms of lattice calculations, the kaon system also provides the perfect place to test lattice methods. Historically, much ground breaking work was done on light systems and even now the state–of–the–art lattice calculations are in light hadron spectroscopy, [52]. Further to this, non–perturbative calculations of light hadron weak matrix elements from lattice calculations are of continuing interest and importance to both experimentalists and lattice devotees alike.

3.1 Indirect CP Violation in $K^0\bar{K}^0$Mixing

K^0 and $\bar{K}^0$ are flavour eigenstates and can mix via second order weak interactions. From these it is possible to construct CP eigenstates, $K_{1,2} = \frac{1}{\sqrt{2}}(K^0 \pm \bar{K}^0)$, $CP|K_{1,2}\rangle = \pm|K_{1,2}\rangle$. However the physically observed mass eigenstates, $K_{L,S}$ contain an admixture of both states,

$$|K_S\rangle = \frac{(|K_1\rangle + \bar{\epsilon}|K_2\rangle)}{\sqrt{1+\bar{\epsilon}^2}} = \frac{\Big((1+\bar{\epsilon})|K^0\rangle + (1-\bar{\epsilon})|\bar{K}^0\rangle\Big)}{\sqrt{2(1+\bar{\epsilon}^2)}} \tag{3.1}$$

$$|K_L\rangle = \frac{(|K_2\rangle - \bar{\epsilon}|K_1\rangle)}{\sqrt{1+\bar{\epsilon}^2}} = \frac{\Big((1+\bar{\epsilon})|K^0\rangle - (1-\bar{\epsilon})|\bar{K}^0\rangle\Big)}{\sqrt{2(1+\bar{\epsilon}^2)}}, \tag{3.2}$$

where $\bar{\epsilon}$ is a small parameter[1]. These physical eigenstates decay predominantly as,

$$K_S \to 2\pi \qquad \text{and} \qquad K_L \to 3\pi, \tag{3.3}$$

due to the major contributions from K_1 and K_2, and with 2π and 3π being CP even and odd final states, respectively. However, $K_{L,S}$ also contain small contributions from the opposite CP eigenstate. As a result, the physical eigenstates can decay via the other channel, though with a much smaller branching fraction. This is indirect CP violation, the initial state particles having a component from each CP eigenstate, which should be compared with direct CP violation where, say, a CP even state decays into a CP odd state. Indirect CP violation in kaon decays is measured by, the CP violating parameter ϵ[2], defined in terms of the ratio of CP violating to CP conserving decays,

$$\epsilon = \frac{A(K_L \to (2\pi)_{I=0})}{A(K_S \to (2\pi)_{I=0})}. \tag{3.4}$$

This CP violating parameter was measured at UA1 in CERN, with current measurement, [53],

$$|\epsilon_{exp}| = (2.259 \pm 0.023) \times 10^{-3}. \tag{3.5}$$

The CP violating parameter, ϵ, can be calculated theoretically, with the main contributions coming from the box diagram, Figure 3.1. This represents the second order weak decay responsible for neutral kaon mixing. The typical scale of the weak decay in this process is given by the W mass. As this scale is much greater than any hadronic scale entering the decay, it is possible to treat this in terms of an effective low energy theory. This invokes all the formalism of the Operator Product Expansion (OPE), to integrate out all the irrelevant, high energy degrees of freedom[3], rewriting the decay amplitude as the matrix element of an effective Hamiltonian, expressed as a sum of operators, $\mathcal{O}_i(\mu)$ with Wilson coefficients, $C_i(\mu)$, where μ is the renormalisation scale. These coefficients can be calculated perturbatively in terms of the appropriate CKM elements and a set of

[1] $\bar{\epsilon}$ is dependent on phase convention taken for flavour eigenstates, so cannot be taken as a physical measure of CP violation.

[2] ϵ is independent of phase convention chosen.

[3] M_W reappears in the effective couplings and Wilson coefficients

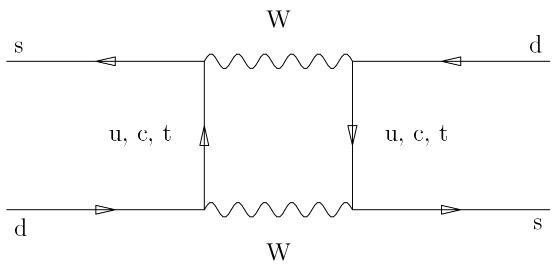

Figure 3.1: Box diagram contributing to CP violation in neutral kaon mixing

universal functions of $x_i = m_i^2/M_W^2$, [54], for internal quarks, $i = u, c, t$. As this decay is a second order weak process, only operators with dimension $d_i \leq 6$ can enter the sum. In short, the large M_W forces the interaction to be short ranged and squeezes the sides of the box diagram together to form an effective four fermion interaction. The only operator for the $\Delta S = 2$ decay with the correct current structure is,[4]

$$(\bar{s}d\bar{s}d)_{LL} \equiv (\bar{s}\gamma^\mu(1-\gamma_5)d)(\bar{s}\gamma_\mu(1-\gamma_5)d). \tag{3.6}$$

All dependence on the scale μ should cancel between Wilson coefficients and operator matrix elements. The first place the strong interaction enters this calculation is in the QCD corrections to these operators. At scales between the scale relevant to the calculation of the matrix element, $\mathcal{O}(2\,\mathrm{GeV})$, and M_W, these corrections are short distance effects and can be calculated perturbatively. This procedure has been carried out for the box diagram, [51, 55, 56], resulting in,

$$\begin{aligned} |\epsilon| = {} & \frac{G_F^2 M_W^2}{16\sqrt{2}\pi^2 \Delta m m_K} Im \left[\eta_1 V_{cd}^2 V_{cs}^{*2} S(x_c) + \eta_2 V_{td}^2 V_{ts}^{*2} S(x_t) \right. \\ & \left. + \; 2\eta_3 V_{td} V_{ts}^* V_{cd} V_{cs}^* S(x_c, x_t)\right] \langle \bar{K^0} | (\bar{s}d\bar{s}d)_{LL} | K^0 \rangle. \end{aligned} \tag{3.7}$$

This form has all the ingredients mentioned above; Wilson coefficients in terms of functions S_i, [54], CKM factors, short distance QCD corrections η_i, [56], and the matrix element of the four fermion operator driving the effective theory of the mixing process. This matrix element is where QCD rears its ugly head for a second time in this calculation, though this time concerning the long distance physics which is intrinsically non–perturbative.

[4] this operator is multiplicatively renormalisable, so only operators with dimension $d_i = 6$ are included.

It is the theoretical calculation of the non-perturbative contributions to the mixing that causes all the problems. Measurements of ϵ and the other well know quantities in Equation (3.7) can be used to gain an accurate measure of the CP violating effects from this decay. However, the main uncertainty arises in the theoretical calculation of the hadronic matrix element. There are many approaches to calculating this matrix element, including chiral perturbation theory, [57], and QCD sum rules, [58], though in this study we offer a calculation based on Lattice QCD.

What is usually calculated is the so called B–parameter, B_K, which gives a comparison between the matrix element and its vacuum saturation approximation (VSA). The VSA involves inserting the lowest state, the vacuum $|0\rangle\langle 0|$, into the four fermion operator. The B–parameter is also a more appropriate quantity to calculate on the lattice, in that a ratio of matrix elements has lower fluctuations, and reduced systematic uncertainties. This defines the B–parameter as,

$$\langle \bar{K}^0|(\bar{s}d\bar{s}d)_{LL}|K^0\rangle|_\mu = \frac{8}{3} f_K^2 m_K^2 B_K(\mu), \tag{3.8}$$

where the VSA is expressed in terms of the kaon decay constant, f_K,

$$\langle 0|\bar{s}\gamma_\mu\gamma_5 d|K^0(q)\rangle = i f_K q_\mu. \tag{3.9}$$

If the VSA is an accurate approximation, $B_K \approx 1$.

This definition describes the B-parameter at the scale of the calculation of the hadronic matrix element. Often, it is more convenient to work with a renormalisation group invariant definition,

$$\hat{B}_K = B_K(\mu)\left(\alpha_{QCD}(\mu)\right)^{\frac{\gamma^{(1)}}{2\beta_0}} = B_K(\mu)\left(\alpha_{QCD}(\mu)\right)^{\frac{-2}{9}}, \tag{3.10}$$

with the exponent coming from the anomalous dimension of the operator and the beta function of the theory.

This concludes the outline of mixing in the neutral kaon system. The basic formalism in terms of the usual operator product expansion was used to motivate the need for a non–perturbative calculation of the $\Delta S = 2$ weak matrix element, which the following sections will elaborate on.

3.2 Kaon Decay Constant f_K

Related to the calculation of the kaon B-parameter, defined in Equation (3.8), is calculation of the kaon decay constant, f_K, defined in Equation (3.9), and other light hadron properties. These have been extensively studied with the same set of gauge configurations in [6], thus offering a check of the correlation functions to be used in determining B_K, and the general methods used to analyse such correlators.

The usual way to calculate decay constant in terms the matrix element of the time component of the axial current is from the combination of the following pseudoscalar two point functions,

$$C_5(t) = \sum_{\vec{x}} \left\langle P_5(\vec{x},t) P_5^\dagger(\vec{0},0) \right\rangle \tag{3.11}$$

$$C_{A_4}(t) = \sum_{\vec{x}} \left\langle A_4(\vec{x},t) P_5^\dagger(\vec{0},0) \right\rangle, \tag{3.12}$$

where $P_5(\vec{x},t) = (\bar{s}\gamma_5 d)$ is the pseudoscalar current and $A_4(\vec{x},t) = (\bar{s}\gamma_4\gamma_5 d)$ is the time component of the axial current.

These correlators are fitted to the following forms,

$$C_5(t) = \frac{Z_5}{m_P} \exp\left(-m_P N_t/2\right) \cosh\left(m_P(N_t/2 - t)\right) \tag{3.13}$$

$$C_{A_4}(t) = \frac{Z_{45}}{m_P} \exp\left(-m_P N_t/2\right) \sinh\left(m_P(N_t/2 - t)\right), \tag{3.14}$$

where pseudoscalar mass, m_P, and the hadronic matrix elements are extracted from the amplitudes,

$$Z_5 = |\langle 0|P_5|P\rangle|^2 \tag{3.15}$$

$$Z_{45} = |\langle 0|A_4|P\rangle||\langle 0|P_5|P\rangle| = f_P m_P |\langle 0|P_5|P\rangle|. \tag{3.16}$$

The pseudoscalar decay constant, f_P, is then determined from the ratio,

$$R(t) = \frac{C_{A_4}(t)}{C_5(t)} \tag{3.17}$$

$$\underset{\text{large t}}{\rightarrow} Z_R \tanh\left(m_P(N_t/2 - t)\right) \tag{3.18}$$

where the amplitude, Z_R, is defined in terms of the matrix elements of the light meson, $f_P m_P / Z_A |\langle 0|P_5|P\rangle|$ and Z_A, is the renormalisation constant for the lattice axial current. The use of this ratio is to obtain a clearer signal to be fitted, with some cancellation of systematic uncertainties between numerator and denominator.

The extraction of the decay constants is done in four stages,

κ_1	κ_2	f_P/Z_A
0.14144	0.14144	0.0621 (9)
0.14144	0.14226	0.0563 (9)
0.14144	0.14262	0.0534 (10)
0.14226	0.14226	0.0505 (10)
0.14226	0.14262	0.0472 (12)
0.14262	0.14262	0.0435 (17)
κ_{crit}	0.14313 (2)	0.0402 (11)

Table 3.1: Pseudoscalar meson decay constants in lattice units.

f_π/Z_A	f_K/Z_A	f_K/f_π
0.040 ± 0.001	0.049 ± 0.001	1.21 ± 0.01

Table 3.2: Extrapolated meson decay constants in lattice units.

1. Calculate the critical kappa value, at which the pion mass vanishes and corresponds approximately to the physical light quark mass, from the mass parameters obtained from Equation (3.13). This calculation is given in Section 2.12 as an example of a lattice calculation.

2. Combining results from fits to the amplitudes of ratio (3.18) and two point function (3.13) to calculate the pseudoscalar decay constant from,

$$\frac{f_P}{Z_A} = Z_R \frac{\sqrt{Z_5}}{m_P}. \tag{3.19}$$

   Values of this for all six light kappa combinations are shown in Table 3.1.

   The pion decay constant, f_π, is determined by the chiral extrapolation of both light kappa values to the critical value. This extrapolated value is included in Table 3.1 and Table 3.2, in lattice units.

3. From the quantities measured it is also possible to calculate the kaon decay constant, f_K, and the ratio, f_K/f_π, which is hoped to have reduced systematic errors as uncertainties in lattice spacing and renormalisation constant cancel in the ratio. To calculate f_K using the pseudoscalar decay constant results in Table 3.1, one light kappa value is extrapolated to the chiral limit,

	lattice estimate	experiment
f_π	$105 \pm 3 \ {}^{+27}_{-\ 4}$ MeV	132 MeV
f_K	$125 \pm 2 \ {}^{+33}_{-\ 5}$ MeV	160 MeV
f_K/f_π	1.21 ± 0.01	1.22
$Z_A = 0.97$, $a^{-1} = 2.7 \ {}^{+0.7}_{-0.1}$ GeV		

Table 3.3: Meson decay constants in physical units.

while the other is interpolated to the strange mass. This used the value $\kappa_s = 0.1419$ from ref. [6]. The results for f_K and ratio f_K/f_π are given in lattice units in Table 3.2.

4. In order to obtain results to be compared with experimental values it is necessary to include a scale and the perturbative renormalisation constant, Z_A. These physical results are given in Table 3.3 along with the experimental measurements. Errors on the lattice results are statistical and include an uncertainty due to variation in the determination of the scale, though of course f_π is used to set the scale in the first place.

These results clearly agree well with those found in ref. [6], which gives us confidence in the correlation functions to be used later and also in the methods used to analyses these correlation functions.

3.3 Kaon B-Parameter B_K

The main uncertainties restricting the extraction of CKM matrix information from mixing in the neutral kaon system are the large theoretical uncertainties arising from the non–perturbative calculation of the matrix element of the $\Delta S = 2$ operator. We attempt this calculation by means of Lattice QCD.

For this calculation, we are interested in the matrix element of the four fermion operator,

$$\mathcal{O}^{\Delta S=2} = (\bar{s}\gamma_u(1-\gamma_5)d)(\bar{s}\gamma_u(1-\gamma_5)d), \tag{3.20}$$

which in practice requires calculation of the matrix element of the parity–even operator,

$$\mathcal{O}^{latt} = (\bar{s}\gamma^\mu d)(\bar{s}\gamma_\mu d) + (\bar{s}\gamma^\mu\gamma_5 d)(\bar{s}\gamma_\mu\gamma_5 d) = \mathcal{V} + \mathcal{A}. \tag{3.21}$$

The chiral symmetry of the lattice theory is explicitly broken by the inclusion of the Wilson term in the fermion action. As a result the operator $\mathcal{O}^{latt}$ mixes with operators of different chirality which are listed below,

$$
\begin{aligned}
\mathcal{O}^{STP} &= \frac{1}{24}\left[\mathcal{S}+\mathcal{T}+\mathcal{P}\right] \\
\mathcal{O}^{VA} &= \frac{-11}{96}\left[\mathcal{V}-\mathcal{A}\right] \\
\mathcal{O}^{SP} &= \frac{-1}{48}\left[\mathcal{S}-\mathcal{P}\right],
\end{aligned}
\tag{3.22}
$$

where we have used the notation,

$$
\begin{aligned}
\mathcal{S} &= (\bar{s}d)(\bar{s}d) \\
\mathcal{P} &= (\bar{s}\gamma_5 d)(\bar{s}\gamma_5 d) \\
\mathcal{V} &= (\bar{s}\gamma^{\mu} d)(\bar{s}\gamma_{\mu} d) \\
\mathcal{A} &= (\bar{s}\gamma^{\mu}\gamma_5 d)(\bar{s}\gamma_{\mu}\gamma_5 d) \\
\mathcal{T} &= \sum_{\mu<\nu}(\bar{s}\sigma^{\mu\nu} d)(\bar{s}\sigma_{\mu\nu} d).
\end{aligned}
\tag{3.23}
$$

We are interested in obtaining a meaningful value for the matrix element of the continuum operator with the correct chirality. In order to obtain this from a lattice calculation a two stage matching procedure must be undertaken. Firstly, the chiral behaviour of the lattice operator is corrected by perturbatively subtracting operators (3.22). Then, as is common with all lattice calculations, the lattice regularised operator must be matched to the continuum. This matching was originally done in ref. [59] up to order g^2. Resulting from this is an expression relating an operator with the correct chiral behaviour and matched to the continuum, $\left(\mathcal{O}^{\Delta S=2}\right)^{cont}$, with those which mix under renormalisation,

$$
\begin{aligned}
\left(\mathcal{O}^{\Delta S=2}\right)^{cont} = &\left(1+\frac{g^2}{16\pi^2}Z(r)\right)\mathcal{O}^{latt} \\
&+\frac{g^2}{16\pi^2}r^2 Z^*(r)\left[\mathcal{O}^{STP}+\mathcal{O}^{VA}+\mathcal{O}^{SP}\right]^{latt}.
\end{aligned}
\tag{3.24}
$$

Of the renormalisation constants calculated, $Z(r)$ is from the matching procedure and $Z^*(r)$ from the perturbative subtraction. These renormalisation coefficients have been calculated for the 'Clover' lattice action, [40],

$$
Z(r=1) = -10.9 \quad ; \quad Z^*(r=1) = 19.4, \tag{3.25}
$$

where r is the Wilson parameter. It is the matrix element of this perturbatively matched and corrected operator that is required for the calculation of the B-parameter.

A check of the matrix elements calculated on the lattice is offered by comparison with the chiral perturbation theory prediction, [48],

$$\langle \bar{K}^0 | (\bar{s}d\bar{s}d)_{LL} | K^0 \rangle = \gamma m_K^2 + \mathcal{O}(m_K^4). \tag{3.26}$$

In previous lattice studies, [1], this exact behaviour was not observed. Two reasons for this were suggested; imperfect perturbative subtraction of operators in determining the continuum matrix element and lattice artefacts with significant $\mathcal{O}(a)$ effects. To combat these problems in this study, we use Lepage Mackenzie 'boosted coupling' in the definition of the renormalised operator and an $\mathcal{O}(a)$ improved 'Clover' lattice action in the numerical calculation of the matrix element.

3.3.1 Lattice Calculation of the B-Parameter

The matrix elements for all the above operators are calculated on the lattice in the usual way, by evaluation of the three point function,

$$G(t_1, t_2) = \sum_{\vec{x},\vec{y}} \langle P_5^\dagger(\vec{x}, t_1) \mathcal{O}(\vec{0}, 0) P_5^\dagger(\vec{y}, t_2) \rangle \tag{3.27}$$

$$\begin{aligned}
&\xrightarrow[\text{large } N_t - t_1, t_2]{} \frac{Z_5}{(2m_K)^2} \langle K^0 | \mathcal{O} | \bar{K}^0 \rangle \exp\left(-m_K(N_t - t_1 + t_2)\right) \\
&\xrightarrow[\text{large } t_1, t_2]{} \frac{Z_5}{(2m_K)^2} \langle 0 | \mathcal{O} | \bar{K}^0 \bar{K}^0 \rangle \exp\left(-m_K(t_1 + t_2)\right).
\end{aligned} \tag{3.28}$$

where the asymptotic form obtained depends on the time ordering of the operators and alters the matrix element extracted. Here we have assumed negligible final state interactions and

$$\langle \bar{K}^0 \bar{K}^0 | P_5^\dagger | K^0 \rangle = \langle \bar{K}^0 | P_5^\dagger | 0 \rangle. \tag{3.29}$$

Both matrix elements will be needed for the calculation of the B-parameter.

Evaluation of the three point function defined in Equation (3.27) is done in the usual way by ensemble average over the 'eight' diagrams shown in Figure 3.2. In terms of quark propagators this corresponds to two traces which, including the relative minus sign due to a single fermion loop, can be written as,

$$\begin{aligned}
G(t_1, t_2) = 2 \{ & Tr\left[S(t_1)\Gamma\gamma_5\right] Tr\left[S(t_2)\Gamma\gamma_5\right] \\
& - Tr\left[S(t_1)\Gamma\gamma_5 S(t_2)\Gamma\gamma_5\right] \}.
\end{aligned} \tag{3.30}$$

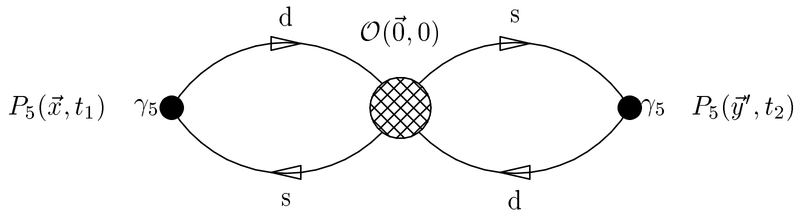

Figure 3.2: An 'Eight' diagram for the four fermion operator, $\mathcal{O}$, with pseudoscalar sources, P_5.

In calculating this, it is useful to define $S(t)$ as,

$$S(t)^{\alpha\beta}_{AB} = \sum_{\vec{x},C,\gamma} \left[S^\dagger_d(\vec{x},t;\vec{0},0)\right]^{\alpha\gamma}_{AC} S_s(\vec{x},t;\vec{0},0)^{\gamma\beta}_{CB}. \tag{3.31}$$

These untraced objects, $S(t)^{\alpha\beta}_{ab}$, are calculated at the outset. Then the matrix elements for all possible operators $\mathcal{O}$ required are determined from Equation (3.30) with traces over colour and spin indices for appropriate combinations of all 16 Dirac matrices Γ.

Often in lattice calculations it is preferable to calculate ratios of quantities rather than the quantities themselves, there being some cancellations of systematic and statistical uncertainties in the ratio. This is the case here, where it is more useful to extract the B-parameter as opposed to the matrix element itself. In particular we attempt to reduce statistical errors by taking the following ratio of three point and two point functions,

$$R(t_1,t_2) = \frac{G(t_1,t_2)}{C_5(t_1)C_5(t_2)} \rightarrow \frac{\langle\mathcal{O}\rangle}{Z_5}, \tag{3.32}$$

which is fitted to a constant which is proportional to the matrix element.

The B-parameter is extracted by fitting the values of the ratio, $R(t_1,t_2)$, as a function of $\frac{8}{3}(f_K m_K)^2/Z_5$. The form of this fit is suggested by chiral perturbation theory,

$$\frac{\langle K^0|\mathcal{O}|\bar{K}^0\rangle}{Z_5} = \alpha + (\gamma+\beta)x = a + bx \tag{3.33}$$

$$\frac{\langle 0|\mathcal{O}|\bar{K}^0\bar{K}^0\rangle}{Z_5} = \alpha + (\gamma-\beta)x = a + b' x \tag{3.34}$$

$$\text{where} \quad x = \frac{8}{3}\left(\frac{C_{A_4}(t)}{C_5(t)}\right)^2 \rightarrow \frac{8}{3}\frac{|\langle 0|A_4|\bar{K}^0\rangle|^2}{Z_5} = \frac{8}{3}\frac{(f_K m_K)^2}{Z_5}.$$

Both matrix elements are required to extract all individual fit parameters.

The B-parameter, at scale set by the lattice calculation, is then given by,

$$B_K(\mu) = Z_A^{-2}\gamma, \tag{3.35}$$

in terms of the axial current renormalisation constant.

In a theory where operator $\mathcal{O} = \mathcal{O}^{(\Delta S=2)}$ is properly renormalised, with the correct chiral behaviour, parameters α and β should vanish and B_K is extracted purely from parameter γ. We see that the operators with wrong chiral behaviour do tend to a constant with vanishing meson mass, as predicted by chiral perturbation theory. As a result there still remains a small discrepancy in the chiral behaviour of the $\Delta S = 2$ matrix element, the reason being that the operators with the wrong chirality were not subtracted completely. Comparison of this study with one using Wilson fermions, [1], can be used to study the effect of improved actions on these lattice artefacts.

3.3.2 Results for B_K

Three point function, 'eight' diagrams, were calculated as outlined in Equation (3.30) for the operators defined in Equations (3.21) and (3.22) and fully matched operator from Equation (3.24). To increase the statistics we use the symmetries of the quark propagators under time reversal, [48], to obtain the relation,

$$G(t_1, t_2) = G(N_t - t_2, N_t - t_1) = G(-t_2, -t_1), \tag{3.36}$$

which is then used to 'fold' the three point function onto its 'backward' half. In practise these three point correlators are only calculated for certain times, keeping $t_2 = 12$ fixed and allowing t_1 to vary.

The matrix elements for each kappa combination were calculated from the ratio of three point and two point functions define in Equation (3.32). Examples of these ratios are shown in Figure 3.3, the plots showing the heaviest and lightest mass combinations. Two plateaus can be seen corresponding to the two matrix elements. Fitting both these plateaus we extract the matrix elements for all six combinations of quark masses. The correlated its for these matrix elements are shown in Table 3.4, along with the fitting ranges and the correlated χ^2.

We study the chiral behaviour of these ratios by fitting the results to the form given in Equation (3.33). This was done for both linear and quadratic fits, to take

		$\langle K\vert\mathcal{O}\vert K\rangle/Z_5$	$\langle 0\vert\mathcal{O}\vert KK\rangle/Z_5$
0.14144	0.14144	-0.0290 (156)	0.1158 (115)
χ^2/dof		16/10	8.9/8
Fit range		[30,40]	[9,17]
0.14144	0.14226	-0.0204 (155)	0.0889 (111)
χ^2/dof		8.9/10	5.2/8
Fit range		[30,40]	[9,17]
0.14144	0.14262	-0.0098 (137)	0.0707 (134)
χ^2/dof		12/12	16/6
Fit range		[30,42]	[10,18]
0.14226	0.14226	0.0001 (133)	0.0647 (111)
χ^2/dof		8.1/12	4.0/8
Fit range		[30,42]	[9,17]
0.14226	0.14262	0.0085 (131)	0.0458 (123)
χ^2/dof		9.4/12	2.5/8
Fit range		[30,42]	[9,17]
0.14262	0.14262	0.0085 (160)	0.0271 (151)
χ^2/dof		7.2/5	0.19/5
Fit range		[37,42]	[12,17]
Linear Fits			
Intercept : a		0.031 (16)	0.022 (13)
Gradient : b		0.433 (140)	0.884 (93)
χ^2/dof		3.7/4	10/4
Quadratic Fits			
Intercept : a		0.044 (18)	0.032 (14)
Gradient : b		0.996 (404)	0.521 (238)
Curvature : c		3.523 (2345)	2.153 (1316)
χ^2/dof		1.4/3	7.2/3

Table 3.4: Values of $R = \langle O\rangle/Z_5$ for all κ combinations from correlated fits. Linear and quadratic fit parameters are also given.

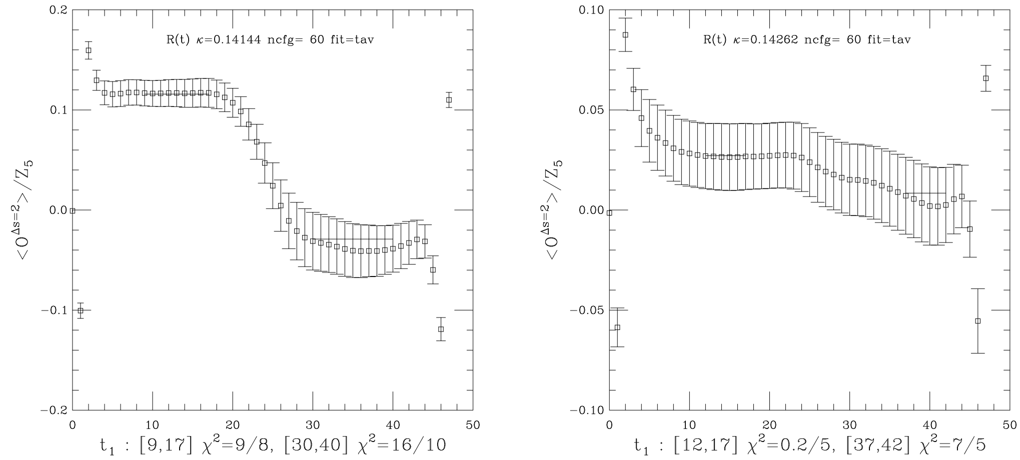

Figure 3.3: Ratio $R(t_1, t_2)$, as a function of t_1 ($t_2 = 12$, fixed), at $\kappa = 0.14144$ and $\kappa = 0.14262$ (best and worst case scenarios). Correlated fits shown with χ^2.

Parameter	Linear Fits	Quadratic Fits
α	0.026 (13)	0.038 (13)
β	−0.226 (88)	0.237 (199)
γ	0.658 (80)	0.759 (265)
δ	-	0.685 (1480)
ϵ	-	2.838 (1194)

Table 3.5: Separated linear and quadratic fit parameters.

into account the possibility of large $\mathcal{O}(m_K^4)$ corrections to the matrix elements. This chiral behaviour and the corresponding correlated linear and quadratic fits are shown in Figure 3.4. Estimates of parameters $\{a, b, c\}$ and $\{a, b', c'\}$ from correlated fits are also shown in Table 3.4, the introduction of parameters c and c' for a quadratic fit.

Within errors the intercepts of the fits to the two matrix elements agree. Estimates of the parameters $\{\alpha, \beta, \gamma\}$ are obtained from combinations of the fit parameters listed in Table 3.4. Defining $\alpha = a$, $\beta = (b - b')/2$, $\gamma = (b + b')/2$ and quadratic fit parameters $\delta = (c - c')/2$, $\epsilon = (c + c')/2$ the results of which are given in Table 3.5. The B-parameter is determined from the parameter γ.

Including the factors of Z_A we quote as values of B_K from linear and quadratic

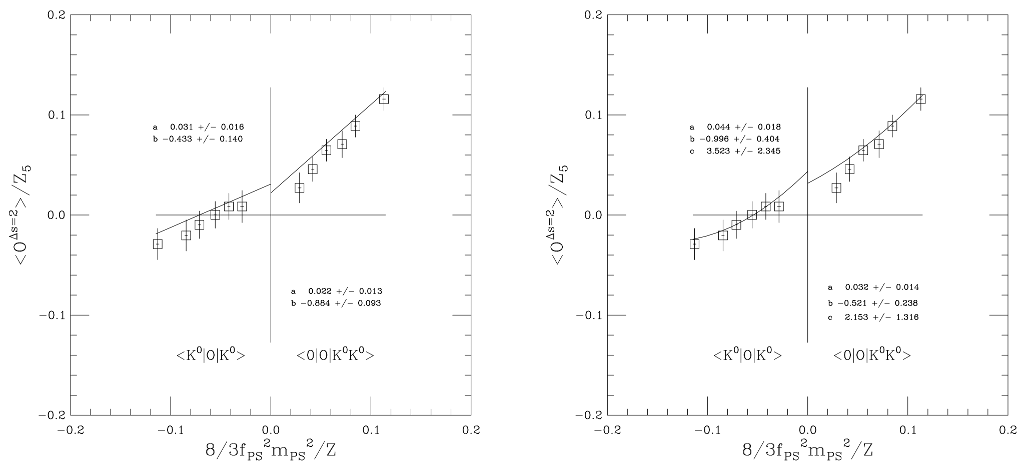

Figure 3.4: Linear and quadratic fits of $\langle \mathcal{O} \rangle / Z_5$ against $\frac{8}{3}(f_K^2 m_K^2 / Z_5)$.

fits,

$$\text{Linear} : B_K(\mu = 2.7\,\text{GeV}) = 0.66 \pm 0.08 \tag{3.37}$$

$$\text{Quadratic} : B_K(\mu = 2.7\,\text{GeV}) = 0.76 \pm 0.26. \tag{3.38}$$

At the scale $\mu = a^{-1} = 2.7$ GeV, taking $\Lambda_{QCD} = 200$MeV with $n_f = 3$, the renormalisation group invariant B-parameter is,

$$\hat{B}_K = (\alpha_{QCD})^{-\frac{2}{9}} B_K(\mu) = 0.88 \pm 0.11\,(\text{Linear}) \tag{3.39}$$

$$= 1.02 \pm 0.35\,(\text{Quadratic}). \tag{3.40}$$

The values obtained for B_K from the linear and quadratic fits agree within errors. However, it was observed that the results obtained from the linear fits were much more stable with the variation in time fitting ranges used to extract the matrix elements from the three point functions. This and the smaller error estimates leads us to quote the results from the linear fits as a final answer.

3.3.3 Comparison with the Wilson Action

The inclusion of the Wilson term to avoid the fermion doubling problem breaks the chiral symmetry of Lattice QCD. These lattice artefacts are a particular problem in the calculation of the kaon B-parameter, which relies on the chiral

Parameter	α	β	γ
Linear Fits (Wilson)	0.080 (30)	0.012 (185)	0.871 (24)
Linear Fits (Clover)	0.026 (13)	0.266 (88)	0.658 (80)

Table 3.6: Results for B-parameter from calculations with Wilson and Clover fermions. (Taken from [1].)

behaviour of the matrix elements for an accurate determination of B_K. It might seem that by reducing these $\mathcal{O}(a)$ effects it could be possible to improve the chiral behaviour for B_K. One of the main aims of this calculation was to see if the use of an $\mathcal{O}(a)$ improved action did in fact offer improved chiral behaviour of the $\Delta S = 2$ matrix element.

The calculation of the kaon B-parameter was originally done by the European Lattice Collaboration, [1], with Wilson fermions on 15 configurations at $\beta = 6.2$ and on a 24^3 lattice. They find,

$$B_K(\mu) = 0.60 \pm 0.20, \qquad \text{quadratic} \tag{3.41}$$

$$= 0.88 \pm 0.20, \qquad \text{linear} \tag{3.42}$$

for the B-parameter, using the values from linear and quadratic fits. Although the actual values of the matrix elements were not quoted kappa by kappa, it was possible to obtain estimates from the graph in the paper, shown in Figure 3.5. We construct a set of jacknife clusters from these estimates and apply the same analysis used to produce the Clover results, in an attempt to obtain a comparison between the two actions for B_K. Unfortunately, these were only estimates to the original data, so there is a small discrepancy between the results quoted in the paper, and those calculated in this analysis. Also, it was not possible to determine the raw matrix element results accurately enough to allow a quadratic fit, which was found to be especially sensitive to small changes in the fitted points.

If the lattice version of the $\Delta S = 2$ operator has the correct chiral behaviour the parameters α and β in Equation (3.33) should vanish. Of these, the intercept α is the most difficult to correct for, [60]. In comparing Wilson and Clover results we take the value of α as the criterion for the 'goodness' of the chiral behaviour of the matrix elements. The values of the fit parameters $\{\alpha, \beta, \gamma\}$ from linear fits are shown in Table 3.6 with errors quoted only for the Clover action results.

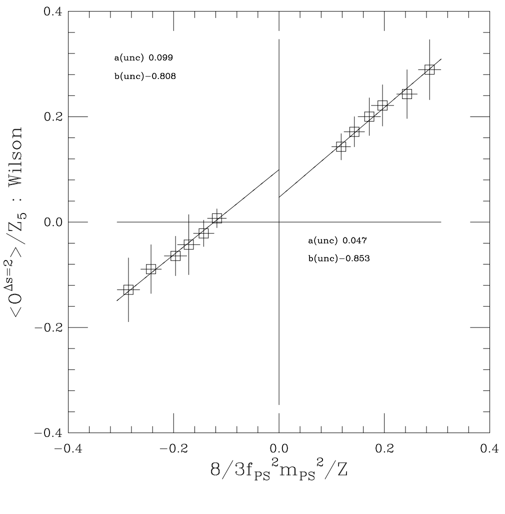

Figure 3.5: Chiral behaviour of the $\Delta S = 2$ operator for Wilson fermions. (Taken from [1].)

From the examination of Table 3.6 it is not possible to determine any definite improvement due to use of the Clover action, though comparisons of the intercepts might suggest a slight improvement. Only through analysis with a fuller set of data in the Wilson case may it be possible to compare these two methods in a more quantitative way. These findings were confirmed by those presented in ref. [61] which compared Wilson and Clover results from simulations at $\beta = 6.0$.

3.3.4 Conclusions

The kaon B-parameter is an important phenomenological quantity, introduced in the theoretical analysis of neutral kaon mixing. An accurate calculation of B_K is required for tightening constraints on the CKM matrix elements while exploring CP violation in the Standard Model. B_K itself, describes all the non–perturbative strong interaction effects on the $\Delta S = 2$ effective operator which drives this weak mixing process.

At present, Lattice QCD offers the only way to calculate the non–perturbative contributions to these weak matrix elements with no model assumptions. In this Chapter we have outlined a method of calculating B_K from Lattice QCD using an $\mathcal{O}(a)$ improved action. We find,

$$B_K(\mu = 2.7\text{Gev}) = 0.66 \pm 0.08, \tag{3.43}$$

which is consistent with others calculations performed with different fermion actions. At present the method and data used was too crude to determine any significant improvement in the chiral behaviour of the matrix elements over the calculation with Wilson fermions.

The main problems encountered in this study arose from two main sources; extraction of the matrix elements from the three point functions and fitting the chiral behaviour of these matrix elements to extract the B-parameter. A possible improvement for the former problem could be through the use of smeared quark propagators. These have been used widely to improve the signal in heavy light calculations and could offer the same advantage to this calculation.

The problem involved in extracting B_K from the chiral behaviour of the matrix elements is more difficult to solve, as it is intrinsic to the use of Wilson formulation of fermions on the lattice. A 'quick fix' can be implemented by adopting the programme of improved perturbative subtraction suggested by Bernard in ref. [48]. Another possibility is to include results from correlation functions of pseudoscalar mesons with non–zero momentum. With these additional results it is possible to extract the fit parameters and B_K from the $\langle \bar{K}^0|\mathcal{O}|K^0\rangle$ matrix element only. This would avoid using the other matrix element which is prone to final state interactions. Perhaps the only way to fully remove the problem of incomplete perturbative subtraction is to match the continuum and lattice operators by non–perturbative methods. This procedure has been attempted for simpler operators, [62], with the aim of applying these non–perturbative renormalisation techniques to the $\Delta S = 2$ operator.

Chapter 4

B-Physics from Lattice QCD

B–Physics is without doubt a fashionable topic in Particle Physics, so much so that grant funding bodies around the world are willing to spend billions on dedicated B–factories. Such interest is not unfounded as B–Physics holds a vital position in testing the consistency of the Standard Model and probing the New Physics that may lie beyond. B–decays offer one of the best possibilities for the measurement of five of the nine CKM matrix elements, including the least well known ones, as well as the possibility of exploiting top quark dependencies to constrain m_t.

In this chapter we discuss one example of B–Physics, $B^0\bar{B}^0$ mixing, and in particular the role that Lattice QCD can play in extracting constraints on CKM matrix elements from this process. In short, this is an attempt to reduce some of the theoretical uncertainties introduced by the strong interaction effects on this decay. In order to do this, it is necessary to introduce some lattice technology required to deal with heavy quarks, and apply this to determine the decay constant of the B–Meson, a vital parameter in B–mixing and one that poses considerable theoretical difficulties.

4.1 Mixing in the Neutral B–System

In Chapter 3, we attempted to study one aspect of CP violation in the kaon system, experimentally seen as neutral meson mixing and quantified by CP violating parameter ϵ_K. Mixing has also been observed in the neutral B–system ($B^0\bar{B}^0$ mixing first seen at ARGUS, [63], but also observed at the LEP experiments and at the Tevatron). However, no CP violation has been observed in this system.

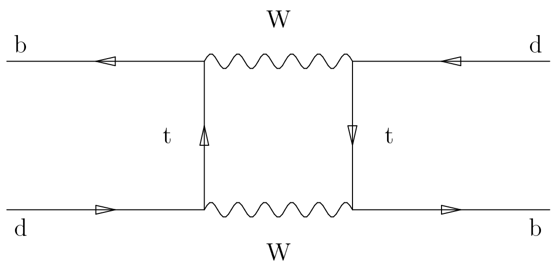

Figure 4.1: Box diagram contributing to CP violation in neutral B mixing. Loop contributes from the top quark only.

The size of the CP violating parameter, ϵ_B, is negligbly small and in what follows we will ignore CP violating effects, i.e. $|B_{H,L}\rangle = |B^0\rangle \pm |\bar{B}^0\rangle$. Instead, in this chapter we consider $B^0\bar{B}^0$ mixing in terms of the theoretical input required to extract accurate estimates of the CKM matrix elements and in particular a calculation of the strong interaction effects entering this process.

Mixing in the B_d system is similar to kaon mixing, with the second order weak process governed by a low energy effective theory. The mixing parameter, x_d, defined in terms of the $B_{H,L}$ mass difference, Δm and decay width, Γ, arises in a similar manner to the kaon system from the box diagram, Figure 4.1. This is now dominated by the top quark contribution, giving,

$$x_d = \frac{\Delta m}{\Gamma} = \tau_B \frac{G_F^2 M_W^2}{6\pi^2} \eta_{QCD} m_B f_B^2 B_B S(x_t) |V_{td}|^2. \tag{4.1}$$

This theoretical expression for the mixing parameter is defined in terms of the B lifetime, τ_B, a known function $S(x_t)$, [54] and the perturbative QCD corrections contained in η_{QCD}, [56]. Here the non–perturbative contributions are contained in the matrix element of the $\Delta B = 2$ operator of the low energy effective theory responsible for the mixing. Again, the matrix element is compared with the vacuum saturation approximation and is parameterised by the decay constant, f_B and B–parameter, B_B,

$$\frac{8}{3} B_B f_B^2 m_B^2 = \langle B^0 | (\bar{b}(1-\gamma_5)d)(\bar{b}(1-\gamma_5)d) | \bar{B}^0 \rangle. \tag{4.2}$$

Most estimates of B_B indicate only small deviations from the vacuum saturation approximation, $B_B \approx 1$, with a recent lattice calculation, [64], giving $B_B = 1.16 \pm 0.07$.

Experimentally, the x_d parameter was measured in e^+e^- scattering at the $\Upsilon(4S)$ energy, creating $B^0\bar{B}^0$ pairs. The B_L and B_S have different masses and decay with different frequencies. One method to measure the mixing is to measure the probability of a B^0 decaying to a $\bar{B}^0$ integrated over time. This time integrated mixing can be characterised by a ratio, r,

$$r = \frac{x^2}{2+x^2} = \frac{N(B^0B^0) + N(\bar{B}^0\bar{B}^0)}{N(B^0\bar{B}^0)} \tag{4.3}$$

in terms of numbers of pairs that mix and then decay, compared to those that just decay. Results from CLEO and ARGUS, [65, 66] quote,

$$x_d = 0.66 \pm 0.11. \tag{4.4}$$

Similar quantities have been measured at LEP, [67, 68, 69, 70], (at the Z resonance, $Z \to b\bar{b}$, and the B hadrons decay semileptonically) and also at $p\bar{p}$ colliders at CERN (UA1) and Fermilab(CDF).

Also of interest is the mixing in the B_s system, which has recently been observed at ALEPH. Knowledge of this would offer an accurate measure of $|V_{td}/V_{ts}|$ without relying on a measurement of m_t,

$$\frac{x_d}{x_s} = \left|\frac{V_{td}}{V_{ts}}\right|^2 \frac{\tau_{B_d}\eta_{B_d}m_{B_d}}{\tau_{B_s}\eta_{B_s}m_{B_s}} \left(\frac{f_{B_d}^2 B_{B_d}}{f_{B_s}^2 B_{B_s}}\right). \tag{4.5}$$

The factors multiplying the CKM matrix elements are $SU(3)$ symmetry breaking terms. This offers another constraint on the CKM matrix elements, though a measurement of x_s is experimentally more difficult, requiring time dependent analyses of the mixing[1].

Although smaller branching ratios of B decays, compared to kaon decays, make the experimental study more difficult, the shear variety of possible decays makes neutral B mesons a rich source for the study of the CKM matrix. Future possible avenues of study arise from the time dependent $B^0 \to J/\psi\, K_s, (\pi^+\pi^-)$ decays, containing both mixing and direct CP violation, offering direct measurement of all the angles of the unitarity triangle.

However, there is still a major obstacle to extracting accurate values of the CKM matrix elements. The top quark mass is not accurately known and, more

[1]the evolution of $B^0(\bar{B}^0)$ states is time dependent, with probabilities of finding $B^0(\bar{B}^0)$ states a time t later are given by, $W_{B^0(\bar{B}^0)}(t) = \frac{1}{2}e^{-\Gamma t}\left(1 \pm \cos\left(\Delta m t\right)\right)$.

importantly for us, there are large theoretical uncertainties in the value of f_B. An accurate determination of f_B would also have important phenomenological implications for the predicted sizes of the CP asymmetries to be studied at future colliders. One attempt to overcome these difficulties is through a non–perturbative calculation of this weak matrix element, by Lattice QCD.

4.2 Heavy Quarks on the Lattice

The scale and resolution of the processes which can be studied by Lattice QCD is determined by the lattice spacing, a. This is typically ~ 0.1 fm, corresponding to scales $a^{-1} \sim 2 - 3$ GeV. In order to minimise the effect of simulating the field theory on a discrete lattice and to fully resolve all important detail, it is only possible to study phenomena on length scales large compared to the lattice spacing. Clearly this causes a major problem when studying systems involving b quarks on the lattice. Simulating quarks with such a large mass,

$$m_b \sim 5\,\mathrm{GeV} \gg a^{-1} \sim 2 - 3\,\mathrm{GeV},$$

the Compton wavelength of the b quark is smaller than the lattice spacing and it could 'see' the granularity of the lattice.

To overcome the difficulties in simulating b quarks at their physical masses, three approaches are often followed;

- simulate quarks with masses well below the true b quark mass, usually around the charm mass. Then extrapolate in terms of pseudoscalar meson mass to the the true B-meson mass, [71, 36]. This may introduce uncertainties arising from $\mathcal{O}(m_Q a)$ effects and the extrapolation.

- treat the heavy quark in the non–relativistic approximation and make a formal expansion of the action in powers of heavy quark velocity. The free parameters in Non Relativistic QCD (NRQCD) are fixed from comparison with the Υ or $J/\psi/\eta_c$ states, [72].

- follow the approach introduced by Eichten, [73], and treat the propagation of heavy quarks by means of an effective field theory, in particular in the infinite quark mass, or static limit.

This last approach will be followed thoughout this work.

4.2.1 Heavy Quark Symmetry

In studying an infinitely heavy quark, the dynamics involved are greatly simplified and QCD gains two new symmetries. Heavy–light systems, such as the B-meson, are particularly useful examples for an introduction to Heavy Quark Symmetry (HQS), with an intuitive understanding offered by simple analogies in atomic physics. Indeed, the B-meson is sometimes referred to as the 'hydrogen atom of QCD'. Such a system has a very heavy quark at the centre of the meson, which is not affected greatly by interaction with the light degrees of freedom. This approximation holds well if the heavy quark mass is much greater than typical momentum transfers within the meson,

$$m_Q \gg \Lambda_{QCD}. \tag{4.6}$$

This is well satisfied for the b quark, but with sizable corrections for the charm quark ($\Lambda_{QCD}/m_c \sim 10\%$). In this limit the heavy quark can be thought of as a static colour source creating a field in which the light quarks and gluons move. This static colour source propagates in time only, with small perturbations due to the interactions with light degrees of freedom. These light degrees of freedom are the 'brown muck' of QCD, whose behaviour is non–perturbative.

With this picture of a heavy light system in mind, how can the new symmetries of QCD be understood?

- flavour symmetry:
  The light degrees of freedom of these systems are the same for all heavy quarks that are heavy enough. In other words, it is not possible to discriminate between the brown muck around different flavours of quarks which satisfy the heavy quark condition. In terms of atomic physics, this is analogous to the isotope effect, the electronic structure of the atom is independent of the number of neutrons in the nucleus.

- spin symmetry:
  The spin of a quark arises from the chromo–magnetic moment, $\mu = g/2m_Q$. This decouples from the theory in the infinite mass limit, the brown muck being oblivious to the spin of the heavy quark. This is also seen in the hydrogen atom analogy, where the hyperfine splitting is dependent on the magnetic moment of the nucleus.

These heavy quark symmetries, first developed by the authors of refs. [74, 75], have been exploited in two main areas; the mass spectra of systems containing a heavy quark can be related using the predictions of HQS, [76], and the matrix elements involved in semi–leptonic B decays can be related in terms of a universal form factor, ξ, the Isgur–Wise function, [77]. Of course to actually calculate these quantities it is necessary to first turn to non–perturbative methods, such as Lattice QCD, to determine the dynamics of the brown muck. For example, the Isgur Wise function has been calculated on the lattice in ref. [78].

The heavy quark symmetries of QCD are only exact in the infinite mass limit. For quarks with a finite mass it is necessary to consider Λ_{QCD}/m_Q symmetry breaking corrections. The Heavy Quark Effective Theory (HQET) has been developed to deal with these corrections in a systematic way. In the next section we outline the HQET and obtain a form for the heavy quark propagator in the infinite mass, static limit.

4.2.2 Heavy Quark Effective Theory

Effective theories are often used in physics when the full theory is intractable. By extracting the important aspects of the full theory, however, some head way can be made by the approximation embodied in the effective theory. One well known example of such an effective field theory is chiral perturbation theory, used to study light quark physics at low momenta. Clearly, heavy quark physics, with the new symmetries outlined above, offers an ideal candidate for description by an effective field theory. In this case the mass of the heavy quark is an irrelevant degree of freedom and is removed in formulating the effective theory. A full field theoretic derivation of HQET from the QCD Lagrangian, including the $1/m_Q$ corrections can be found in [79]. Here instead we outline a simpler treatment to extract the first term in the effective Lagrangian motivated by the physical ideas of heavy quark symmetry. The $1/m_Q$ corrections will only be mentioned later in a slightly different context, where they are treated as perturbations to this leading term, Section 5.3.

We begin by determining the Feynman rules of the HQET. The heavy quark symmetry is introduced by parameterising the meson momentum, P^μ_{meson},

$$P^\mu_{meson} \approx p^\mu = m_Q v^\mu + k^\mu, \tag{4.7}$$

in terms of the heavy quark velocity, v^μ, which explicitly introduces the heavy quark mass dependence, and a residual momentum, k^μ. The heavy quark is now nearly on-shell, with its motion characterised by the velocity, defined to satisfy,

$$\not{v}\not{v} = v \cdot v = 1. \tag{4.8}$$

This residual momentum characterises all the small perturbations due to interactions with the light degrees of freedom and acts as a measure of how far the quark is off shell.

In the $m_Q \to \infty$ limit, the usual QCD Feynman rules for the fermion propagator and fermion-gauge interaction become,

$$\frac{i}{\not{p} - m_Q} \to \frac{i}{v \cdot k}\frac{1+\not{v}}{2} \tag{4.9}$$

$$-ig\gamma^\mu \frac{\lambda^a}{2} \to -igv^\mu \frac{\lambda^a}{2}. \tag{4.10}$$

The projection operator, $(1 \pm \not{v})/2$, defines the heavy quark field in terms of a two component spinor, h_v, which satisfies, $\frac{(1+\not{v})}{2} h_v = h_v$. In perturbative calculations with these Feynman rules, the projection operators can always be connected with spinors h_v, as a result of which the projection operators can be omitted from the Feynman rules. These projection operators separate field components for heavy quark and anti–quark, which must now be treated as completely independent fields. The rules clearly contain the essence of the heavy quark symmetry, in that they are independent of the heavy quark mass, and contain no spin dependence. The effective field theory from which these Feynman rules are obtained is described by the effective Lagrangian, [80],

$$\mathcal{L}_v^{eff} = i\bar{h}_v v_\mu D^\mu h_v, \tag{4.11}$$

for a heavy quark field, h_v, propagating with velocity v, and related to the original quark fields by, $Q(x) \approx e^{im_Q v \cdot x} h_v(x)$. This is the leading term in the HQET Lagrangian.

In what follows later, we use the static limit of this effective field theory. The static Lagrangian describes a heavy quark in its rest frame, $v = (1, \vec{0})$, [81],

$$\mathcal{L}_{static}^{eff} = h^\dagger i D^0 h. \tag{4.12}$$

Although the perturbative expansion offers a simple expression for the free propagator of a heavy quark, from a lattice point of view we are interested in evaluating a Path Integral using the heavy quark propagator in a background field. This is found from the solution of,

$$D^0 S_h(x,y) = \delta^{(4)}(x,y). \tag{4.13}$$

Constructing a suitable lattice version of the covariant derivative, a solution for the propagator exists in terms of a product of link variables in the time direction,

$$S_h(x,y) = \delta^{(3)}(\vec{x}-\vec{y})\theta(x^4-y^4)U_4^\dagger(\vec{x},x^4-1)U_4^\dagger(\vec{x},x^4-2)\ldots U_4^\dagger(\vec{x},y^4), \tag{4.14}$$

for a forward propagating heavy quark. Similar solutions exist for heavy anti–quarks.

An alternative path to this propagator, offering a heuristic derivation of the HQET, can be obtained directly from the QCD Lagrangian. In the static limit the quark mass is much greater than other momentum scales. The equation for a quark propagator in terms of the Dirac operator simplifies to,

$$(\gamma_0 \mathcal{D}_0 + m_Q)S_0(x,y) = \delta^{(4)}(x,y). \tag{4.15}$$

This has as formal solution,

$$\begin{aligned} S_0(x,y) = \mathcal{P}_{\vec{x}}\left(\begin{array}{c} y^4 \\ x^4 \end{array}\right)\delta(\vec{x}-\vec{y})\Big[&\theta(y^4-x^4)\exp\left(-m_Q(y^4-x^4)\right)\left(\frac{1+\gamma_4}{2}\right) \\ &+\theta(x^4-y^4)\exp\left(m_Q(x^4-y^4)\right)\left(\frac{1-\gamma_4}{2}\right)\Big], \end{aligned} \tag{4.16}$$

for the heavy quark propagator. $\mathcal{P}_{\vec{x}}$ is the Polyakov phase picked up as the static quark propagates in time in a background field which contains all gluonic interactions. This is defined as the path ordered integral of the gauge fields,

$$\mathcal{P}_{\vec{x}}\left(\begin{array}{c} y^4 \\ x^4 \end{array}\right) = \mathcal{P}\exp\int_{x^4}^{y^4} dz A_4(\vec{x},z). \tag{4.17}$$

The utility of calculating this propagator on the lattice is its simple form. The Polyakov phase was met earlier in constructing a gauge invariant fermion action which for the lattice version was constructed from link variables, $U_\mu(\vec{x},t)$. Clearly this static propagator is now just a time ordered product of links in the time direction,

$$\mathcal{P}_{\vec{x}}\left(\begin{array}{c} y^4 \\ x^4 \end{array}\right) \equiv \left\{\begin{array}{ll} U_4(\vec{x},x^4)U_4(\vec{x},x^4+a)\ldots U_4(\vec{x},y^4-a) & (y^4>x^4) \\ U_4^\dagger(\vec{x},x^4-a)U_4^\dagger(\vec{x},x^4-2a)\ldots U_4^\dagger(\vec{x},y^4) & (x^4>y^4) \end{array}\right. . \tag{4.18}$$

This is known as a Wilson line and corresponds to a static quark hopping in time on a constant spatial lattice site. When quark fields have been rescaled and spin dependencies reintroduced, the heavy quark propagator from Equation (4.18) and HQET agrees with the form given in Equation (4.16).

In the absence of practical lattice calculations with b quarks at their physical mass, this static heavy quark propagator offers an interesting and useful approach to heavy quark physics and one which can be obtained without the computationally expensive inversion of the full Dirac matrix. However, before these can used to probe heavy quark physics, it is necessary to consider the effect of the matching procedure when using an effective field theory. In principle there are now three field theories that need to be matched; full continuum QCD, the continuum effective field theory and the effective field theory defined with a lattice regulator, all of which can provide perturbative expansions. Historically the perturbative calculation of the renormalisation constants was carried out in two parts,

- firstly relate the 'full' continuum operators to the corresponding operators in the continuum effective theory,
- then match the continuum effective theory to the effective theory on the lattice.

This can be done in one step, by requiring the quantum corrections of full continuum QCD match those of the effective field theory on the lattice.

This concludes the outline of the HQET and in particular the definition of the heavy quark propagator in the infinite mass limit. However, practical calculations in the static limit require the introduction of a piece of lattice technology, smeared interpolating operators.

4.3 Smeared Interpolating Operators

Calculating matrix elements and particle masses in the static limit introduces problems with the extraction of the ground state from the large time behaviour of the Euclidean correlators. For example, consider the zero momentum two point correlator of operator $\mathcal{O}(\vec{x},t)$ which has quantum numbers suitable for study of hadrons, h. On inclusion of a complete set of states, this becomes,

$$C(t) = \sum_{\vec{x}} \left\langle \mathcal{O}(\vec{x},t)\mathcal{O}^{\dagger}(\vec{0},0) \right\rangle$$

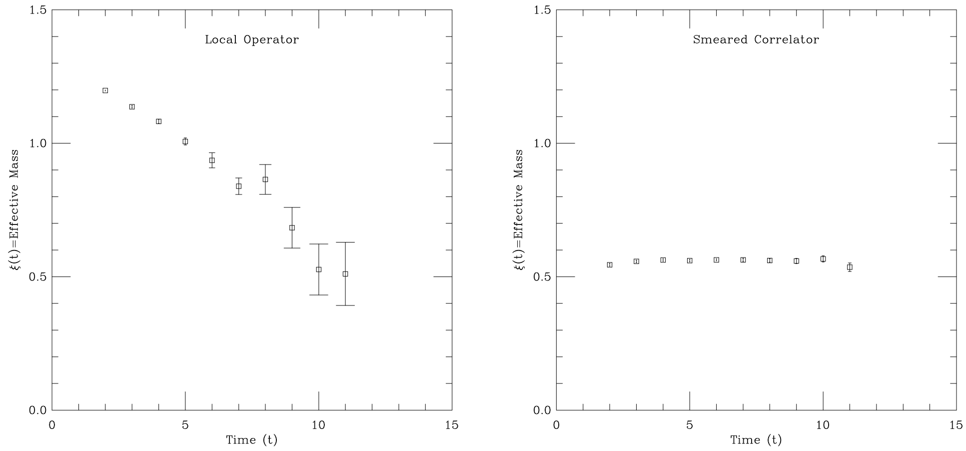

Figure 4.2: Effective mass plots from local and smeared operators.

$$= \frac{|\langle 0|\mathcal{O}(0)|h_0\rangle|^2}{2E_0} \exp(-E_0 t) a(t) \tag{4.19}$$

$$\text{where,} \quad a(t) = \left(1 + \sum_{n=1}^{\infty} \frac{E_0}{E_n} \frac{|\langle 0|\mathcal{O}(0)|h_n\rangle|^2}{|\langle 0|\mathcal{O}(0)|h_0\rangle|^2} \exp(-(E_n - E_0)t)\right). \tag{4.20}$$

Included in a complete set of states is an infinite tower of energy levels with $|h_0\rangle$ the lightest hadronic state, and $|h_n\rangle$ the nth excited state. In all lattice calculations it is hoped that this lightest state dominates in the asymptotic time limit and $a(t) \to 1$. The approach of $a(t) \to 1$ requires contributions from the excited states to be exponentially damped in time and depends crucially on the choice of interpolating operators. However, with local operators in static correlators, it is often not possible to take a large enough time length to isolate the ground state plateau, before statistical noise swamps any signal. Added to this are large excited state contaminations introduced by the closeness of the ground and first excited states. This can be seen clearly in the comparison of effective mass plots from correlators of the local axial current and a smeared current in Figure 4.2. For correlators with exponential time behaviour, $C(t) = Z\exp(-mt)$, the effective mass is defined as, $m^{eff}(t) = \frac{C(t)}{C(t+1)}$. The correlator from local current never achieves an asymptotic value and statistical errors dominate in the large time limit. One way to improve this situation is through the use of extended or 'smeared' interpolating operators.

Interpolating operators for matrix elements are only required to have the correct quantum numbers to connect the two external states, leaving a degree of arbitrariness in their definition. This arbitrariness is exploited in smearing. The idea behind smearing involves choosing an interpolating operator which increases the overlap between the operator and the ground state, thus increasing the signal from this state. The aim of this is to extract a clean ground state signal for as small times as possible, before statistical errors dominate the signal. Local operators only sample the current at a single point, x say, whereas extended operators include contributions to the operator from the current at neighbouring lattice sites,

$$\mathcal{O}^S_\Gamma(\vec{x},t) \equiv \sum_{\vec{y}} \bar{Q}(\vec{y},t) f^S(\vec{x},\vec{y}) \Gamma q(\vec{x},t). \tag{4.21}$$

$\mathcal{O}^S_\Gamma$ is an example of a smeared operator for the current, $\bar{Q}\Gamma q$, with a general smearing function, $f^S(\vec{x},\vec{y})$. Such smearing functions can be generated in many different ways and we compare calculations using both gauge fixed smearing functions and those calculated in a gauge invariant fashion. Within these two classes the smearing functions are 'optimised' by including different forms for the wavefunction used to approximate the heavy quark and by varying the extent of the smearing function. For example, the smeared correlator shown in Figure 4.2, uses a groundstate exponential smearing function of radius, $r_0 = 5$ lattice units and generated in the Coulomb gauge. A great deal of work has been done on this optimisation, one example using multi–state smearing methods, which accounts for contributions from excited states, [3].

On a point of notation we refer to a smeared correlator, $C^{RS}(t)$, say, as smeared with source of type S and with sink of type R. Such a distinction becomes particularly important when dealing with correlation functions with one interpolating operator left local, equivalent to, $f^L(\vec{x},\vec{y}) = \delta^{(3)}(\vec{x}-\vec{y})$[2]. Although (SL), local source smeared sink, and (LS), smeared source and local sink, are equal in the limit of infinite configurations, for a finite sample the statistical errors are greatly reduced for the LS case. This can be understood from the form of the correlators; LS correlators sample the quark propagators over many spatial lattice points, whereas SL correlators contain only contributions from $\vec{x} = \vec{0}$. A good example of this occurs in the determination of f_B^{static}. This involves the

[2] LS correlators are required to extract local matrix elements.

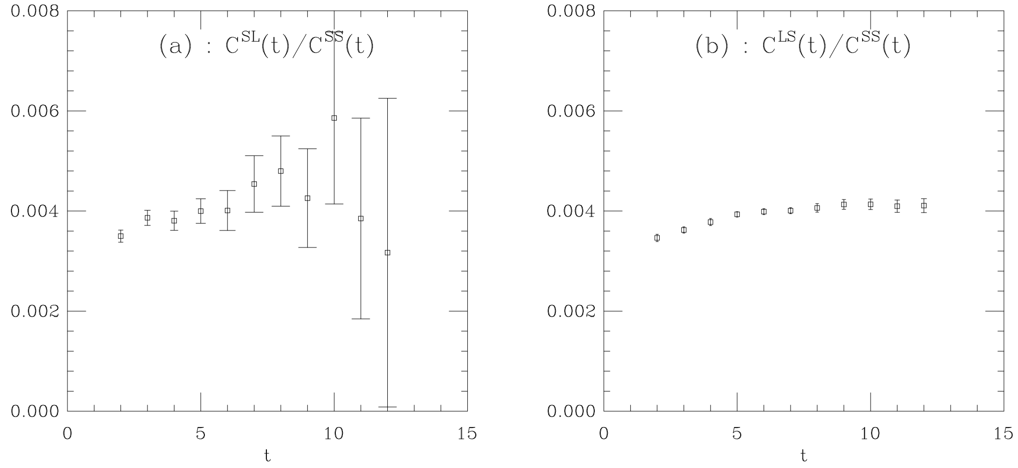

Figure 4.3: Ratios (a) $C^{SL}(t)/C^{SS}(t)$ and (b) $C^{LS}(t)/C^{SS}(t)$. Correlators for pseudoscalar mesons with the heavy quark treated in the static limit, and smeared with gauge invariant smearing.

calculation of the ratio, $Z^L/Z^S = C^{SL}(t)/C^{SS}(t)$, or $C^{LS}(t)/C^{SS}(t)$, with the graphs of the two ratios compared in Figure 4.3.

In practise, the smeared correlators are generated from a set of smeared heavy propagators. For example, consider a general smeared–smeared two point correlator,

$$C_\Gamma^{RS}(t) = \sum_{\vec{x},\vec{y},\vec{z}} \left\langle \left(\bar{Q}(\vec{y},t) f^R(\vec{y},\vec{x}) \Gamma q(\vec{x},t)\right) \left(\bar{q}(\vec{0},0) f^S(\vec{z},\vec{0}) \Gamma Q(\vec{z},0)\right)\right\rangle \quad (4.22)$$

$$= -\sum_{\vec{x},\vec{y},\vec{z}} Tr\left\{S_q(\vec{x},t;\vec{0},0)\Gamma f^R(\vec{y},\vec{x}) S_Q(\vec{z},0;\vec{y},t) f^S(\vec{z},\vec{0})\Gamma\right\}. \quad (4.23)$$

Typically we calculate a set of smeared propagators,

$$S_Q^{RS}(\vec{x},t;\vec{0},0) = \sum_{\vec{y},\vec{z}} f^R(\vec{y},\vec{x}) S_Q(\vec{y},t;\vec{z},0) f^S(\vec{z},\vec{0}). \quad (4.24)$$

This is especially useful when dealing with static quark propagators, where the propagator is a product of links, and the data requirements are more manageable.

Having explained the need for smearing, we now turn to the actualities of the smearing techniques applied in the rest of this work. A comparison of these different techniques is included later, with reference to the smeared operator 'test–bed' calculation, f_B^{static}.

4.3.1 Coulomb Gauge Smearing

Historically, the first use of extended operators considered a smearing function consisting of a simple sum of delta functions, [82]. This method produced smearing sources which were not gauge covariant. To obtain a signal from a gauge dependent object, smearing functions in a fixed gauge were introduced. The Coulomb gauge was chosen for its simple application, gauge fixing at each timeslice independently. The first smearing functions considered in ref. [83], were simple 'cubes'. These consisted of the local current sampled at all points in a cube of spatial lattice sites, with contributions weighted equally,

$$f^{cube}(\vec{x},\vec{y}) = \begin{cases} 1 & a \,\text{and}\, b \,\text{and}\, c \leq r_0 \\ 0 & \text{otherwise} \end{cases} , \tag{4.25}$$

where we define $(a,b,c) = \vec{x} - \vec{y}$ as the position relative to the centre of the smearing function. Variations of this simple form have been used. A doubly smeared cube was constructed from a convolution of the cube with itself,

$$f^{double}(\vec{x},\vec{y}) = \begin{cases} (1-\frac{a}{2r_0}) \times (1-\frac{b}{2r_0}) \times (1-\frac{c}{2r_0}) & a \,\text{and}\, b \,\text{and}\, c \leq 2r_0 \\ 0 & \text{otherwise} \end{cases} , \tag{4.26}$$

and exponential smearing functions,

$$f_n^{exp}(\vec{x},\vec{y}) = r^n \exp\left(-r/r_0\right), \qquad r = \sqrt{a^2+b^2+c^2}. \tag{4.27}$$

These exponential smearing functions were motivated by the wavefunctions of the hydrogen atom, which also offer the possibility of studying excited states. Examples of these smearing functions are shown in Figure 4.4.

All of these smearing functions introduce some average length scale, corresponding to the extent of the smearing. Following earlier work studying a variety of smearing radii, [84], we choose $r_0 = 5$ lattice units for cube, double and exponential smearing functions.

Although the Coulomb gauge smearing technique allowed for greater flexibility in the actual smearing functions used, it did have certain drawbacks, mainly the shear computational effort required. Not only was it necessary to calculate the gauge transformations numerically, though these could be reused elsewhere, but to apply the smearing functions to create smeared quark propagators was also numerically intensive. Take, for example, the worst case scenario of construction of smeared smeared correlators. The computation required to smear a

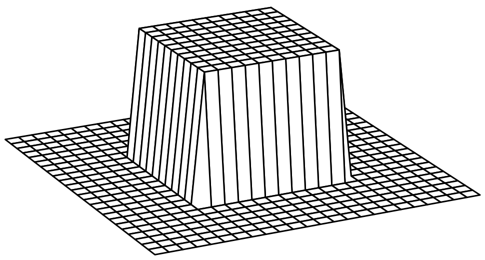

Cube Smearing

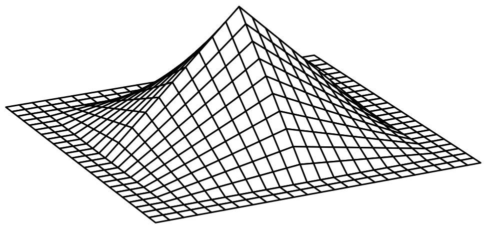

Double Smearing

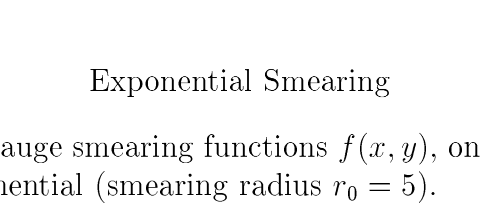

Exponential Smearing

Figure 4.4: Coulomb gauge smearing functions $f(x,y)$, on a 24^2 grid using cube, double cube and exponential (smearing radius $r_0 = 5$).

heavy propagator goes as n^2, where $n = 24^3$ (the extent of the smearing function) is a large number. For the selection of smearing functions used, this was a considerable computational overhead. A possible way to reduce this was to use a fast fourier transform to compute the convolution of smearing functions for the smeared smeared case, [85], which scales as $n \log n$. However, this method was not implemented for the work presented here.

4.3.2 Gauge Invariant Smearing

An alternative smearing was proposed by the Wuppertal group, [86], which generated smearing functions in a gauge covariant manner. The idea behind this was to smear a delta function using a scalar wavefunction. A non–local source term, $S(\vec{x}, \vec{0})$, was calculated from the scalar propagator solution of the three dimensional, gauge invariant, Klein Gordon equation,

$$K(\vec{x}, \vec{x}')S(\vec{x}', \vec{0}) = \delta(\vec{x}, \vec{0}) \tag{4.28}$$

with $K(\vec{x}, \vec{x}') = 1 - \kappa_s \vec{D}^2$, discretised accordingly.

However Wuppertal smearing turns out to have a significant computational overhead for smearing at the sink. We use a variation of this method, Jacobi smearing, [2], to solve for $S(\vec{x}', \vec{0})$ as a power series in κ_s with N terms. The Jacobi smearing function, $J(\vec{x}, \vec{0})$, is calculated by an iterative process,

$$J(\vec{x}, \vec{0}) = \sum_{n=0}^{N} \kappa_s^n \Delta^n(\vec{x}, \vec{x}')\delta_{\vec{x}', \vec{0}} \tag{4.29}$$

$$\Delta(\vec{x}, \vec{x}') = \sum_{i=1}^{3}\{\delta_{\vec{x}', \vec{x}-\hat{i}} U_i^\dagger(\vec{x} - \hat{i}, t) + \delta_{\vec{x}', \vec{x}+\hat{i}} U_i(\vec{x}, t)\} \tag{4.30}$$

which has the advantage of being much quicker computationally.

For scalar kappa values less than some critical value, this series converges to the Wuppertal smearing source. For κ_s greater than this value the series diverges, but still offers a valid smearing function for any value of N. This smearing has been used widely within the UKQCD collaboration, [2], and a value of $\kappa_s = 0.25$ is fixed. The smearing radius is varied with N the number of iterations of the Jacobi algorithm and is calculated by,

$$r^2 = \frac{\sum_{\vec{x}} |\vec{x}|^2 |J(\vec{x}, \vec{0})|^2}{\sum_{\vec{x}} |J(\vec{x}, \vec{0})|^2} \tag{4.31}$$

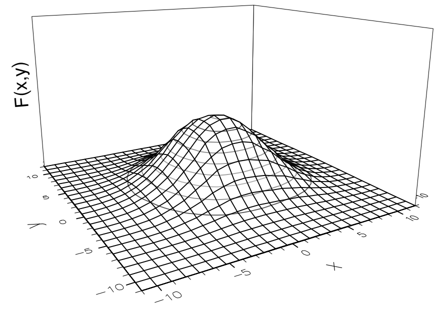

Figure 4.5: A smearing function $F(x,y) = \sqrt{|S|^2}\Big|_{z=0}$, normalised to unit volume, on a $24^3 \times 48$ lattice using Jacobi smearing ($\kappa_S = 0.250, N = 50$). (Taken from [2].)

where $|J(\vec{x},\vec{0})|^2 = \sum_{a,b} J_{ab}(\vec{x},\vec{0})J^*_{ab}(\vec{x},\vec{0})$. This process can be thought of as a diffusion type process, with a delta function expanding with iteration time. Following an initial study of smeared static correlators in ref. [36], we choose $N = 140$. An example of this smearing function is given in Figure 4.5.

Where the gauge invariant smearing benefits, is in the computational effort required to calculate smeared propagators. The effort required to calculate these went as nN where $n = 24^3$, the lattice volume, and N the number of Jacobi iterations. To construct a LS propagator, the zeroth iteration of the Jacobi algorithm was simply a set of links, all elements zero except for unity at the origin. For SL propagators, the initial set of links was the local Wilson line, $\mathcal{P}_{\vec{x}}(0,t)$. For SS type smearing, no extra effort was required, as the Jacobi algorithm was applied with the SL propagator as the zeroth iteration.

4.4 Decay Constant of the B–Meson

An accurate determination of the decay constant of the B–meson has a critical part to play in extraction of CKM matrix elements from neutral B–meson mixing. Much effort has been applied in the determination of a reliable theoretical estimate for this quantity, but as yet no final result has been obtained. Indeed a large part of this effort has been directed toward the calculation of the matrix element in the static limit of QCD. This has its own particular problems and uncertainties, the main one being the extraction of a clean ground state signal. In this section we attempt a calculation of f_B^{static}.

The B–meson decay constant, f_B, is defined in the continuum in terms of the matrix element of the axial current, $A_\mu(x) = \bar{b}\gamma_\mu\gamma_5 q$,

$$\langle 0|A_\mu|B(p)\rangle = ip_\mu f_B. \tag{4.32}$$

The standard way of extracting this from a lattice calculation is through the large time behaviour of the zero momentum B–meson propagator. This is obtained from the two point correlation function of the time component of the local axial current,

$$\begin{aligned} C(t) &= \sum_{\vec{x}} \langle A_4^L(\vec{x},t) A_4^{L\dagger}(\vec{0},0)\rangle && (4.33) \\ &\underset{\text{large t}}{\rightarrow} \left(Z^L\right)^2 \exp\left(-M_B t\right) && (4.34) \\ \text{where,}\quad \left(Z^L\right)^2 &= \frac{|\langle 0|A_4^L(0)|B\rangle|^2}{2M_B} = \frac{f_B^2 M_B}{2}, && (4.35) \end{aligned}$$

is the local amplitude, defined in terms of the matrix element of the axial current.

In treating the b quark in the static approximation, the decay constant is related to the local amplitude, Z^L, by,

$$f_B^{static}\sqrt{M_B} = \sqrt{2}\, Z_A^{static}(M_B a, \alpha_s)\, Z^L\, a^{-3/2}, \tag{4.36}$$

with powers of the lattice spacing giving a dimensionful result. Z_A^{static} is the renormalisation constant for the axial current in the HQET. Further to this, we must make two main changes to Equations (4.33) and (4.34), which are altered in the static limit.

Firstly, the exponent M_B is replaced by an effective mass, ξ, to be thought of as the 'binding energy' of the B–meson. This is not a true mass, in that it contains the $\exp\left(-m_b t\right)$ factors absorbed from the static quark propagator, $\xi = M_B - m_b$. These factors are in terms of the bare quark mass, which are divergent in the $a \rightarrow 0$ limit, [87]. At present theses $1/a$ divergences cannot be dealt with. The main consequence of this is that finite hadronic masses cannot be obtained directly from the static theory. It is, however, possible to calculate mass differences in this limit, as shown in Chapter 5. A further consequence is that, until some means of non–perturbative subtraction of these divergences is formulated, the $\mathcal{O}(1/m_b)$ corrections to the static approximation cannot be included in the calculation of f_B.

The second problem involved in simulating with static quarks lies in the asymptotic behaviour of the two point correlators. As was discussed in Section 4.3, calculating static matrix elements with local currents it is virtually impossible to isolate the ground state before the statistical fluctuations swamp any signal. This introduces the need for 'smeared' operators, Section 4.3, which increase the overlap of the operator with the ground state, allowing for measurements of the lowest state, the B-meson. With these extended currents we can calculate various smeared correlation functions,

$$C^{RS}(t) = \sum_{\vec{x}} \left\langle A_4^R(\vec{x},t) A_4^{S\dagger}(\vec{0},0) \right\rangle \tag{4.37}$$

$$\to Z^R Z^S \exp\left(-\xi^{RS} t\right), \tag{4.38}$$

where indices R and S indicate different smearing functions, including one corresponding to the local current. In what follows, there will be frequent references to the effective mass. For the correlators in Equation (4.38), this is defined as,

$$m^{eff} = \log\left(\frac{C(t)}{C(t+1)}\right). \tag{4.39}$$

The decay constant is defined in terms of the local amplitude, Z^L, which can be extracted from these smeared correlation functions in two ways,

1. • fit ratio,

$$R(t) = \frac{C^{LS}(t)}{C^{SS}(t)} \to \frac{Z^L}{Z^S}, \tag{4.40}$$

   to a constant, shown in Figure 4.6,

   • and then fit

$$C^{SS}(t) \to (Z^S)^2 \exp\left(-\xi^{SS} t\right), \tag{4.41}$$

   to extract Z^S. The effective mass plot for $C^{SS}(t)$ is shown in Figure 4.7(a),

   • from which,

$$Z^L = R \times Z^S. \tag{4.42}$$

This will be labeled as smeared–smeared (SS) method.

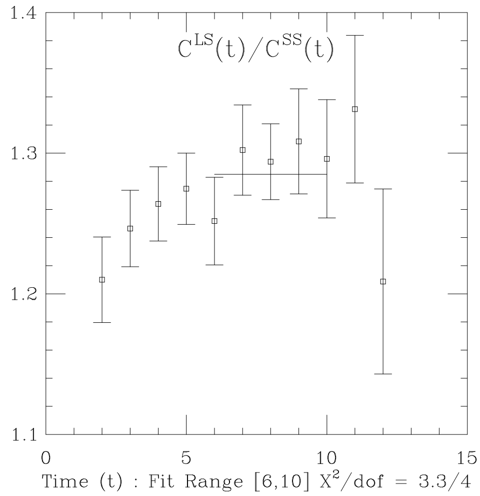

Figure 4.6: Ratio of $R(t) = C^{LS}(t)/C^{SS}(t)$ for exponential smearing.

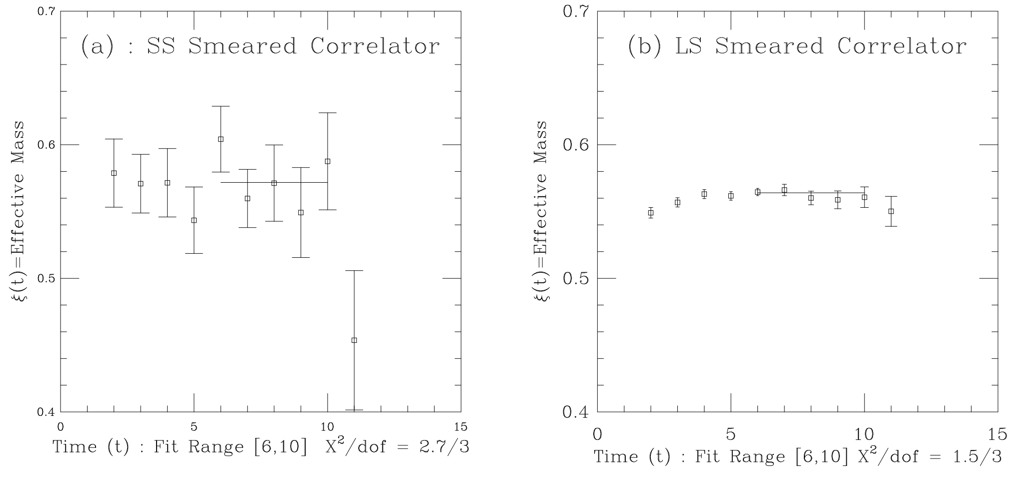

Figure 4.7: Effective mass plots of (a) C^{SS} and (b) C^{LS} for exponential smearing.

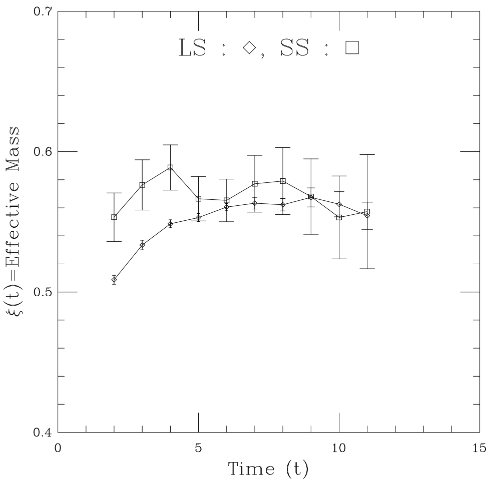

Figure 4.8: Combined effective mass plots of C^{SS} and C^{LS}. Provides a consistency check on smeared correlators.

2. • fit ratio,

$$R(t) = \frac{C^{LS}(t)}{C^{SS}(t)} \to \frac{Z^L}{Z^S}, \tag{4.43}$$

to a constant,

• and then fit,

$$C^{LS}(t) \to Z^L Z^S \exp\left(-\xi^{LS} t\right), \tag{4.44}$$

to extract $P = Z^L Z^S$. The LS effective mass plot shown in Figure 4.7(b),

• from which,

$$Z^L = \sqrt{R \times P}. \tag{4.45}$$

This will be labeled as local–smeared (LS) method.

A consistency check exists on the C^{SS} and C^{LS} correlators, as the effective masses must be the same, $\xi^{SS} = \xi^{LS}$. This is demonstrated in Figure 4.8 for gauge invariant smearing. The advantage of using the LS method is the reduced statistical errors compared to the SS case (as borne out by the results in Tables 4.1 and 5.1). Countering this, however, is the observation that the LS effective masses reach their asymptotic value from below, introducing some uncertainty

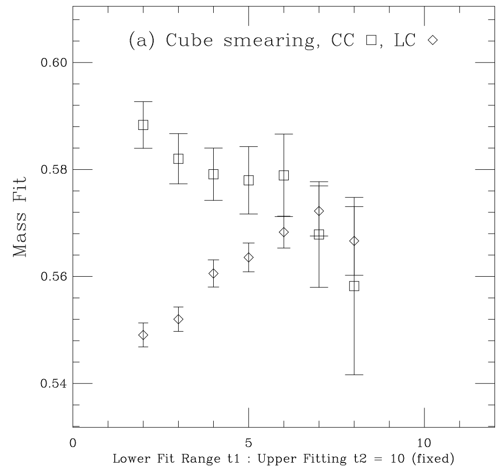

Figure 4.9: Correlated mass fits : LS and SS : vary lower fit range, keeping upper time fixed, $t_2 = 10$, for cube smearing.

as to whether the lightest state has indeed been isolated. This is demonstrated in Figure 4.9 which plots the results from fits of the mass, varying the lower fitting time ($t_1 = 2,\ 8$) with fixed end time for upper fit range ($t_2 = 10$). To emphasise the difference between the LS and SS approach to the asymptotic limit, we consider the 'worst case', looking at the stability of the fits from cube smeared correlators. We find that the fits from the SS correlators are reasonably stable with changing fit range, where as the fits from the LS correlator approach an asymptotic value from below. Both of these factors, of agreement between LS and SS effective masses and the stability of the fits, are taken into account when searching for an appropriate fitting range.

With the values of Z^L extracted by these various methods, and a 'true' ground state signal isolated, we use Equation (4.36) to obtain f_B^{static},

$$f_B^{static} = \sqrt{\frac{2}{M_B}}\, Z_A^{static}(M_B a, \alpha_s)\, Z^L\, a^{-3/2}. \tag{4.46}$$

The renormalisation constant of the axial current, Z_A^{static}, from the matching procedure of the continuum to the lattice regularised static effective theory, has been calculated for the Clover action in [43]. We follow the Lepage Mackenzie prescription and use a boosted coupling, from which we take $Z_A^{static} = 0.79$. For the mass of the B-meson, we use $M_B = (5279 \pm 2)$ MeV, [53], and take as scale $a^{-1} = 2.7\ ^{+0.7}_{-0.1}$ GeV. It should be noted that the uncertainty due to the lattice spacing occurs as 3/2 powers of a^{-1}.

By using these values for the renormalisation constant and the scale, we necessarily introduce some uncertainty into the calculation. A way often used to reduce such uncertainties is to take a ratio, where it is hoped that there will be cancellations of these systematics. Such a quantity exists here in the form of the dimensionless ratio f_{B_s}/f_{B_d}. This is calculated from the matrix element at its critical value compared to the value interpolated to the strange mass,

$$\frac{f_{B_s}^{static}}{f_{B_d}^{static}} = \frac{Z^L(\kappa_s)}{Z^L(\kappa_c)}\sqrt{\frac{M_{B_d}}{M_{B_s}}}. \tag{4.47}$$

Required for this is the $B_s - B_d$ mass splitting which is calculated in Section 5.1.

Although in terms of lattice calculations, f_B^{static} represents an interesting and extremely important result, phenomenologically speaking what is of greater interest is a value for f_B itself. How can we get f_B from f_B^{static}? As was mentioned earlier, there are at least two approaches to studying heavy quarks on the lattice. We have followed the approach which considers the infinite quark mass limit. It is also possible to calculate the heavy–light decay constants using propagating quarks, [36], albeit at quark masses lower than the b quark mass. To combine results from these two regimes, we look to the HQET which predicts a scaling law for heavy–light pseudo–scalar mesons,

$$f_P\sqrt{M_P} = const(\alpha_S(M_P))^{-2/\beta_0}, \qquad M_P \to \infty, \tag{4.48}$$

which can be used to interpolate between the propagating and static results.

In fact, it was found in ref. [88], that this scaling law contains sizable $\mathcal{O}(1/m_Q)$ corrections. These can be quantified by parameterising the scaling law as,

$$f_P\sqrt{M_P} = A\left(1 + \frac{B}{M_P} + \frac{C}{(M_P)^2}\right). \tag{4.49}$$

Calculation of f_B^{static} gives only the first term in this expansion, but fit to the results with propagating quarks can be used to fix the other constants and obtain a value for the pseudoscalar decay constant at $M_P = M_B$.

4.4.1 Results for f_B^{static}

The building blocks for this calculation are the simple two point functions of the time component of the axial operator, Equation (4.33). These were calculated at three light kappa values and for all possible smearings. In following the two procedures outlined above it was necessary to fit to three types of functions; C^{SS}, C^{LS} and C^{LS}/C^{SS}. To choose the fit ranges, a number of criteria were applied; agreement of correlated and uncorrelated fits, $\chi^2/dof \sim 1$, agreement of effective masses from C^{SS} and C^{LS} correlators and stability of the fits with respect to changes in fit range. These fit ranges for the correlators are given in the results table. Values for the fits obtained with the value from extrapolation of the light quark masses to the chiral limit are shown in Table 4.1. Values for the decay constant f_B^{static}, including all factors of scale and renormalisation constant are also listed. This table is complemented by the values of the effective masses for these fits, which are given in Table 5.1 in Section 5.1. The eight results quoted come from all different smearing functions used, following the two methods outlined earlier in Equations (4.42) and (4.45) for extracting Z_L from the correlation functions available.

To quote a final answer for f_B^{static} we take a series of weighted averages for the correlated fits, quoting errors from statistics and uncertainty in lattice spacing. We average over all combinations of LS and SS,

$$\text{CUBE}: \left(260 \pm 9 \ \ {}^{+108}_{-\ 14}\right) \text{MeV} \tag{4.50}$$

$$\text{DOUBLE}: \left(256 \pm 12 \ \ {}^{+106}_{-\ 14}\right) \text{MeV} \tag{4.51}$$

$$\text{EXP}: \left(249 \pm 9 \ \ {}^{+102}_{-\ 14}\right) \text{MeV} \tag{4.52}$$

$$\text{GI}: \left(248 \pm 7 \ \ {}^{+102}_{-\ 14}\right) \text{MeV}. \tag{4.53}$$

The values obtained for f_B^{static} vary with the smearing method used, though there is agreement of all results within errors. Another point to note is the very small statistical errors, especially for the LS fits, perhaps indicating an underestimation of the errors involved. A 'best' estimate of f_B^{static} is given by the results from the exponential or gauge invariant smearings. these smearing functions were found to be the most stable in the fitting procedure.

Comparison of the results with those of other groups is shown in Figure 4.10. The values for the points plotted are taken from ref. [3], and includes results

Smearing	144	226	262	Z_L	f_B^{static} (GeV)
LC	0.143 (5)	0.131 (5)	0.125 (5)	0.119 (5)	0.256 (10)
χ^2/dof	0.4/1, 8.0/6	1.7/1, 5.3/6	1.8/1, 4.5/6	0.2	
$[9, 11]$, $[5, 11]$					
LD	0.146 (5)	0.132 (5)	0.126 (5)	0.119 (5)	0.257 (11)
χ^2/dof	0.01/1, 0.6/2	0.2/1, 0.5/2	0.1/1, 0.4/2	0.3	
$[9, 11]$, $[9, 11]$					
LE	0.137 (2)	0.126 (2)	0.121 (2)	0.116 (2)	0.249 (4)
χ^2/dof	1.5/3, 3.3/4	2.0/3, 2.6/4	2.4/3, 2.6/4	0.2	
$[6, 10]$, $[6, 10]$					
GI LE	0.134 (3)	0.125 (2)	0.120 (2)	0.115 (2)	0.247 (5)
χ^2/dof	1.2/3, 4.4/5	1.2/3, 2.6/5	0.9/3, 2.5/5	0.2	
$[6, 10]$, $[5, 10]$					
CC	0.149 (7)	0.137 (7)	0.131 (8)	0.127 (7)	0.273 (16)
χ^2/dof	0.1/1, 8.0/6	0.1/1, 5.3/6	0.1/1, 4.5/6	0.8	
$[7, 9]$, $[5, 11]$					
DD	0.150 (7)	0.136 (7)	0.131 (7)	0.119 (7)	0.256 (14)
χ^2/dof	3.4/3, 0.6/2	3.1/3, 0.5/2	3.0/3, 0.4/2	1.5	
$[6, 10]$, $[9, 11]$					
EE	0.140 (6)	0.128 (6)	0.123 (6)	0.114 (6)	0.245 (14)
χ^2/dof	2.8/3, 3.3/4	2.6/3, 2.6/4	2.5/3, 2.6/4	1.3	
$[6, 10]$, $[6, 10]$					
GI EE	0.139 (4)	0.128 (4)	0.123 (4)	0.116 (4)	0.250 (9)
χ^2/dof	0.3/3, 4.5/5	0.9/3, 2.6/5	1.4/3, 2.5/5	0.01	
$[6, 10]$, $[5, 10]$					

Table 4.1: B-Meson Decay Constant f_B^{static}. Values of pseudoscalar decay constant for three light quark masses, with extrapolated value included. Correlated χ^2/dof are quoted.

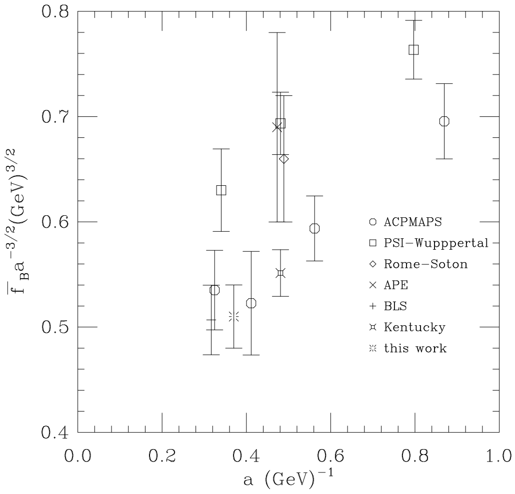

Figure 4.10: Comparison of results for $\tilde{f}$ against scale. (Taken from [3].)

from refs. [3, 89, 88, 84, 90, 85]. In order to compare different calculations from different β on the same graph, the function,

$$\tilde{f} = Z_L a^{-\frac{3}{2}} (\mathrm{GeV})^{-\frac{3}{2}}, \tag{4.54}$$

is plotted against the lattice spacing a. This removes differences in values of the renormalisation constant Z_A^{stat} used by the various groups.

Taking for our result from the exponential smearing,

$$Z_L = 0.115 \pm 0.006, \tag{4.55}$$

the value from this study to be compared with those in Figure 4.10 is,

$$\tilde{f} = 0.510 \pm 0.030 \ {}^{+211}_{-\ 28}, \tag{4.56}$$

where the first error is statistical with the second from uncertainty in the scale, at $a = 0.37$.

4.4.2 Calculation of $f_{B_s}^{static}/f_{B_d}^{static}$

Combining the values obtained for the ratio $Z_L(\kappa_s)/Z_L(\kappa_c)$ with the values of the $B_s - B_d$ mass splitting in Section 5.1. We are able to determine $f_{B_s}^{stat}/f_{B_d}^{stat}$,

$$\frac{f_{B_s}^{stat}}{f_{B_d}^{stat}} = \frac{Z_L(\kappa_s)}{Z_L(\kappa_c)}\sqrt{\frac{M_{B_d}}{M_{B_s}}} = \frac{Z_L(\kappa_s)}{Z_L(\kappa_c)}\sqrt{\frac{M_{B_d}}{M_{B_d} + \Delta m}} \tag{4.57}$$

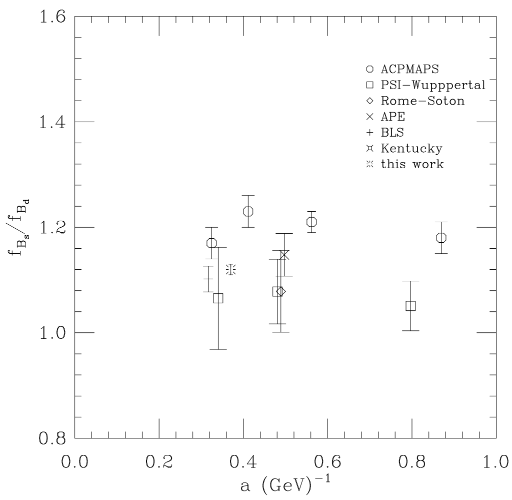

Figure 4.11: Comparison of results for f_{B_s}/f_{B_d} against scale. (Taken from [3].)

with $M_{B_d} = 5.279$ GeV, taken from experimental measurement. This was done for all smearing types and a weighted average for the results given below,

$$\text{CUBE} : 1.117 \pm 0.006 \tag{4.58}$$

$$\text{DOUBLE} : 1.113 \pm 0.008 \tag{4.59}$$

$$\text{EXP} : 1.128 \pm 0.012 \tag{4.60}$$

$$\text{GI} : 1.120 \pm 0.005, \tag{4.61}$$

The error in this case is purely statistical.

We compare the results obtained here with those published in ref. [3] and including results from [3, 89, 88, 84, 90, 85]. The combined plot is shown in Figure 4.11.

4.4.3 Calculation of f_B

The above results are those relating to f_B^{static}. In order to extract the decay constant of the B–Meson, f_B, for comparison with continuum physics, it is necessary to combine these results with those determined by the use of simulations based on propagating quarks. The value of f_B with b quarks at their physical mass is found from an interpolation in the heavy–light pseudoscalar mass, M_P to the

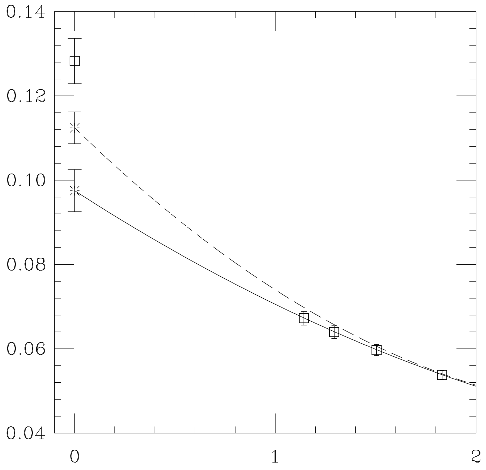

Figure 4.12: Scaling Violations : Φ against inverse meson mass. Full line; fit to four propagating points only. Dotted line; fit to three lightest propagating points and static point.

B-meson mass, M_B. The inclusion of the static point is used to further constrain the physical values of f_B obtained from the interpolation. In previous calculations, [36], this caused many problems as the static point could not be included in a fit with the propagating results.

We follow the treatment given in [36], attempting to quantify the deviations from the scaling law, (4.48), by studying the quantity,

$$\Phi = Z_A \hat{\Phi}(M_P) \equiv (\alpha_s(M_P)/\alpha_s(M_B))^{2/\beta_0} f_P \sqrt{M_P} \tag{4.62}$$

$$= \sqrt{2} Z_A^{stat} \hat{\Phi}^{stat}(M_P \to \infty) \equiv (f_P \sqrt{M_P})^{stat}, \tag{4.63}$$

as a function of $1/M_P$. This is plotted in Figure 4.12, including both results from propagating quarks and the static point at $1/M_P = 0$. In order to directly compare static and propagating results it is necessary to include factors of α_s, which arise from corrections to the scaling law away from the $M_P \to \infty$ limit, as well as the appropriate renormalisation constants. We approximate $\alpha_s(M_P)$ by,

$$\alpha_s(M) = \frac{2\pi}{\beta_0 \log\left(M/\Lambda_{QCD}\right)}, \tag{4.64}$$

taking $\Lambda_{QCD} = 200$ MeV, $\beta_0 = 11 - \frac{2}{3} n_f$ and $n_f = 0$ in the quenched approximation.

We attempt fits to Φ as either linear or quadratic functions of $1/M_P$,

$$\Phi(M_P) = A\left(1 - \frac{B}{M_P}\right), \tag{4.65}$$

or

$$\Phi(M_P) = C\left(1 - \frac{D}{M_P} + \frac{E}{M_P^2}\right), \tag{4.66}$$

though it was found that a quadratic fit best approximated the data.

We fit these functions twice, once using all four light κ_h values and then the four propagating results with the static result. This is shown in Figure 4.12, with the perturbative value for the renormalisation constant of the axial vector, $Z_A = 0.97$. It was not possible to obtain a consistent fit to include the static point and those from simulations with propagating quarks.

Clearly the problem originally seen in ref. [36] has not been resolved with this calculation of f_B^{static}. The authors mention possible reasons for the discrepancy; uncertainties in the renormalisation constants and residual discretisation error effects in the simulations of propagating quarks. We are unable to comment further on these suggestions, instead we quote their value for f_B,

$$f_B = 160 \pm 6 \ {}^{+\,53}_{-\,19}. \tag{4.67}$$

4.4.4 Comparison of Smearing Functions

One of the main aims of this calculation of f_B^{static} by use of smeared correlators is to attempt to improve the signal of the ground state contributions. Various smearing functions have been used, the details of which were outlined in Section 4.3. This section attempts to compare the ability of these smearing functions to offer good signals for the various correlators studied.

Unfortunately, such comparison is not clear cut as there are no well defined ways to determine the 'goodness' of a smearing function. In order to make any comment on these smearing functions, we turn to the criteria used to determine the fit ranges chosen; the existence of a plateau at early times, comparison of uncorrelated and correlated fits, goodness of fit i.e. χ^2/dof, stability of fits obtained with varying fit ranges and agreement between effective masses of LS and SS type correlators.

These criteria are studied from the following sets of graphs. Figure 4.13 shows the effective mass plots of the SS and LS correlation functions. This demonstrates

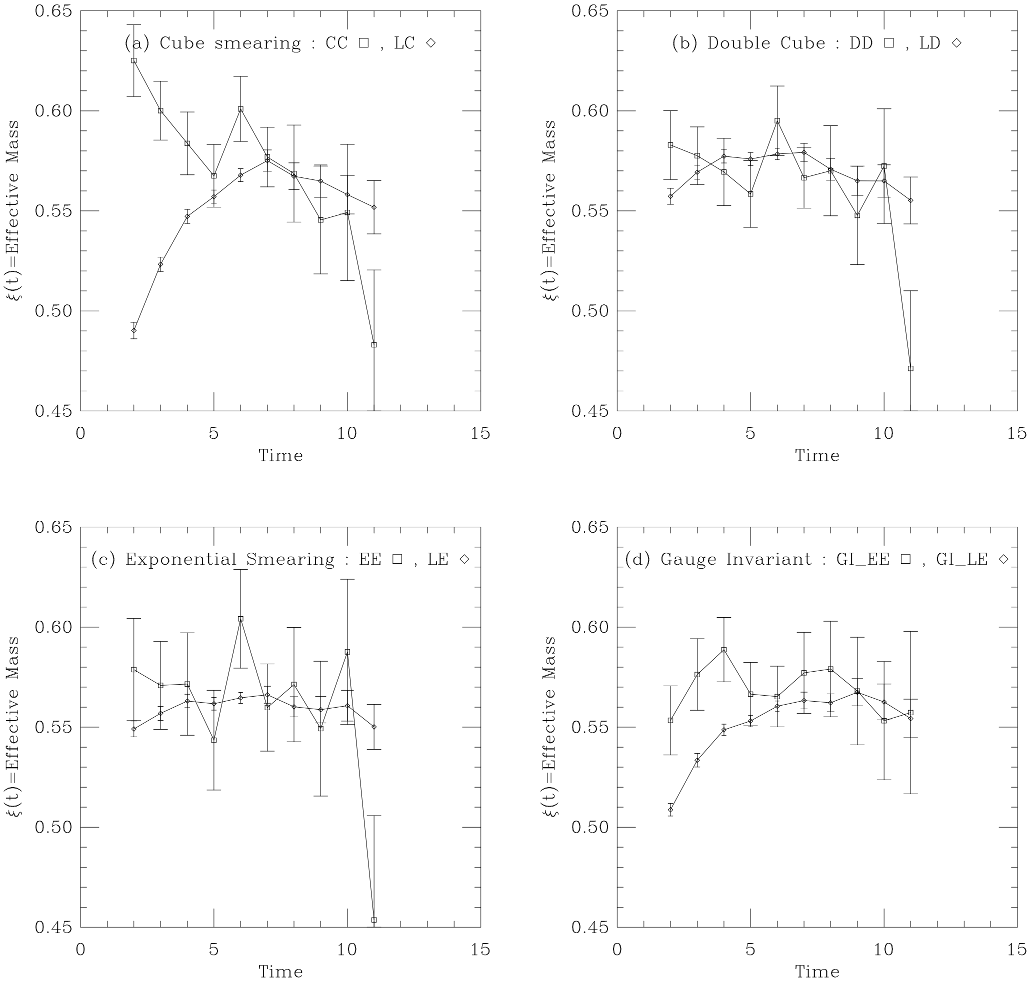

Figure 4.13: Comparison of Smearing Functions : Effective Masses of SS and LS Correlators (a) Cube, (b) Double Cube, (c) Exponential (d) Gauge Invariant.

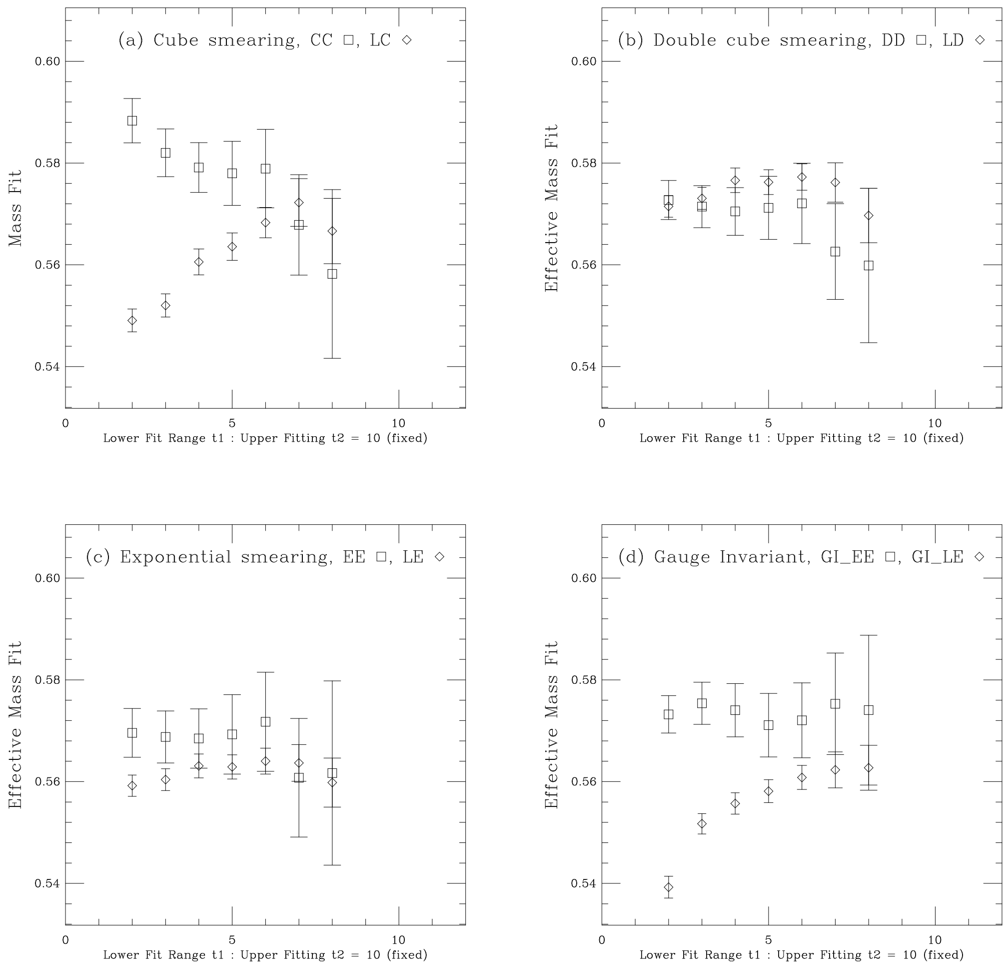

Figure 4.14: Comparison of Smearing Functions : Fits of Effective Masses of SS and LS Correlators, with Varying Time Range ($t_2 = 10$ fixed).

the time at which a plateau sets in and also the agreement of effective masses for SS and LS correlators. Figure 4.14, on the other hand, plots mass fits against the lower time of the fitting range, keeping the upper time of the fitting range fixed (t_2=10). This shows the stability of the mass fits, over varying time intervals.

What features do these graphs show? One important aspect is the approach of the LS correlators to the asymptotic from below. For both exponential and double smearings plateaux exist at early times and the LS and SS correlators agree well over a wide time range. These features are seen to a lesser extent from the gauge invariant smearing. These findings are borne out further by Figure 4.14, where the mass fits for double and exponential type smearings are very stable over a range of time fits, but gauge invariant smearing shows this only for the SS version. Perhaps it is not surprising that the most naive smearing function, the simple cube, does not compare as well as these others.

Smearing is a necessary evil when dealing with calculations involving static quarks, without which no ground state signal at all could be extracted. A variety of different smearing functions have been used to attempt to isolate the ground state B–Meson, all with relative benefits and varying degrees of success. Clearly, this comparison barely scratches the surface of the subject and there is much work to be done in refining the smearing process.

4.4.5 Conclusions

The decay constant of the B–Meson is an important quantity. Phenomenologically it is the main theoretical uncertainty in $B^0\bar{B}^0$ mixing which, with B–parameter, contains all non–perturbative strong interaction effects. From a lattice perspective, this calculation pushes both the analytical field theoretic techniques, using the Heavy Quark Effective Theory, and also the technology involved in extracting clean signals by the use of extended interpolating operators.

In this chapter, we have used the technique introduced by Eichten treating the heavy quark propagator with an expansion in heavy quark mass. Calculations using the lowest order term in this expansion were performed to determine the decay constant of the B-meson in the static limit, f_B^{static}. This was done with a variety of smearing functions, generated by both gauge invariant and Coulomb gauge methods. As a final answer we quote the result from exponential and gauge invariant smearing methods,

$$f_B^{static} = \left(248 \pm 8 \ {}^{+102}_{-\ 14}\right) \text{ MeV}. \tag{4.68}$$

where the first error is purely statistical and the second from uncertainty in the lattice spacing.

With the growing interest in mixing in the B_s system, the ratio f_{B_s}/f_{B_d} is also an important quantity. Calculation of a dimensionless ratio is also desirable on the lattice, where it avoids the systematic errors introduced by the renormalisation constant and the lattice spacing. In the static limit, we quote a final answer,

$$\frac{f_{B_s}^{static}}{f_{B_d}^{static}} = 1.12 \pm 0.01. \tag{4.69}$$

In order to extract a measurement of f_B it is necessary to combine data from calculations using both static and propagating quarks. We attempt a fit using a parameterisation of the scaling law which includes $1/M_P$ corrections. It was found that it was not possible to reconcile the results obtained from the static and propagating methods.

Although we say ‘final’ answer, the range of values obtained from different smearing functions cannot be ignored. Indeed the spread of results among the ‘world data’ for calculations of f_B^{static} shows that the calculation is far from finished. A straight forward refinement of the method applied here would be in a global fit to the parameters of C^{SS}, C^{LS} and C^{LS}/C^{SS}. This would improve the consistency of the results from LS and SS methods. Clearly an essential aspect of any further study of f_B^{static} is the use of smearing. We have demonstrated the use of various ground state smearing functions. However, to include some information from an excited state smearing function using a multi–state smearing method as outlined in [3], would be useful and informative.

On a more speculative note, we mention two possibilities for the future. Non–perturbative renormalisation has been mentioned already for the renormalisation constant of the axial current. In ref. [62] the author also mentions the possibility of a non–perturbative calculation of Z_A^{stat}. Also to be considered is the possibility of including the $1/m_b$ corrections of HQET in the calculation of f_B. A preliminary study is presented in ref. [91]. Perhaps only with the inclusion of these two procedures will the seemingly simple calculation of f_B be fully understood.

Chapter 5

Heavy Quark Spectroscopy

With increasing experimental activity focused on heavy flavour physics, the spectrum of hadrons containing heavy quarks, in particular the b quark, is slowly being mapped out. Indeed, the spectroscopy of heavy hadrons will continue to be refined as dedicated B physics machines come on–line in the near future. On the theoretical front, the Standard Model, though a great success in many areas, still has a large number of free parameters which must be determined from experiment. Standard theoretical techniques, however, offer no means to determine hadronic masses. Lattice QCD, meanwhile, offers the only first principles approach to studying hadron spectroscopy.

The success of state–of–the–art Lattice QCD calculations with light hadrons is demonstrated in ref. [52]. In recent years considerable progress has been made in the study of heavy–light systems both in terms of numerical calculations and theoretical developments. In this chapter we continue to use the approach of Eichten, [73], in considering the heavy quark propagator in terms of an expansion in inverse powers of the quark mass. In particular we consider primarily the lowest order term in this expansion, the so called static limit. With this static formulation, the only choice we have is to measure mass differences.

In studying the propagation of hadrons containing one heavy quark treated by the static formalism, we are unable to measure finite masses, M_P. Instead, only binding energies, $\xi = M_P - m_Q$, can be extracted, containing dependence on the bare quark mass m_Q. These bare masses are linearly divergent in the $a \to 0$ limit, [87], requiring non–perturbative renormalisation, which as yet cannot be attempted. However, if we are able to measure two particles, P_1 and P_2, say, containing the same heavy quark, Q, the difference in binding energies is independent of bare quark mass,

$$\xi_1 - \xi_2 = (M_{P_1} - m_Q) - (M_{P_2} - m_Q) = M_{P_1} - M_{P_2}. \qquad (5.1)$$

In this way we can determine finite physical mass splittings.

In the calculation of the $B_s - B_d$ and $\Lambda_b - B_d$ mass splittings we only consider results from the lowest order term in the $1/m_Q$ expansion, the mass splittings arising from the different light quark dependencies. The vector–pseudoscalar splitting is slightly different, in that is arises from the spin dependent term in the effective action, which only occurs at first order in $1/m_Q$. We calculate the mass splitting by considering this spin dependent term as a perturbation to the static result.

5.1 Mass of B_s

Following the outline above concerning the extraction of physical mass splittings from simulations involving the static heavy quarks, it is possible to calculate the $B_s - B_d$ mass difference. This mass difference is also of interest experimentally, with the study of B_s mesons becoming accessible from current accelerators.

In this case, we are studying two particles which differ in their light quark make up, $B_d = \bar{b}d$ and $B_s = \bar{b}s$. In terms of lattice simulations this corresponds to studying the same correlation functions, though at different light quark masses or kappa values. These correlation functions have been used in the determination of the decay constant of the B–Meson, in Section 4.4, and take the following asymptotic form,

$$\begin{aligned} C(t) &= \sum_{\vec{x}} \langle A_4(\vec{x},t) A_4^\dagger(\vec{0},0) \rangle \\ &\underset{\text{large t}}{\rightarrow} Z^2 \exp(-\xi t). \end{aligned} \qquad (5.2)$$

The dependence of the effective mass, $\xi = \xi(\kappa_l)$, on light kappa value can be used to extract the $M_{B_s} - M_{B_d}$ mass difference. It is assumed that these effective masses are linear in light kappa value and we fit the effective masses to the following form,

$$\xi(\kappa_l) = A + \frac{B}{\kappa_l}, \qquad (5.3)$$

to extract parameters A and B. The mass difference is then determined from these parameters by,

$$(M_{B_s} - M_{B_d})^{cont} = (M(\kappa_l = \kappa_s) - M(\kappa_c))^{latt}\, a^{-1} = B \times \left(\frac{1}{\kappa_s} - \frac{1}{\kappa_c}\right) \times a^{-1}, \tag{5.4}$$

where $\kappa_s = 0.1419$, [6], corresponds to the strange quark mass. From paper [92] the authors quote $m_{B_s} - m_{B_d} = (71 \pm 13 - 16)$ MeV. Experimentally, [93], the mass splitting is found to be,

$$\Delta m = m(B_s) - m(B_d) = (\,96 \pm\, 6\,)\,\text{MeV}. \tag{5.5}$$

5.1.1 Results

The correlators for this mass difference have been used to calculate f_B^{static}, Section 4.4. Indeed, the effective mass resulting from fits to the B-meson correlator was one of the main criteria for choosing fitting range for the particular correlation function. In this calculation we use the effective mass fits from both LS and SS type correlators and from all possible different smearings. Table 5.1 contains the mass fits for all three light kappa values, the mass splitting in lattice units and the physical result with the inclusion of the scale from the lattice spacing. The error quoted in the table are purely statistical calculated with a scale $a^{-1} = 2.7$ GeV. An error due to the uncertainty in the scale is quoted in the combined results,

$$\text{SS} : \left(74 \pm 6\ \ {}^{+19}_{-\ 3}\right)\ \text{MeV} \tag{5.6}$$

$$\text{LS} : \left(62 \pm 4\ \ {}^{+16}_{-\ 2}\right)\ \text{MeV} \tag{5.7}$$

from weighted averages to the four LS type correlators and four SS type correlators. The result consists of a central value for the weighted average, a statistical error and a systematic error due to uncertainties in the lattice spacing. Clearly this last effect, in terms of lattice spacing, is the largest uncertainty.

The results quoted indicate a difference between the mass splitting determined from the LS and SS type correlators. At first sight this seems to be at odds with the criteria used to choose the fitting ranges, that is, agreement between mass fits for LS and SS correlators. However, looking at Table 5.1 we can see that the fits to the effective masses do agree within errors. It is the interpolation to the strange mass that introduces the differences in the values obtained for the mass

Smearing	144	226	262	$\Delta m \times a$	Δm(GeV)
LC χ^2/dof $[9, 11]$	0.562 (7) 0.4/1	0.544 (8) 1.7/1	0.535 (9) 1.8/1	0.026 (2) 0.1	0.072 (6)
LD χ^2/dof $[9, 11]$	0.565 (6) 0.01/1	0.546 (7) 0.2/1	0.536 (8) 0.1/1	0.026 (2) 0.8	0.070 (5)
LE χ^2/dof $[6, 10]$	0.564 (3) 1.5/3	0.548 (3) 2.0/3	0.541 (3) 2.4/3	0.023 (1) 0.01	0.063 (2)
GI LE χ^2/dof $[6, 10]$	0.561 (2) 1.2/3	0.545 (3) 1.2/3	0.539 (3) 0.9/3	0.022 (1) 0.04	0.060 (2)
CC χ^2/dof $[7, 9]$	0.575 (12) 0.1/1	0.557 (14) 0.1/1	0.549 (15) 0.1/1	0.024 (3) 0.2	0.066 (7)
DD χ^2/dof $[6, 10]$	0.572 (8) 3.4/3	0.554 (9) 3.1/3	0.547 (10) 3.0/3	0.028 (2) 0.4	0.074 (5)
EE χ^2/dof $[6, 10]$	0.572 (10) 2.8/3	0.553 (12) 2.6/3	0.547 (13) 2.5/3	0.030 (3) 1.2	0.080 (9)
GI EE χ^2/dof $[6, 10]$	0.572 (7) 0.3/3	0.553 (8) 0.9/3	0.546 (8) 1.4/3	0.028 (2) 0.1	0.075 (4)

Table 5.1: Effective Masses. $\Delta m = m_{B_s} - m_{B_d}$ for B-Meson correlators. χ^2 given for correlated fits and extrapolation.

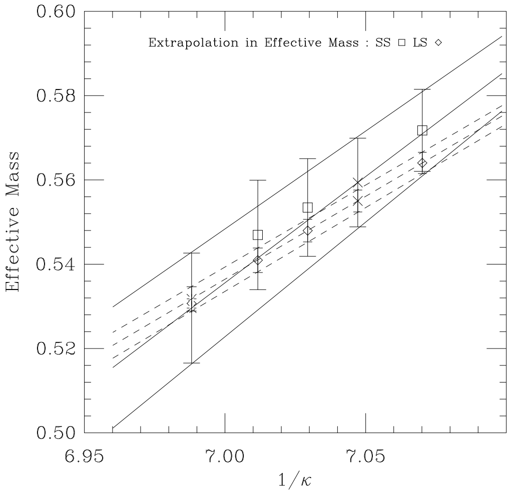

Figure 5.1: Extrapolation of effective masses for LS(dotted line) and SS(full line) correlators, for exponential smearing. Values at strange mass marked by a cross.

splitting. This is demonstrated in Figure 5.1 which shows the correlated fits with errors to the LS and SS correlators for exponential smearing. The values at κ_s are also marked. Although the actual values including those from extrapolations agree, it is the difference or gradient that is relevant in this case. This is slightly different for the LS and SS cases.

The differences between these can be understood in terms of asymptotic values of the various correlators. Although the LS correlators have far lower statistical error, there still may be some doubt as to whether these smearing functions really do attain an asymptotic plateau. In Section 4.4.4 it was seen that the SS correlators, although seeming more 'noisy' obtained fits which were in fact remarkably stable, a good indication that the ground state has been isolated. This was not the case for the LS correlators.

As a best estimate of the $B_s - B_d$ mass splitting we quote the value given in Equation (5.6). This agrees well with other works, with a full comparison of the results shown in Figure 5.2, including results from refs. [3, 89, 88, 84, 90, 85]. We also include Figure 5.3 which contains results of simulations on the same gauge configurations, with propagating quarks at several finite mass values. The static result at infinite mass and the experimental point, at M_B are also plotted on this

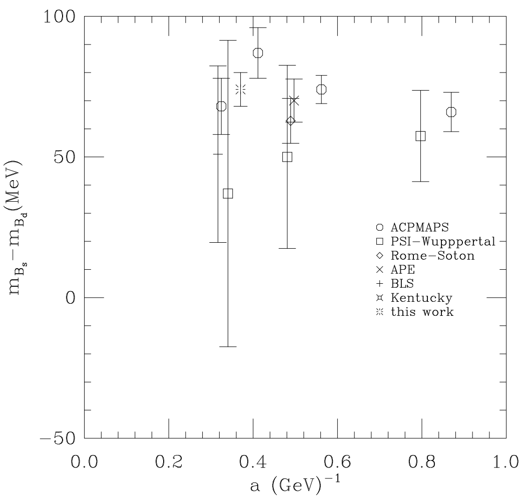

Figure 5.2: Comparison of results for $m_{B_s} - m_{B_d}$ against scale. (Taken from [3].)

graph.

5.2 Mass of Λ_b

Beautiful baryons are now well within the grasp of experimentalists since the discovery of the Λ_b at CERN's UA1 detector, [94]. With the experimental side opening up it is interesting to see what can be determined theoretically and in particular from lattice calculations. An initial lattice study, [92], was made using Wilson fermions giving a first determination of the Λ_b mass. This section aims to attempt a similar calculation with an improved action.

In Section 5.1 the determination of the $B_s - B_d$ mass splitting was obtained from quantities with the same heavy quark dependence, but with different light quark contents. A similar analysis can be applied when studying heavy baryons. The Λ_b contains one heavy quark and two light quarks coupled in a spin 0, isospin 0 singlet combination. The resulting linear divergences from treating the heavy quark in the static limit are the same as for the B meson. Thus, by comparing the time behaviour of a Λ_b with the B-mesons used earlier, it is possible to calculate the $\Lambda_b - B$ mass difference.

As usual for most lattice calculations, particle properties are extracted from

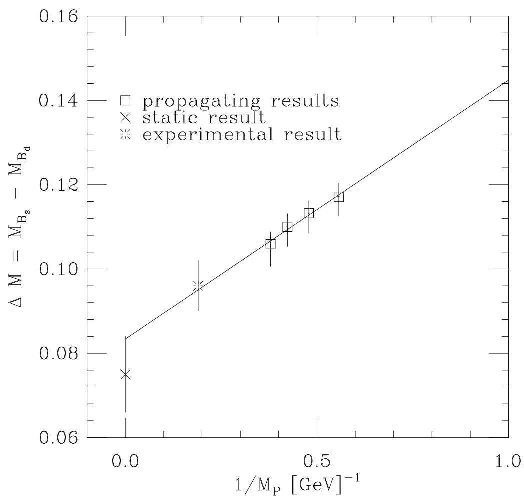

Figure 5.3: Extrapolation of $B_s - B_d$ mass difference in $1/M_P$. (Taken from [4].)

the large time behaviour of a two point correlator. For the Λ_b the local interpolating operator, representing a heavy quark, Q, coupled to two light quarks in a spin singlet, is,

$$\Lambda(\vec{x},t)_\delta = \epsilon^B_{AC} Q^A_\delta(x) \left(u^T_B(x) \mathcal{C} \gamma_5 d^C(x) \right), \tag{5.8}$$

where $\mathcal{C}$ is the charge conjugation operator. Using this, the zero momentum baryon propagator has the following asymptotic form,

$$C_{\Lambda_b}(t) = \sum_{\vec{x}} \langle \Lambda(\vec{x},t) \Lambda^\dagger(\vec{0},0) \rangle \underset{\text{large t}}{\rightarrow} Z_{\Lambda_b} \exp\left(-\xi_{\Lambda_b} t\right). \tag{5.9}$$

As with B–mesons, the Λ_b contains only one heavy quark. The linear divergences contained in the 'binding energy', ξ_{Λ_b}, can be canceled by calculating the difference,

$$\xi_{\Lambda_b} - \xi = (m_{\Lambda_b} - m_B)^{latt} \equiv \Delta m_{\Lambda_b}. \tag{5.10}$$

We fit the ratio of the two point correlator, Equation (5.9), to that for the B meson and extract the mass difference in lattice units from an exponential fit to the large time behaviour of the ratio,

$$R_\Lambda(t) = \frac{C_{\Lambda_b}(t)}{C(t)} \underset{\text{large t}}{\rightarrow} \text{const.} \exp\left(-\Delta m_{\Lambda_b} t\right). \tag{5.11}$$

In order to get any signal at all from this ratio it was necessary to use a smeared interpolating operator to isolate the ground state, Λ_b. This was done

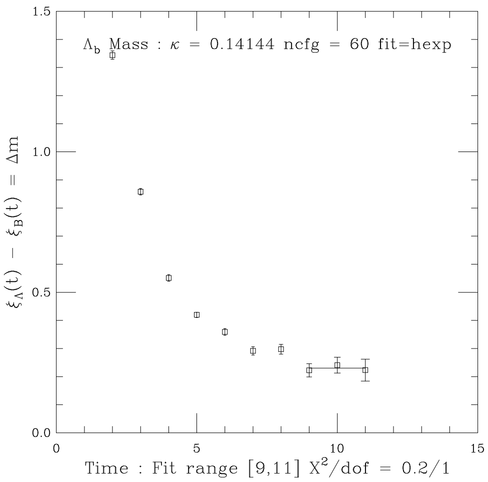

Figure 5.4: Effective mass difference, $\Delta m_{\Lambda_b}(t) = \log\left(R_\lambda(t)/R_\Lambda(t+1)\right)$. GI SS correlator used for both Λ_b and B meson interpolating operators.

in a similar way to the smearing of the B mesons, though in the baryonic case there are two light quarks. For simplicity, we consider the di–quark pair as a local object and smear this with respect to the heavy quark,

$$\Lambda^S(\vec{x},t)_\delta = \sum_{\vec{y}} \epsilon^B_{AC} Q^A_\delta(\vec{y},t) f^S(\vec{x},\vec{y}) \left(u^T_B(\vec{x},t) C\gamma_5 d^C(\vec{x},t)\right). \tag{5.12}$$

where the smearing functions, $f^S(\vec{x},\vec{y})$, are those described in Section 4.3. The baryon correlation functions are calculated in the usual way; a smeared heavy quark propagator is constructed and then combined with the light quark singlet $\left(u^T_B(\vec{x},t) C\gamma_5 d^C(\vec{x},t)\right)$.

The measurements of Δm_{Λ_b} were taken for the set of three light quark masses and for all smearing combinations. Linear extrapolation to κ_{crit} was required for a measurement of the mass splitting at the physical light quark mass. Inclusion of factors of the lattice spacing gives the mass difference in physical units,

$$M_{\Lambda_b} - M_B = \Delta m_{\Lambda_b}(\kappa_{crit})\, a^{-1}\,(\text{GeV}). \tag{5.13}$$

In [92], the authors quote $M_{\Lambda_b} - M_B = (\,720 \pm 160 - 130\,)$ MeV for the $\Lambda_b - B$ mass splitting using a similar method to the one presented in this section. At the time of publication, however, the authors were unable to comment on the consistency of this result with experiment. Since then the Λ_b mass has been measured,

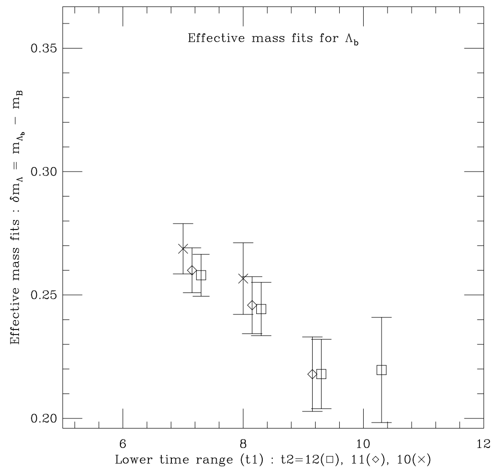

Figure 5.5: Mass fits for $\Lambda_b - B$ mass splitting. Upper time range varies in $t_2 \in [10, 12]$, while fits vary with lower time range.

[94, 95], and the Particle Data Book quotes an average $\Lambda_b = (\,5641 \pm 50\,)$ MeV with $M_B = (\,5279 \pm 2\,)$ MeV. Experimentally, this gives $M_{\Lambda_b} - M_B = (\,362 \pm 50\,)$ MeV. It is of interest to see whether this calculation with an $\mathcal{O}(a)$ improved action and larger statistical sample gives any improvement on the original lattice calculation with Wilson fermions and also to compare it with the confirmed experimental results.

5.2.1 Results

Two point correlation functions for the propagator of the Λ_b were calculated from Equation (5.9) with all smearing functions of the type defined in Equation (5.12). These correlation functions were used to construct the ratio R_Λ form which the mass differences Δm_{Λ_b} were extracted. An effective mass plot is shown in Figure 5.4 with the effective mass defined as $\Delta m_{\Lambda_b} = \log\left(R_\Lambda(t)/R_\Lambda(t+1)\right)$. It seems from Figure 5.4 that a plateau is obtained. However, caution should be taken in ascribing this to the isolation of the ground state as this would only be made completely clear by a simulation of higher statistics with a longer time extent.

Fits for the mass difference Δm_{Λ_b} were made over the time interval $t \in [9, 11]$. Table 5.2 lists mass differences for three light kappa values, extrapolated to κ_{crit}

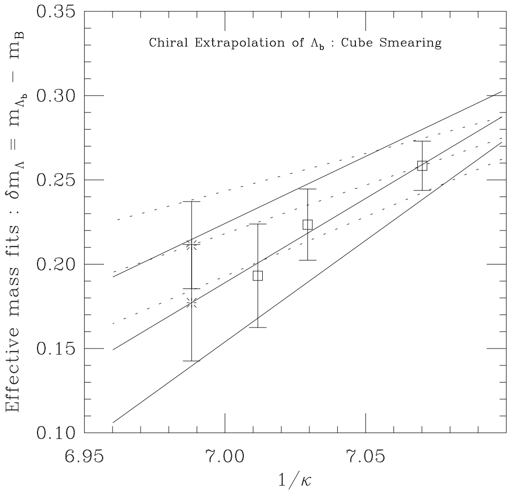

Figure 5.6: Chiral Extrapolation of $\Lambda_b - B$ mass splitting comparing uncorrelated and correlated fits. Cube smearing of LS type smearing shown.

in lattice units and expressed in physical units. We may justify using this small fitting range by looking at how the effective mass fits change with fitting time range. The fits for the SS exponential smearing are shown in Figure 5.5 with upper time range varying in the region $t_2 \in [10, 12]$ and effective mass fits plotted against lower fit time. The fits obtained with $t_1 \geq 9$ seem stable to variation in fit range indicating the beginning of a plateau in effective mass. It was also noted that good agreement was lacking between the uncorrelated and correlated chiral extrapolations of the mass differences. This is clearly demonstrated in Figure 5.6. In this case the correlated fit seems to take into account the large error on the lightest mass value and gives a fit of a higher, and perhaps more sensible, value than the uncorrelated fit.

Combining the results obtained from all smearing types in a weighted average we quote as best estimates for the $\Lambda_b - B$ mass splitting,

$$\text{SS} : \left(429 \pm 83 \ {}^{+111}_{-\ 16}\right) \text{MeV} \tag{5.14}$$

$$\text{LS} : \left(554 \pm 58 \ {}^{+144}_{-\ 21}\right) \text{MeV} \tag{5.15}$$

where again we have quoted a statistical error and an uncertainty due to the lattice spacing.

Smearing	144	226	262	$\Delta m_{\Lambda_b} a$	Δm_{Λ_b} (GeV)
LC	0.258 (15)	0.223 (21)	0.193 (31)	(u) 0.177 (35) (c) 0.211 (26)	(u) 0.478 (93) (c) 0.571 (70)
χ^2/dof	0.03/1	0.08/1	0.1/1	2.2	
LD	0.265 (14)	0.231 (17)	0.204 (21)	(u) 0.187 (24) (c) 0.209 (21)	(u) 0.504 (64) (c) 0.563 (57)
χ^2/dof	0.5/1	0.3/1	0.08/1	3.8	
LE	0.262 (14)	0.228 (17)	0.207 (23)	(u) 0.188 (25) (c) 0.201 (20)	(u) 0.509 (67) (c) 0.542 (54)
χ^2/dof	0.5/1	0.2/1	0.01/1	0.7	
GI LE	0.266 (11)	0.226 (15)	0.188 (20)	(u) 0.169 (22) (c) 0.203 (19)	(u) 0.455 (60) (c) 0.547 (50)
χ^2/dof	0.0/1	0.05/1	0.2/1	7.6	
CC	0.230 (18)	0.194 (31)	0.172 (49)	(u) 0.154 (54) (c) 0.173 (31)	(u) 0.416 (146) (c) 0.467 (84)
χ^2/dof	0.0/1	0.01/1	0.1/1	0.2	
DD	0.219 (16)	0.176 (31)	0.144 (50)	(u) 0.124 (54) (c) 0.157 (33)	(u) 0.334 (147) (c) 0.424 (90)
χ^2/dof	0.04/1	0.2/1	0.2/1	0.6	
EE	0.218 (15)	0.181 (24)	0.165 (37)	(u) 0.144 (42) (c) 0.146 (31)	(u) 0.388 (112) (c) 0.394 (83)
χ^2/dof	0.02/1	0.5/1	1.2/1	0.01	
GI EE	0.230 (16)	0.189 (21)	0.157 (28)	(u) 0.137 (32) (c) 0.160 (27)	(u) 0.369 (86) (c) 0.431 (74)
χ^2/dof	0.2/1	0.8/1	0.9/1	2.0	

Table 5.2: $\Lambda_b - B$ effective mass differences, for three light kappa and extrapolated to the chiral limit. All fits done over range $[9, 11]$, with both uncorrelated, (u), and correlated, (c), results given. χ^2 given for correlated fits.

Clearly this is an improvement on the calculation using Wilson fermions and goes some way towards a value comparable with the experimental result. Again, the main problem seems to be in cleanly extracting the ground state baryon from the Euclidean correlator. This can be seen in two places. In Figure 5.4 a 'plateau' is only obtained after nine time steps leaving only a short time range from which to extract a ground state before the signal stops[1]. Also, from the results in Table 5.2, we see higher values of the mass difference values from the LS correlators compared to the SS correlators suggesting that a true plateau has not been reached for the LS case. With greater time extent and higher statistics, however, these issues should be less relevant. As a best estimate we quote the figure in (5.14) as our final result.

The most obvious improvement would be to include smearing of the light quarks relative to each other. As mentioned earlier, for reasons of simplicity the two light quarks in the baryon were taken as being local to each other with smearing only of this di–quark pair relative to the heavy quark. Clearly this is somewhat unphysical in that the light quarks in a baryon are not expected to be in the same position relative to the heavy quark at the centre. By using smearing between the light quarks one could hope to better model such a baryon. Work is being carried out with such smeared light quarks and propagating heavy quarks, [96].

In using the static theory we can only look at the first term in an expansion of this mass difference as powers of m_B. Using propagating quarks, however, it is possible to determine the $1/M_P$ corrections to this static limit. This has been done by the authors of ref. [5] and they find $\Delta m_{\Lambda_b} = (\,458 \pm 144 \pm 18\,)$ MeV, with corrections of the order 20% to the static theory. Extrapolation of their results to the infinite mass limit would give results compatible with those found here, though perhaps the static results are still a little high. This again points to the problems of extracting a clean signal for the ground state contributions. This is clearly seen in Figure 5.7, which includes the values of Δm_{Λ_b} at several values of M_P, the static value for both Clover and Wilson, [92], fermions and the experimental value.

[1] no measurements were taken after timeslice 12

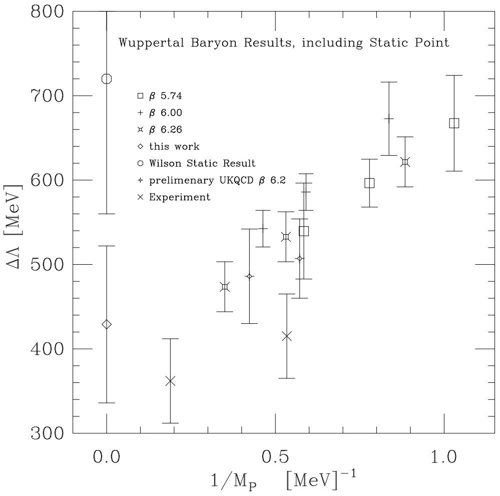

Figure 5.7: $\Lambda_b - B$ Mass Splittings against $1/M_P$, with inclusion of static point. (Taken from [5].)

5.3 $B^* - B$ Mass Splitting

Throughout this thesis the properties and spectrum of hadrons containing a beauty quark have been studied by means of an effective field theory. This was based on Eichten's expansion of the heavy quark propagator in powers of m_Q. In particular the static limit of this theory is concerned only with the lowest order term in this expansion. However, the mass difference between the vector and pseudoscalar meson states arises from spin dependent terms in the action. To lowest order in the expansion in m_Q these states are degenerate in mass. To measure the vector pseudoscalar mass splitting it is necessary to take into account the $\mathcal{O}(1/m_Q)$ corrections to the static theory. As such, the calculation of this mass difference acts as a test of the heavy quark formalism and in particular the effect of the chromo–magnetic operator correction term. It also plays an important role in testing the effect of 'Clover improvement' on lattice measurements, following directly from the conclusions of ref. [92] which presents the original calculation of the $B^* - B$ mass splitting, with Wilson fermions. The discrepancy between their results and experimental values was attributed to either the heavy quark expansion or to lattice systematic errors. The following calculation will attempt to go some way in establishing the validity of these conclusions.

Keeping only the first two terms of Eichten's expansion of the heavy quark propagator gives,

$$S_Q(x;y) = \exp\left(-m_Q(x^4 - y^4)\right)\left(S_0(x;y) + \frac{1}{2m_Q}S_1(x;y)\right), \tag{5.16}$$

with the leading term the static propagator, as given earlier in Equation (4.16), and second term with four contributions,

$$S_1 = S_{\vec{D}^2} + S_\sigma + S_{\vec{D}_r} + S_{\vec{D}_l}. \tag{5.17}$$

These four correction terms, corresponding to kinetic, chromo–magnetic and end–point operators, have the following forms, given in terms of the static propagator, $S_0(x;y) \sim \mathcal{P}_{\vec{x}}(t_x, t_y)\delta^{(3)}(\vec{x} - \vec{y})$,

$$\begin{aligned}
S_{\vec{D}^2}(x;y) &= \left(\frac{1+\gamma_4}{2}\right)\int_{y^4}^{x^4} dw^4 \mathcal{P}_{\vec{x}}(x^4, w^4) \\
&\qquad\qquad \vec{D}^2(\vec{x}, w^4)\mathcal{P}_{\vec{y}}(w^4, y^4)\delta^{(3)}(\vec{x} - \vec{y}) && (5.18)\\
S_\sigma(x;y) &= \left(\frac{1+\gamma_4}{2}\right)\sum_{i<j}\int_{y^4}^{x^4} dw^4 \mathcal{P}_{\vec{x}}(x^4, w^4) \\
&\qquad\qquad \sigma_{ij}F_{ij}(\vec{x}, w^4)\mathcal{P}_{\vec{y}}(w^4, y^4)\delta^{(3)}(\vec{x} - \vec{y}) && (5.19)\\
S_{\vec{D}_r}(x;y) &= -\left(\frac{1+\gamma_4}{2}\right)\mathcal{P}_{\vec{x}}(x^4, y^4)(\vec{\gamma}\cdot\vec{D}(\vec{x}, y^4))\delta^{(3)}(\vec{x} - \vec{y}) && (5.20)\\
S_{\vec{D}_l}(x;y) &= -\left(\frac{1-\gamma_4}{2}\right)(\vec{\gamma}\cdot\vec{D}(\vec{x}, x^4))\mathcal{P}_{\vec{x}}(x^4, y^4)\delta^{(3)}(\vec{x} - \vec{y}). && (5.21)
\end{aligned}$$

Measurements of the properties of the pseudoscalar and vector mesons come from two point correlation functions, defined as,

$$\begin{aligned}
C_{B^*}(t) &= -\frac{1}{3}\sum_{\vec{x},k}\left\langle \gamma^k S_Q(x;0)\gamma^k S_q(0;x)\right\rangle && (5.22)\\
C_B(t) &= -\sum_{\vec{x}}\left\langle \gamma^4\gamma_5 S_Q(x;0)\gamma^4\gamma_5 S_q(0;x)\right\rangle && (5.23)
\end{aligned}$$

At lowest order, including only the first term in the heavy quark expansion, the two point functions $C_B(t)$ and $C_{B^*}(t)$ propagate with the same mass. This can be seen by comparing the Dirac structure of both correlation functions,

$$\gamma_4\gamma_5\left(\frac{1+\gamma_4}{2}\right)\gamma_4\gamma_5 = -\frac{1}{3}\gamma_k\left(\frac{1+\gamma_4}{2}\right)\gamma_k, \tag{5.24}$$

i.e. $C_B^0(t) = -\frac{1}{3}C_{B^*}^0(t)$.

The contributions from the correction terms in Equations (5.18), (5.20) and (5.21) are the same for both pseudoscalar and vector two point functions. It is only the spin dependent term given in Equation (5.19) that enters with a different constant of proportionality,

$$\gamma_4\gamma_5\sigma_{ij}\gamma_4\gamma_5 = \gamma_k\sigma_{ij}\gamma_k. \tag{5.25}$$

It is this chromomagnetic operator term that differentiates between pseudoscalar and vector correlation functions, providing the only contribution to the mass splitting.

As with the other calculations in this section we can define a set of quantities which allow us to extract a finite mass difference. To measure the $B^* - B$ mass splitting it is useful to define the following local correlation functions, in terms of the spin dependent correction to the static propagator, (5.19), and the static propagator itself,

$$C_V(t) = -\sum_{\vec{x}} \left\langle \gamma^4\gamma_5 S_\sigma(x;0)\gamma^4\gamma_5 S_l(0;x)\right\rangle \tag{5.26}$$

$$C_P(t) = -\sum_{\vec{x}} \left\langle \gamma^4\gamma_5 S_0(x;0)\gamma^4\gamma_5 S_l(0;x)\right\rangle. \tag{5.27}$$

To model the behaviour of this spin dependent correlator in terms of a mass splitting, the ratio of these two correlation functions is considered and the spin term is treated as a perturbation to the static correlator. This ratio can easily be seen to behave linearly with time,

$$R_\sigma(t) = \frac{C_V(t)}{C_P(t)} \tag{5.28}$$

$$\rightarrow C_\sigma + D_\sigma t, \tag{5.29}$$

with the mass splitting found from,

$$m_{B^*}^2 - m_B^2 = Z_\sigma \, \frac{4}{3} \, D_\sigma a^2 \, (\mathrm{GeV})^2, \tag{5.30}$$

where Z_σ is the renormalisation constant of the chromomagnetic moment operator of the heavy quark. This renormalisation constant was calculated from the one loop corrections to the chromomagnetic operator, matched between the heavy quark effective theory on the lattice and the continuum regulators. The original calculation in ref. [44], was carried out for Wilson fermions. However, using the

'Clover' improved action has no effect on the calculation of the renormalisation constant. Z_σ comes from the renormalisation of an operator defined purely in terms of heavy quark physics, whereas improvement only changes the light physics content. For $\beta = 6.2$, at a scale $a^{-1} \approx 2.7$ GeV and with a boosted coupling, we take,

$$Z_\sigma = Z_{mag} Z_{mag}^{latt} = 1.45. \tag{5.31}$$

The calculation in ref. [92], was the first to use this technique to measure the vector pseudoscalar mass splitting. They used Wilson fermions and obtained a result, $M_{B^*}^2 - M_B^2 = (0.28 \pm 0.06\,)\mathrm{GeV}^2$ (using $Z_\sigma = 1.45$). Experimentally, the $B^* - B$ mass difference is measured at CLEO above the $\Upsilon(4s)$ energy, creating B^*B pairs. The B^* decays, $B^* \to \gamma B$, and the energy of the photon measured. The Particle Data Group quotes, [97], $M_{B^*} - M_B = (46.0 \pm 6.0\,)$ MeV, giving a value $M_{B^*}^2 - M_B^2 = (0.488 \pm 0.007\,)\mathrm{GeV}^2$.

5.3.1 Lattice Calculation

The two point correlation functions for the spin dependent correction to the heavy quark propagator are calculated in a similar way to those of the lowest order. It is useful to define an effective Wilson line, including the small perturbations due to insertion of the field tensor along the ordinary Wilson line. This effective Wilson line is then used in exactly the same way as the original Wilson lines, in Equation (5.27), as the basis for the two point correlator, Equation (5.26).

To construct an effective Wilson line we discretise the spin dependent correction terms to the propagator, in Equation (5.19), which gives,

$$\begin{aligned}\mathcal{P}_{\vec{x}}^{eff}(t,0) &= \sum_{i<j}\sum_{w^4=0}^{t} \mathcal{P}_{\vec{x}}(t,w^4)\sigma_{ij}F_{ij}(\vec{x},w^4)\mathcal{P}_{\vec{y}}(w^4,0) \\ &= \sum_{w^4=0}^{t} \mathcal{P}_{\vec{x}}(t,w^4)\left(\sum_{i,j<k}\sigma_i\epsilon_{ijk}F_{jk}(\vec{x},w^4)\right)\mathcal{P}_{\vec{y}}(w^4,0), \end{aligned} \tag{5.32}$$

where the lattice definition of the field tensor, F_{jk}, is defined in terms of plaquettes in the (j,k)th plane. The field tensor was discussed in Section 2.4 in terms of 'Clover' improved actions with the field tensor shown in Figure 2.2. Expressed as a sum of plaquettes,

$$\begin{aligned}F_{jk}(\vec{x},t) = \frac{1}{8i}\,&[U_{j,k}(\vec{x},t) + , U_{k,-j}(\vec{x},t) \\ &+ U_{-j,-k}(\vec{x},t) \,+\, U_{-k,j}(\vec{x},t) \,-\, h.c.]\,. \end{aligned} \tag{5.33}$$

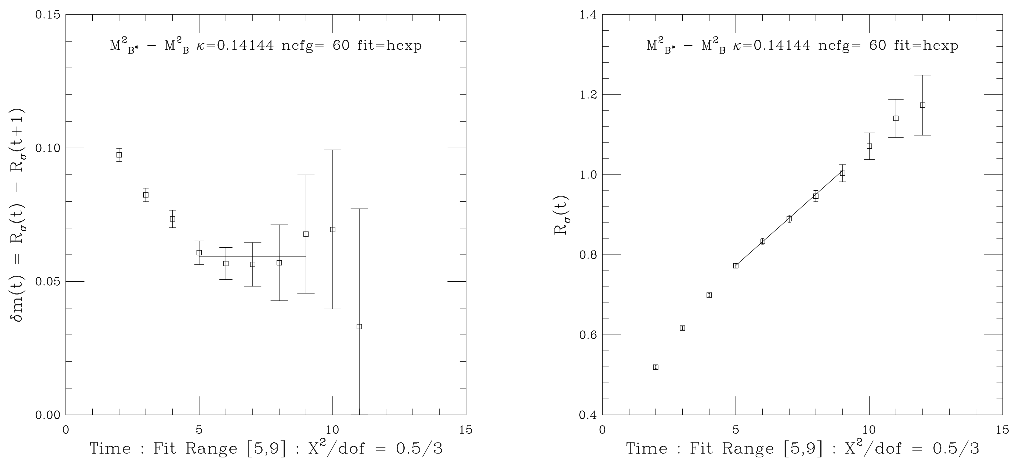

Figure 5.8: (a) Effective mass difference $\delta m = R_\sigma(t) - R_\sigma(t+1)$ with time and (b) ratio $R_\sigma(t)$ for vector pseudoscalar mass splitting. Gauge invariant smearing used.

The plaquette on the lattice was defined earlier, Figure 2.1, as,

$$U_{\mu\nu}(x) = U_\mu(x)U_\nu(x+\hat{\mu})U^\dagger_\mu(x+\hat{\nu})U^\dagger_\nu(x). \tag{5.34}$$

With the effective Wilson lines of Equation (5.32) calculated, the two point function is determined in exactly the same way as outlined earlier for studying f_B^{static}, Section 4.4, but now with the simple Wilson line, $\mathcal{P}_{\vec{x}}(t,0)$ replaced by the effective Wilson line, $\mathcal{P}^{eff}_{\vec{x}}(t,0)$. It should be noted, in this latter case the heavy quark propagator now combines off–diagonal components of the light quark propagator. This is to be expected by the inclusion of a term which breaks the spin symmetry of the Heavy Quark Effective Theory. A further advantage of constructing these effective Wilson lines is that they can be smeared in exactly the same way as the original Wilson lines, with the smearing procedure originally discussed in Section 4.3.

5.3.2 Results

As with all calculations in the static effective theory, smeared interpolating operators are required to obtain any signal with the two point correlation functions in Equations (5.26) and (5.27). A variety of smearing functions, both gauge in-

$R_\sigma(t)$	144	226	262	Critical	$m^2_{B^*} - m^2_B(\mathrm{GeV})^2$
LC	0.041 (4)	0.042 (4)	0.043 (5)	0.042 (5)	0.444 (48)
χ^2/dof	1.6/3	1.1/3	1.0/3	0.7	
LD	0.042 (3)	0.042 (3)	0.042 (3)	0.042 (4)	0.448 (37)
χ^2/dof	2.6/3	1.7/3	1.4/3	1.6	
LE	0.040 (3)	0.040 (3)	0.039 (3)	0.040 (3)	0.424 (35)
χ^2/dof	1.5/3	0.6/3	0.2/3	1.9	
GI LE	0.039 (2)	0.039 (2)	0.039 (3)	0.040 (3)	0.420 (28)
χ^2/dof	0.5/3	0.1/3	1.0/3	0.3	
GI EE	0.036 (2)	0.037 (2)	0.037 (3)	0.038 (2)	0.405 (26)
χ^2/dof	0.03/1	0.3/1	0.5/1	0.4	

Table 5.3: Values for mass splitting, δm_σ from linear fit to ratio $R(t)$, extrapolation to the chiral limit and physical value. Correlated fits and χ^2/dof given.

variant and Coulomb gauge were used, though it was only possible to calculate a smeared–smeared correlator for the gauge invariant smearing.

To check the ratio (5.28) did actually isolate the ground state contributions, an effective mass difference was calculated, $\delta m_\sigma(t) = R_\sigma(t) - R_\sigma(t+1)$. An example of this effective mass is shown in Figure 5.8(a). With a plateau confirmed, R_σ was fitted to the asymptotic form in Equation (5.29) and parameters C_σ and D_σ extracted. An example of the linear behaviour of the ratio is also shown in Figure 5.8(b). In all LS cases the fit range was chosen to be $t \in [5,9]$, but for the gauge invariant SS case, the plateau set in earlier, and a time range $t \in [2,4]$ was used. The values from three light kappa and the chirally extrapolated result are shown in Table 5.3. We note good agreement with the uncorrelated and correlated fits and only include the correlated fits in the table. The final column in this table shows the corresponding continuum result in physical units, using central value only for the scale, $a^{-1} = 2.7$ GeV, and with the inclusion of the renormalisation constant of the chromo–magnetic operator.

As a final answer, we take a weighted average over the LS type results, and quote for $m^2_{B^*} - m^2_B$,

$$\mathrm{SS}: \left(0.405 \pm 0.026 \;\, {}^{+237}_{-\;29}\right)(\mathrm{GeV})^2 \tag{5.35}$$

$$\mathrm{LS}: \left(0.431 \pm 0.037 \;\, {}^{+252}_{-\;31}\right)(\mathrm{GeV})^2 \tag{5.36}$$

where the first error is purely statistical and an error due to uncertainty in the

Measurement	Clover	Wilson	Experiment
$B_s - B_d$(MeV)	$74 \pm 6 \ ^{+19}_{-\ 3}$	$71 \pm 13 \ ^{+}_{-16}$	96 ± 6
$\Lambda_b - B$ (MeV)	$429 \pm 83 \ ^{+111}_{-\ 16}$	$720 \pm 160 \ ^{+}_{-130}$	362 ± 50
$B^* - B$ (GeV)^2	$0.431 \pm 0.037 \ ^{+252}_{-\ 31}$	$0.28 \pm 0.06 \ ^{+}_{-7}$	0.488 ± 0.007

Table 5.4: Results of heavy quark spectroscopy. clover, wilson and experimental results given.

lattice spacing.

The major source of error is introduced due to uncertainty in the lattice spacing, this mass splitting having quadratic dependence on the choice of scale. All values from different smearing functions agree well, even between the LS and SS types. There is a marked improvement over the results obtained from use of the Wilson action and a strong agreement with the experimental result. In this case the use of an improved action, and in particular one which introduces this improvement by use of a 'Clover' like term, seems to improve the results based on matrix elements dependent on this same chromo–magnetic operator.

5.4 Conclusions

The calculation of hadronic masses from first principles is an intrinsically non–perturbative problem. The main practical means of attacking such a calculation is by Lattice QCD to calculate the strong interaction effects binding the quarks into hadrons.

In this chapter, we have used Lattice QCD techniques, in conjunction with theoretical techniques for treating the dynamics of heavy quarks, to determine mass splittings of hadrons containing one heavy quark, in particular the $B_s - B_d$, $\Lambda_b - B$ and $B^* - B$ mass splittings. The final results of these calculations are shown in Table 5.4, along with the results using Wilson fermions from ref. [92], and experimental measurements from ref. [53]. For the lattice results we quote two errors; the first purely statistical and the second due to uncertainty in the calibration of the lattice spacing.

These results were obtained by use of an improved action, one of the aims of such calculations being to see the effect of this improvement on the results obtained. The $B_s - B_d$ mass splitting agrees well between Clover and Wilson though is a little low compared to the experimental mass. The difference between Clover and Wilson, results for the $\Lambda_b - B$ splitting is most likely a statistical effect, though further studies with higher statistics and longer time extents could change this. The vector pseudoscalar mass splitting shows a marked improvement, a result also seen with simulations with light quarks, [4].

Chapter 6

Conclusions

Lattice QCD is a powerful tool for the calculation of non–perturbative phenomena in particle physics. In this thesis we have used the techniques of Lattice QCD with large scale numerical simulations to calculate several quantities which depend crucially on the effects of the strong interaction. These include, weak matrix elements, containing all the long distance physics of a low energy effective field theory and hadron masses, depending on the confinement of quarks in hadrons.

In Chapter 3 we calculated the kaon B-parameter. This is the quantity in neutral kaon mixing containing all the strong interaction effects on the weak decay. We find $B_K = 0.66 \pm 0.08$. This calculation was done with an $\mathcal{O}(a)$ improved action. We compared the results with those found from a calculation with Wilson fermions. Slight improvement was observed though use of this improved action, though the effect was not conclusive.

In Chapter 4, we studied the decay constant of the B-meson, using a formulation of heavy quarks in the static limit of the HQET. From this calculation, we find $f_B^{static} = 248 \pm 8\ {}^{+102}_{-\ 14}$ MeV. To remove the uncertainty in scale and renormalisation constant we calculated the dimensionless ratio $f_{B_s}^{stat}/f_{B_d}^{stat} = 1.12 \pm 0.01$. Using a parameterisation of the heavy quark scaling relation we compared results for the decay constant from propagating quarks with the result in the infinite mass limit. It was still not possible to obtain a consistent fit to all points. In the calculation of quantities containing static quarks, smeared interpolating operators were required to extract the ground state. We compared the effect on f_B^{static} of a variety of smearing functions and observed that Coulomb gauge exponential and gauge invariant smearings best satisfied the criteria for good smearing functions.

Heavy quark spectroscopy was studied in Chapter 5 and we calculated three mass splittings in the B-system; $B_s - B_d$, $\Lambda_b - B$ and the $B^* - B$ mass differences. The first two mass splittings were calculated from the lowest order term in the HQET expansion in quark mass. We find, $m_{B_s} - m_{B_d} = 74 \pm 6 \ {}^{+19}_{-\ 3}$ MeV and $m_{\Lambda_b} - m_B = 429 \pm 83 \ {}^{+111}_{-\ 16}$ MeV. These agree well with experiment, simulations with propagating quarks and also show slight improvement over results with an earlier calculation with Wilson fermions, mainly due to better statistics. The vector–pseudoscalar mass splitting required the calculation of the spin dependent correction to the static quark propagator. From this we obtained $m_{B^*}^2 - m_B^2 = 0.431 \pm 0.037 \ {}^{+252}_{-\ 31}(\mathrm{GeV})^2$, a result much closer to the experimental value than the original Wilson calculation. In this measurement of a spin sensitive quantity, use of an improved action did indeed lead to an improved result.

None of the calculations presented here are particularly new, instead they represent a set of quantities that *ought* to be calculated on the existing gauge configurations. Perhaps the main conclusion from this thesis is that with larger statistical samples, on finer lattices, using improved actions and employing smearing techniques, the systematic uncertainties of lattice calculations are beginning to come under control. Things look bright for the lattice community with their results slowly being accepted by a wider audience, a process which cannot fail to continue as the simulations become ever more accurate and understood.

Appendix A

The Standard Model Lagrangian

The Standard Model is a combination of three gauge theories, based on the gauge group,

$$SU(3) \otimes (SU(2)_L \otimes U(1)_Y)\,, \tag{A.1}$$

the with the corresponding gauge bosons, G^a_μ, $(a = 1, \ldots, 8)$, W^i_μ, $(i = 1, 2, 3)$ and B_μ, and gauge couplings, g_3, g_2 and g_1, respectively, and which have as their generators, $T^a = \lambda^a/2$, $\sigma^i = \tau^i/2$ and 1.

The fermion content of the Standard Model is three families, $A = 1, 2, 3$ consisting of left handed quark $SU(2)$ doublets, Q^A_L, right handed quark singlets, u^A_R and d^A_R, left handed lepton doublet, l^A_L, right handed lepton singlet, e^A_R.

In this Appendix, we specify the Lagrangain that governs the dynamics of the Standard Model,

$$\mathcal{L}_{SM} = \mathcal{L}_{Gauge} + \mathcal{L}_{Fermion} + \mathcal{L}_{Higgs} + \mathcal{L}_{Yukawa} + \mathcal{L}^{\theta}. \tag{A.2}$$

We take each sector in turn:

- Gauge sector:

$$\mathcal{L}_{Gauge} = -\frac{1}{2}G^a_{\mu\nu}G^{a\mu\nu} - \frac{1}{2}F^i_{\mu\nu}F^{i\mu\nu} - \frac{1}{2}H_{\mu\nu}H^{\mu\nu} \tag{A.3}$$

where $a = 1, \ldots, 8$, $i = 1, 2, 3$ and,

$$G^a_{\mu\nu} = \partial_\mu A^a_\nu - \partial_\nu A^a_\mu - f^a_{bc}A^b_\mu A^c_\nu \tag{A.4}$$

$$F^i_{\mu\nu} = \partial_\mu W^i_\nu - \partial_\nu W^i_\mu - \epsilon^i_{jk}W^j_\mu W^k_\nu \tag{A.5}$$

$$H_{\mu\nu} = \partial_\mu B_\nu - \partial_\nu B_\mu, \tag{A.6}$$

are the field tensors of the $SU(3)$, $SU(2)$ and $U(1)$ gauge groups respectively, with the structure constants f^a_{bc}, ϵ^i_{jk} and 1.

- fermion sector:

$$\mathcal{L}_{Fermion} = \bar{\psi} i \gamma^\mu D_\mu \psi, \tag{A.7}$$

for covariant derivatives,

$$D_\mu Q_L^A = \left(\partial_\mu - i\frac{g_3}{2}\lambda^a A_\mu^a - i\frac{g_2}{2}\tau^i W_\mu^i - i\frac{g_1}{6}B_\mu\right) Q_L^A \tag{A.8}$$

$$D_\mu u_R^A = \left(\partial_\mu - i\frac{g_3}{2}\lambda^a A_\mu^a - i\frac{2g_1}{3}B_\mu\right) u_R^A \tag{A.9}$$

$$D_\mu d_R^A = \left(\partial_\mu - i\frac{g_3}{2}\lambda^a A_\mu^a + i\frac{g_1}{3}B_\mu\right) d_R^A \tag{A.10}$$

$$D_\mu l_L^A = \left(\partial_\mu - i\frac{g_2}{2}\tau^i W_\mu^i + i\frac{g_1}{2}B_\mu\right) l_L^A \tag{A.11}$$

$$D_\mu e_R^A = \left(\partial_\mu + i g_1 B_\mu\right) e_R^A \tag{A.12}$$

- Higgs sector

$$\mathcal{L}_{Higgs} = (D_\mu \Phi)^\dagger (D_\mu \Phi) - \mu \Phi^\dagger \Phi + \lambda (\Phi^\dagger \Phi)^2 \tag{A.13}$$

where

$$D_\mu \Phi = \left(\partial_\mu - i\frac{g_2}{2}\tau^i W_\mu^i - i\frac{g_1}{2}B_\mu\right) \Phi. \tag{A.14}$$

- Yukawa sector:

$$\mathcal{L}_{Yukawa} = \lambda_{AB}^l \bar{l}_L^A \Phi e_R^B + \lambda_{AB}^u \bar{Q}_L^A \tilde{\Phi} u_R^B + \lambda_{AB}^d \bar{Q}_L^A \Phi d_R^B + h.c., \tag{A.15}$$

where $\tilde{\Phi} = i\tau_2 \Phi^*$, and λ_{AB} are the cross generational Yukawa couplings.

- topological terms:

$$\mathcal{L}^\theta = -\frac{1}{2} tr G_{\mu\nu} \tilde{G}^{\mu\nu} - \frac{1}{2} tr F_{\mu\nu} \tilde{F}^{\mu\nu} - \frac{1}{2} tr H_{\mu\nu} \tilde{H}^{\mu\nu} \tag{A.16}$$

where $\tilde{G}^{\mu\nu} = \frac{1}{2}\epsilon^{\mu\nu\lambda\rho} G_{\lambda\rho}$. This term can be written as a total divergence, which only contributes as a surface term to the action.

Bibliography

[1] M. Gavela *et al.*, Nucl. Phys. **B306**, 677 (1988).

[2] UKQCD Collaboration, C. Allton *et al.*, Phys. Rev. D **47**, 5128 (1993).

[3] A. Duncan *et al.*, FERMILAB-PUB-94/164-T (1994).

[4] UKQCD Collaboration, C. Allton *et al.*, Edinburgh preprint 93/523, April 1993. (1993).

[5] C. Alexandrou *et al.*, PSI-PR-94-92 (1994), hep-lat 9407027.

[6] UKQCD Collaboration, C. Allton *et al.*, Phys. Rev. D **49**, 474 (1994).

[7] L. Ryder, *Quantum Field Theory* (Cambridge University Press, Cambridge, 1986).

[8] I. Aitchison and A. Hey, *Gauge Theories in Particle Physics* (Hilger, Bristol, 1982).

[9] T. Cheng and L.-F. Li, *Gauge Theories of Elementary Particle Physics* (Oxford University Press, Oxford, 1988).

[10] P. Higgs, Phys. Rev. Lett. **12**, 132 (1964).

[11] N. Cabibbo, Phys. Rev. Lett. **10**, 1802 (1963).

[12] J. Kobayashi and M. Maskawa, Prog. Theor. Phys. **49**, 652 (1973).

[13] CDF Collaboration, F. Abe *et al.*, Fermilab Pub 94/097–E (1994).

[14] Particle Data Group, Phys. Rev. D **45**, (1992).

[15] L. Wolfenstein, Phys. Rev. Lett. **51**, 1945 (1983).

[16] A. Buras, M. Misiak, M. Münz, and S. Pokorski, MPI–Ph/93–77, TUM–T31–50/93, hep-ph 9311345 (1993).

[17] A. Ali, DESY 92-152 (1993), to be published in Proceedings of XXVIth International Conference on High Energy Physics, Dallas, Texas, USA.

[18] A. Ali and D. London, DESY 93-022 (1993).

[19] K. G. Wilson, Phys. Rev. D **10**, 2445 (1974).

[20] R. Feynman and A. Hibbs, *Quantum Mechanics and Path Integrals* (McGraw-Hill, New York, 1965).

[21] T. Banks *et al.*, Phys. Rev. D **15**, 1111 (1977).

[22] L. Susskind, Phys. Rev. D **16**, 3031 (1977).

[23] K. G. Wilson, in *New Phenomena in Subnuclear Physics*, edited by A. Zichichi (Plenum, New York, 1977).

[24] G. Kilcup and S. Sharpe, Nucl. Phys. **B283**, 493 (1987).

[25] H. Neilson and M. Ninomiya, Nucl. Phys. **B185**, 203 (1981).

[26] M. Creutz, *Quarks, Gluons and Lattices* (Cambridge University Press, Cambridge, 1983).

[27] K. Symanzik, in *Mathematical Problems in Theoretical Physics*, edited by R. Schrader, R. Seiler, and D. Uhlenbrock (Springer, Berlin, 1982), Vol. 153, p. 47.

[28] B.Sheikholeslami and R. Wohlert, Nucl. Phys. **B259**, 572 (1985).

[29] G. Heatlie *et al.*, Nucl. Phys. **B352**, 266 (1991).

[30] N. Metropolis, A. Rosenbluth, A. Teller, and E. Teller, Journal of Chemical Physics **21**, 1087 (1953).

[31] A. Kennedy, J. Kuti, S. Meyer, and B. Pendleton, Phys. Rev. Lett. **54**, 87 (1985).

[32] C. Parinello, S. Petrarca, and A. Vladikas, Phys. Lett. **B268**, 236 (1991).

[33] M. Paciello *et al.*, Phys. Lett. **B276**, 163 (1992).

[34] M. Paciello *et al.*, Phys. Lett. **289**, 405 (1992).

[35] J. Mandula and M. Ogilvie, Phys. Lett. **B248**, 156 (1990).

[36] UKQCD Collaboration, R. M. Baxter *et al.*, Phys. Rev. D **49**, 1594 (1994).

[37] M. Gell-Mann, R. Oakes, and B. Renner, Phys. Rev. **175**, 2195 (1968).

[38] M. Bochicchio *et al.*, Nucl. Phys. **B262**, 331 (1985).

[39] G. P. Lepage and P. B. Mackenzie, Nucl. Phys. B (Proc. Suppl.) **20**, 173 (1991).

[40] A. Borrelli, C. Pittori, R. Frezzotti, and E. Gabrielli, Nucl. Phys. **B409**, 382 (1993).

[41] E. Eichten and B. Hill, Phys. Lett. **B240**, 193 (1990).

[42] O. Hernandez and B. Hill, Phys. Lett. **B289**, 417 (1992).

[43] A. Borrelli and C. Pittori, Nucl. Phys. **B385**, 502 (1992).

[44] J. Flynn and B. Hill, Phys. Lett. **B264**, 173 (1991).

[45] C. Michael, Phys. Rev. D **49**, 2616 (1994), hep-lat 9310026.

[46] UKQCD Collaboration, C. Allton *et al.*, Nucl. Phys. **B407**, 331 (1993).

[47] D. Toussaint, in *From Actions to Answers*, edited by T. DeGrand and D. Toussaint (World Scientific, Singapore, 1990).

[48] C. Bernard, in *From Actions to Answers*, edited by T. DeGrand and D. Toussaint (World Scientific, Singapore, 1990).

[49] A. Simpson, Ph.D. thesis, University of Edinburgh, 1991.

[50] J. Christenson, J. Cronin, V. Fitch, and R. Turlay, Phys. Rev. Lett. **13**, 138 (1964).

[51] M. Gaillard and B. Lee, Phys. Rev. **D10**, 897 (1974).

[52] F. Butler *et al.*, hep-lat 9405003 (1994).

[53] Particle Data Group, Phys. Rev. D **50**, (1994).

[54] T. Inami and C. Lim, Progr. Theor. Phys. **65**, 297 (1981), ibid **65** (1981) 1772.

[55] F. Gilman and M. Wise, Phys. Rev. **D27**, 1128 (1983).

[56] A. Buras, M. Jamin, and P. Weisz, Nucl. Phys. **B347**, 491 (1990).

[57] J. Donoghue, E. Golowich, and B. holstein, Phys. Lett. **119B**, 412 (1982).

[58] A. Pich and E. de Rafael, Nucl. Phys. **B358**, 331 (1991).

[59] G. Martinelli, Phys. Lett. **B141**, 395 (1984).

[60] R. Gupta *et al.*, Phys. Rev. D **47**, 5113 (1993).

[61] APE Collaboration A. Donini, (1994), to appear in 'Lattice 94' conference proceedings, Bielefeld, Germany.

[62] C. Pittori, (1994), to appear in 'Lattice 94' conference proceedings, Bielefeld, Germany.

[63] ARGUS Collaboration A. Albrect *et al.*, Phys. Lett. **192B**, 245 (1987).

[64] ELC Collaboration As. Abada *et al.*, Nucl. Phys. **B376**, 172 (1992).

[65] CLEO Collaboration H. Albrect *et al.*, Z. Phys. **C55**, 357 (1992).

[66] ARGUS Collaboration M. Artuso *et al.*, Phys. Rev. Lett. **62**, 2233 (1989).

[67] ALEPH Collaboration D. Decamp *et al.*, Phys. Lett. **B258**, 236 (1991).

[68] DELPHI Collaboration A. Abreu *et al.*, Phys. Lett. **B301**, 145 (1993).

[69] L3 Collaboration B. Adeva *et al.*, Phys. Lett. **B288**, 395 (1992).

[70] OPAL Collaboration P.D. Acton *et al.*, Phys. Lett. **B276**, 379 (1992).

[71] C. Allton *et al.*, Phys. Lett. **B292**, 408 (1992), hep-lat 9208018.

[72] C. Davies, Nucl. Phys. B (Proc. Suppl.) **34**, 135 (1994).

[73] E. Eicthen, Nucl. Phys. **B(Proc. Suppl.)4**, 170 (1988).

[74] N. Isgur and M. Wise, Phys. Lett. **B232**, 113 (1989).

[75] N. Isgur and M. Wise, Phys. Lett. **B237**, 527 (1990).

[76] N. Isgur and M. Wise, Phys. Rev. Lett. **66**, 1130 (1991).

[77] N. Isgur and M. B. Wise, Phys. Rev. D **42**, 2388 (1990).

[78] S. Booth *et al.*, Phys. Rev. Lett. **72**, 462 (1994), hep-lat 9308019.

[79] M. Neubert, SLAC-PUB-6263, hep-ph 9306320 (1993).

[80] H. Georgi, Phys. Lett. **B240**, 477 (1990).

[81] E. Eicthen and B. Hill, Phys. Lett. **B234**, 511 (1990), ibid **B243** (1990) 427.

[82] A. Billoire, E. Marinari, and G. Parisi, Phys. Lett. **B162**, 160 (1985).

[83] APE Collaboration, P. Bacilieri *et al.*, Phys. Lett. **B214**, 115 (1988), nucl. Phys., **B317**, 509, (1989).

[84] APE Collaboration, C.R. Allton *et al.*, npb **413**, 461 (1994).

[85] T. Draper and C. McNeile, Nucl. Phys. **B(Proc. Suppl.)34**, 453 (1994).

[86] S. Güsken *et al.*, Nucl. Phys. **B (Proc. Suppl.)17**, 361 (1990), phys. Lett., **B227**, 266, (1989).

[87] L. Maiani, G. Martinelli, and C. Sachrajda, Nucl. Phys. **B368**, 281 (1992).

[88] C. Allton *et al.*, Nucl. Phys. **B349**, 598 (1991).

[89] C. Alexandrou *et al.*, CERN-TH 6692/92 (1992).

[90] C. Bernard, J. Labenz, and A. Soni, Phys. Rev. D **43**, 2536 (1994).

[91] G. Martinelli, (1994), to appear in 'Lattice 94' conference proceedings, Bielefeld, Germany.

[92] M. Bochicchio *et al.*, Nucl. Phys. **B349**, 598 (1991).

[93] CSB2 Collaboration Lee-Franzini *et al.*, Phys. Rev. Lett. **65**, 2947 (1990).

[94] UA1 Collaboration Albajar *et al.*, Phys. Lett. **B273**, 540 (1991).

[95] R422 Collaboration Bari *et al.*, Nuovo Cimento **104A**, 1787 (1991).

[96] UKQCD Collaboration N. Stella *et al.*, , work in progress.

[97] CLEO Collaboration Akerib *et al.*, Phys. Rev. Lett. **67**, 1692 (1991).